TÉCNICO LISBOA

Kinetics of CO_2 methanation over a Ni/alumina industrial catalyst

Rogéria Paula Martins Bingre do Amaral

Dissertação para obtenção do Grau de Mestre em

Engenharia Química

Orientadores:

Professor Doutor Carlos Henriques

Professora Doutora Filipa Ribeiro

Doutor Sébastien Thomas

Júri:

Presidente: Professor Sebastião Alves (IST)

Orientadores: Professor Doutor Carlos Henriques (IST)

Vogais: Professor José Madeira Lopes (IST)

September 2016

Acknowledgements

I would like to start by thanking to Professors Carlos Henriques and Filipa Ribeiro for showing me this opportunity and for working very hard to make it possible, especially during the obstacles in the beginning.

I want to thank to all my co-workers Audrey, Geraldine, Jeremy, Ksenia, Marina, Pauline, Qian, QinQin, Valentin and Yvan for making my adaptation very fast and easy with all the activities and those talks during coffee breaks. Thank you for had always given me help when I asked and do not mind with my poorly and almost inexistent French. You were my family while I was there.

It is especially to Dr. Sébastien Thomas that I want to give a huge thank you for everything during these six months: for the opportunity given (and also Anne-Cecile), for the warm welcome in that cold month, for all the orientation provided to this work, for repeating the same thing several times when I couldn't understand. The availability and friendliness that you revealed exceed clearly your duties and also my best expectations.

Finally, I am grateful to my parents and closest friends for all the unconditional support during this period. Mãe, Pai you were always there when I needed and always encouraging me to go further.

Resumo

O aumento do consumo de energias renováveis gera desafios respeitantes ao armazenamento do excesso de electricidade produzida de maneira a satisfazer os intervalos onde não há produção. Actualmente, o maior projecto em curso para a utilização eficiente das energias renováveis, “Power-to-Gas”, consiste em electrolizar a água com o excesso de electricidade produzido para obter oxigénio e hidrogénio. Com este último é possível reagir com dióxido de carbono (um dos maiores poluentes actuais) para produzir metano.

Este trabalho consiste na modelação e estudo cinético dessa reacção (metanação de CO_2) bem como as reacções paralelas (metanação de CO e *reverse water-gas shift*) através de um catalisador industrial níquel/alumina.

Inicialmente foi feito um estudo bibliográfico dos vários trabalhos realizados envolvendo metanação de CO_2 principalmente em catalisadores de níquel. Vários mecanismos de reacção diferentes foram encontrados para as reacções em estudo, tendo em conta o tipo de catalisador usado assim como o modelo cinético que melhor descreve o comportamento das reacções.

Várias técnicas de caracterização do catalisador foram realizadas de maneira a se conhecer melhor as condições óptimas de trabalho. De seguida, efectuou-se inúmeros testes catalíticos de forma a avaliar a influência dos produtos e reagentes envolvidos na velocidade da reacção. Todos os resultados experimentais foram testados nos modelos encontrados na literatura.

Finalmente foi proposto um modelo cinético para as três reacções em estudo e calculados os seus parâmetros correspondentes, bem como o mecanismo para cada uma das reacções.

Palavras-Chave: catalisador níquel/alumina; metanação de CO_2; metanação de CO; *reverse water-gas shift*; modelo cinético

Abstract

The increase of the consumption of renewable energies creates challenges concerning the storage of the excess of electricity produced to fill the gaps where there is no production. Currently, the biggest ongoing project to the efficient use of renewable energies, Power-to-Gas, consists in electrolyze water with the excess of electricity to produce oxygen and hydrogen. With hydrogen it is possible to react with carbon dioxide (one of the biggest world pollutants) to produce methane.

This work focused in the kinetic study and modelling of this reaction (CO_2 methanation) and also of the parallel reactions (CO methanation and reverse water-gas shift) over an industrial nickel/alumina catalyst.

Initially it was made a bibliographic study of the several works made in CO_2 methanation mainly in nickel catalyst. Several different reaction mechanisms were found to the reactions in study, taking into account the type of catalyst used and the kinetic model that best describe the behaviour of the reactions.

Several techniques of characterization of the catalyst were realized in order to better know the optimal conditions of work. Then it was made catalytic tests to evaluate the influence of the products and reactants involved in the reaction rate. All the experimental data were tested in the models found in literature.

Finally it was proposed a kinetic model for the three reactions and the correspondent parameters calculated. It was also proposed a mechanism for each reaction.

.

Keywords: nickel/alumina catalyst; CO_2 methanation; CO methanation; reverse water-gas shift; kinetic model

Table of Contents

List of Tables

List of Figures

Abbreviations and Acronyms

Ads. – adsorption

Ar - Argon

BET – Brunauer-Emmet-Teller

Conv – conversion

Diss. - dissociative

FR – flow rate

GHSV – gas hourly space velocity

K – thermodynamic constant of the reaction

K_i – adsorption constant of the component i

LHHW – Langmuir-Hinshelwood Hougen-Watson

Non-diss. – non-dissociative

OR – overall reaction

RDS – rate determining step

RWGS – reverse water-gas shift

SNG – synthetic natural gas

TPR – temperature programmed reduction

WGS – water-gas shift

XRD – x-ray diffraction

ΔG_r - free energy of Gibbs

ΔH_r^0 – heat reaction

ΔS – entropy

1. Introduction

1.1 Exposition of the problem

As the greenhouse effect depends mainly on the emissions of CO_2, it is important to reduce these emissions. In terms of consume of fossil fuel, the Natural Gas, mainly methane, is the cleanest fossil fuel for electricity production but its source is limited.

With the increasing of the use of renewable sources, the storage of electric energy is a big concern, to provide electricity without the use of batteries, because renewable sources cannot provide base load electric power due to their intermittent nature (e.g., wind energy). So the excess of electric energy can be converted into chemical energy by transferring it into fuels such as hydrogen, synthetic natural gas (SNG) or methanol through the "Power to Gas" system. The methanation of CO_2 has the potential to solve both of these problems. The process is being developed is the conversion of CO_2 into methane using hydrogen produced via electrolysis of water (ideally with the excess of electric energy from renewable sources).

Producing methane using CO_2 as a reactant avoids the liberation of this gas to atmosphere and provides methane for electricity production. As emissions are constant in other industries, the source of methane will be (ideally) unlimited.

By the production of methane from CO_2 it is possible to implement three strategies for reducing CO_2 emission: reduce the amount of CO_2 produced, storage and usage of CO_2.

1.2 Current projects

At the present, international organizations and industries are involved in this technique. In Denmark, Haldor Topsoe is working on a "Power to Gas" project [1]; in UK, ITM Power manufactures integrated hydrogen energy solutions to enhance the utilization of renewable energy [2]; the company Hydrogenics in Canada is pioneer in this project [3]; CEA [4], GEG and Saipem in France aim at creating a demonstration plant; instead in Germany Total, Siemens and other organizations have invested in the realization of a biogas plant, wind turbines and electrolysis unit for hydrogen generation. E.ON has launched in 2013 a project for the construction of a "Power to Gas" pilot plant [5]. Institutions as FIW and IWES are investigating the conversion of the surplus of electric energy from wind turbines in synthetic natural gas. [6]

Mostly of the projects take place in Germany due to the transformation of the Germany energy system towards a system that is 100% based on renewable energies which is associated by an increasing demand for chemical storage of electric energy and the compensation of fluctuating wind and solar energy provision. [7]

1.3 Fundamentals

The reaction involved in this process is described by:

$$CO_{2(g)} + 4H_{2(g)} \rightarrow CH_{4(g)} + 2H_2O_{(g)} \quad (1)$$

This is the Sabatier reaction observed by Paul Sabatier over a Nickel catalyst in 1902. It has a heat reaction, $\Delta_r H_{298K}^o$, of -165 kJ.mol^{-1} and it is typically operated at temperatures between 200ºC and 550ºC depending on the catalyst used. [8]

A two-step reaction mechanism is assumed for this reaction. In the first step, carbon dioxide and hydrogen are converted to carbon monoxide and water via the reverse water-gas shift ($\Delta_r H_{298K}^o$ = 41 kJ.mol^{-1}) [8]:

$$CO_2 + H_2 \rightleftarrows CO + H_2O \quad (2)$$

In the subsequent reaction, methane is formed from carbon monoxide and hydrogen ($\Delta_r H_{298K}^o$ = -206 kJ.mol^{-1}) [8]:

$$CO + 3H_2 \rightarrow CH_4 + H_2O \quad (3)$$

The produced gas can be upgraded to SNG to be fed into the natural gas grid.

Besides methane and water, also higher saturated hydrocarbons are formed. The most stable is ethane ($\Delta_r H_{298K}^o$ = -132 kJ.mol^{-1}) [8]:

$$2CO_2 + 7H_2 \leftrightarrows C_2H_6 + 4H_2O \quad (4)$$

It can also occur precipitation of carbon according with the follow reaction ($\Delta_r H_{298K}^o$ = -90 kJ.mol^{-1}) [8]:

$$CO_2 + 2H_2 \leftrightarrows C + 2H_2O \quad (5)$$

The methanation reactions of carbon monoxide and carbon dioxide are widely used in ammonia synthesis plants to remove traces of CO since this component acts like a poison to the ammonia synthesis catalyst. Refineries also use this process to remove CO from hydrogen in order to make it more pure.

In this work, it will be mainly studied the first three reactions. The next figure shows the influence of the temperature in the free energy of Gibbs, calculated by the thermochemistry data in gas phase [9]. It is important to know the behaviour of such reactions in function of temperature, in order to accomplish the best yield from methane production.

$$\Delta G_r(T) = \Delta H_r(T) - T \times \left(\sum \Delta S_{prod} - \sum \Delta S_{reag}\right) \quad (6)$$

From the free energy of Gibs, it is also possible to calculate the thermodynamic constant of each reaction.

$$K(T) = exp\left(\frac{-\Delta G_r(T)}{R \times T}\right) \quad (7)$$

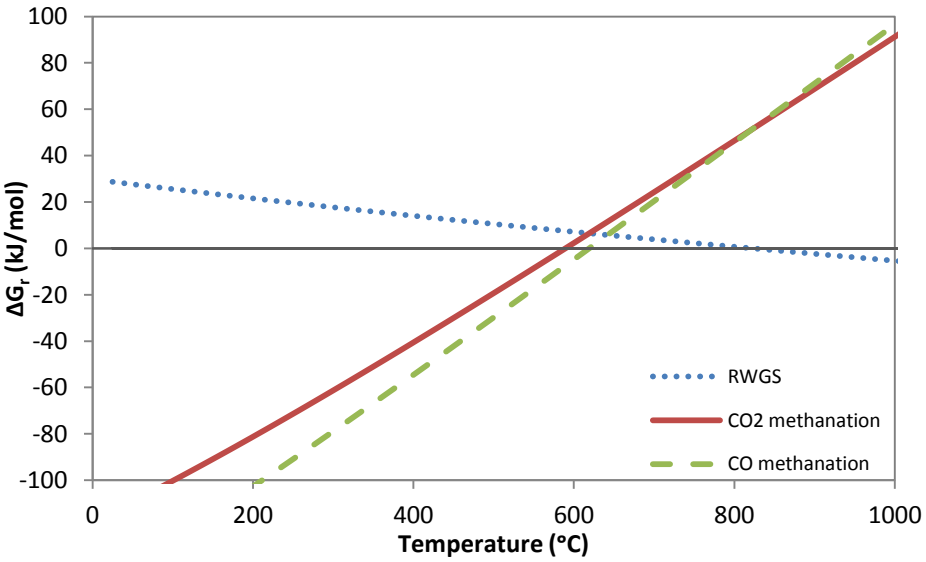

Figure 1: Influence of the temperature in the free energy of each reaction

If ΔG<0, the corresponding reaction is favoured and the equilibrium is shifted towards the products. In other hand, if ΔG>0, the equilibrium is shifted towards the reactants. As it can be seen in Figure 1, formation of methane through carbon dioxide and hydrogen is favoured till a maximum temperature of 600ºC, but the formation of carbon monoxide is favoured by temperatures above 800ºC.

However, temperature is not the only important parameter. In Figure 2, conversion of carbon dioxide at equilibrium is affected by the methanation reaction as a function of temperature and pressure: conversion of carbon dioxide increases with increasing pressure and decreasing temperature.

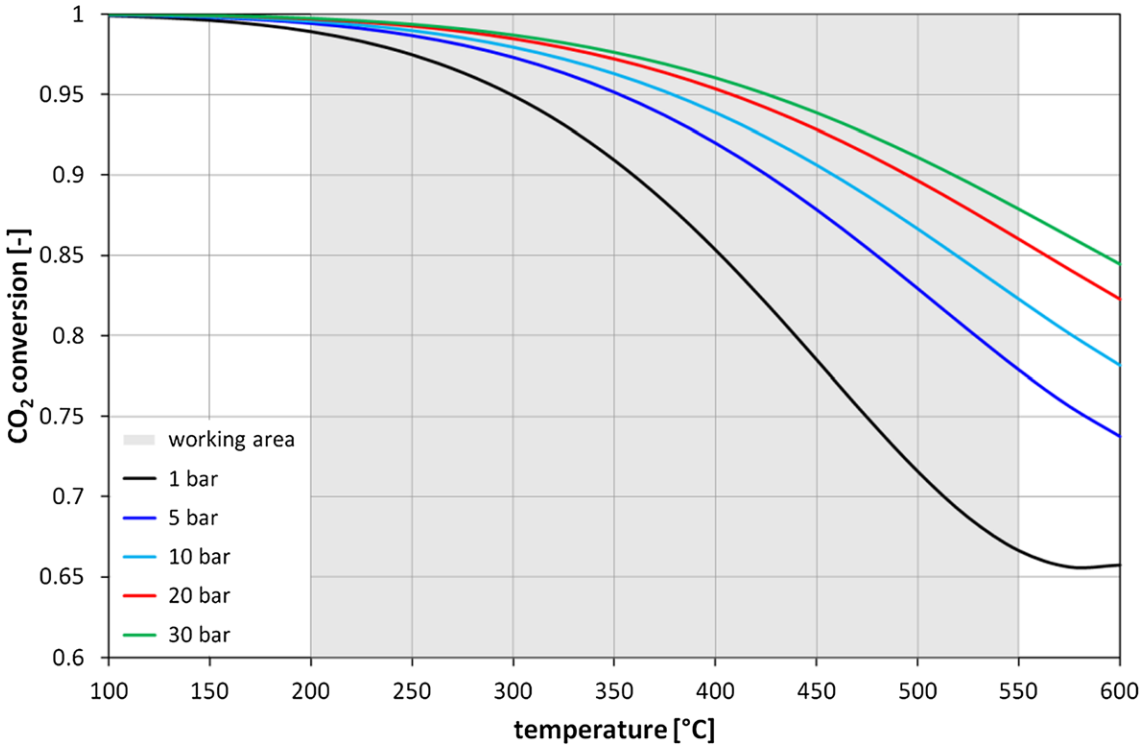

Figure 2: Influence of temperature and pressure on CO_2 conversion (CO_2/H_2=1/4) [8]

Apart from the thermodynamic considerations, the choice of catalyst has a significant influence on the methanation reaction. The catalyst based on nickel presents a high activity and comparatively low price.

It needs to resist fasting temperature changes between 50ºC and 100ºC occurring within a few seconds and caused by changes of the operating point.

Below 200ºC there is the potential formation of highly toxic nickel carbonyl from carbon monoxide. On the other hand, above 550ºC there is deactivation of the catalyst by sintering or carbon formation. So, in conclusion, catalyst should operate in temperature range by the gray shaded box in Figure 2. [8]

1.4 State of the art

In order to facilitate the discussion of the results and to provide a foundation for discussion of material in the sections below, a review of the studies in methanation was made.

Recently, much research has been made in order to find a catalyst for CO_2 methanation. These studies have provided significant information about the reaction kinetics and thermodynamic behaviours. However, little is yet known about the reaction mechanism of carbon dioxide methanation.

According with Darensbourg *et al*. [10], recent studies have lead to a general consensus that the CO_2 methanation reaction occurs through an adsorbed CO intermediate. Still there are two major mechanisms proposed for the methanation of CO_2 by:

1) Bahr – transformation of the CO_2 to CO prior to methanation
2) Medsforth – pathways not requiring the transformation of CO_2 to CO first, with the possibility that much of the reaction takes place in the gas phase rather than on the catalyst surface

In first approximation, on the study of Medsforth [11] over a nickel catalyst, prepared with different promoters, it is proposed the following mechanism that serves as a base for several studies ahead:

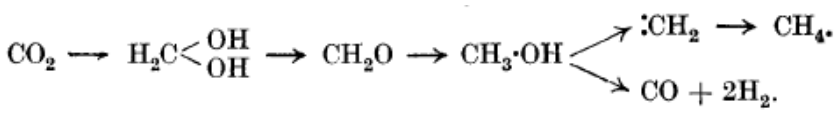

Figure 3: Mechanism proposed to explain the presence of CO

This expression explains the formation of carbon monoxide that has been found in the exit gases by various workers, particularly where a large excess of hydrogen is not used.

However, a simpler hydrogenation can take place, where a compound is dehydrated to give the monoxide and water:

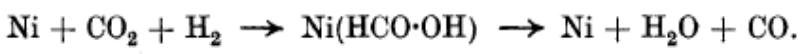

Figure 4: A simpler mechanism for CO_2 hydrogenation

For the reaction of CO methanation, a similar mechanism is given, with the formation of the same intermediate (formaldehyde):

$$CO + 2H_2 \longrightarrow H_2C{\cdot}HOH \longrightarrow :CH_2 \longrightarrow CH_4.$$

Figure 5: Mechanism similar to CO_2 methanation proposed to CO methanation

Herwijnen *et al*. [12] studied the methanation of CO_2 on a supported nickel catalyst with partial pressures of CO_2 below 0,02 atm, at atmospheric pressure and at temperatures between 200 and 230ºC.

They have made the assumption of Langmuir chemisorptions which leads to the general form of kinetic equation:

$$r = \frac{k_\infty . \exp(-E/RT) . g(p) . (1-\beta)}{(1 + f(p,T))^m} \quad (8)$$

Where $g(p)$ is the pure kinetic term which is followed by $(1-\beta)$ that is a correction for the deviation from thermodynamic equilibrium. In the denominator, f(p,T) comes from the coverage balance over the actives sites and m is the number of active sites involved in the rate-determining step. However calculation of the equilibrium composition shows that for CO as well as for CO_2 the conversion is complete up to 400ºC. This means that the value of β is so small that it can be neglected. Furthermore, the partial pressure of hydrogen is very large compared with the carbon oxide what implies $g(p)$ is only a function of the carbon oxide concentration.

For the methanation of CO_2, the next equation is obtained assuming the temperature dependency of the rate constant but that K_{CO_2} (adsorption constant of CO_2) can be constant:

$$r = \frac{k_\infty . \exp(-E/RT) . P_{CO_2}}{(1 + K_{CO_2} . P_{CO_2})^2} \quad (9)$$

Using regressions on the measured conversion it is obtained the follow expression in $mol.h^{-1}.g^{-1}$:

$$r = \frac{1.36 \times 10^{12} \times \exp(-25\,300/RT) \times P_{CO_2}}{(1 + 1270 \times P_{CO_2})^2} \quad (10)$$

In terms of CO methanation, the equation presented is equal taking into account that the reactant involved in that case is CO.

Franko *et al*. [13] reviewed mechanisms and proposed kinetic equations in previous studies and they affirmed that any mechanistic theory must explain the following:

(a) No methanol is observed. Only it is formed when CO is hydrogenated over copper-zinc oxide, with only one of the two bonds to oxygen being broken.
(b) No formaldehyde is formed, which would almost necessitate methanol as an intermediate.
(c) Methylene radical, CH_2, have been detected.
(d) Metal carbonyls are not present.
(e) The reaction occurs on the surface of the catalyst and not in the gas phase.

(f) There is conflicting evidence about the ratios of $CO:H_2$ sorbed on the surface. However, evidence is good that an equimolar ratio of the gases desorbs irrespective of the ratio of the original mixture. This leads to the postulate of some sort of weakly bonded HCOH complex.

Accordingly with the reference of Vlasenko and Uzefovich [14] the mechanism for hydrogenolysis of CO_2 to methane on nickel-chromium catalyst proceeds in the following way:

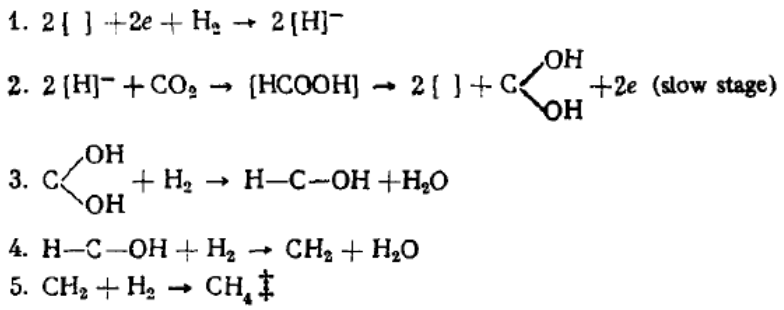

Figure 6: Mechanism proposed by Vlasenko and Uzefovich

According to this scheme, the process is initiated by the activation of only the hydrogen on the catalyst surface, after which the reaction takes place in the gas volume.

Through some studies they concluded that CO_2 is not hydrogenated in the presence of CO, however this is not totally right since it does not take into account that simultaneous with methane formation is the formation of water which reacts with CO to make CO_2 by the water-gas shift reaction.

The synthesis of methane from CO_2 and hydrogen was also studied by Binder and White [15] over a reduced nickel catalyst, where the surface reaction between the CO_2 and hydrogen appeared to be rate controlling.

$$r = \frac{C_1 \left[P_{CO_2} P_{H_2}^2 - \frac{P_{CH_4} P_{H_2O}^2}{K_1 P_{H_2}^2} \right]}{[P_{H_2}^{1/2} + C_2 P_{CO_2} + C_3]^5}$$

$$r = \frac{C_1' \left[P_{CO_2} P_{H_2}^4 - \frac{P_{CH_4} P_{H_2O}^2}{K_1} \right]}{[P_{H_2}^{1/2} + C_2' P_{CO_2} + C_3']^9}$$

Figure 7: Kinetic model proposed by Binder and White

The first equation was derived assuming that the rate-controlling step is the reaction of one molecule of adsorbed CO_2 with two molecules of dissociated adsorbed hydrogen. The second equation is based on the assumption that the rate-determining step is the reaction of one molecule of adsorbed CO_2 with four molecules of adsorbed hydrogen. In this particular case it was not possible to prove reaction mechanism by the study of the kinetic data.

The next study analysed was performed by Dalmon *et al*. [16] over nickel catalysts, where it was proposed the mechanism of Bahr's model:

$$CO_{2,gas} \rightleftharpoons Ni_4CO_{ads.} + NiO_{ads} \quad (11)$$

$$Ni_4CO_{ads.} \rightleftharpoons Ni_3C_{surf.} + NiO_{ads} \quad (12)$$

$$Ni_3C_{surf.} + NiO_{ads} + 3H_2 \rightleftharpoons CH_4 + H_2O \quad (13)$$

They concluded that the carbon polymerisation should be larger at higher C concentration and this concentration is smaller in CO_2 hydrogenation, accordingly with volumetric adsorption measurements reported in this study. Therefore it would be expected less heavy hydrocarbons in CO_2 hydrogenation, since that at atmospheric pressure the C concentration is thermodynamically weak to favour the formation of hydrocarbons larger than methane. Moreover, adsorbed oxygen atoms which are relatively more abundant in the case of CO_2 adsorption may act as a geometric diluent, thus contributing to the decrease in the C – C formation.

For the larger reaction rate observed for CO_2 hydrogenation, they have observed that Ni_4CO_{ads} can be formed at lower temperatures suggesting that the corresponding adsorption activation energy is smaller.

Accordingly with the study of Bartholomew *et al* [17], the kinetic model of the methanation of CO_2 is based on a complex Langmuir-Hinshelwood mechanism involving dissociative adsorption of CO_2 to CO and atomic oxygen followed by hydrogenation of CO via a carbon intermediate to methane. The scheme of the mechanism is presented in Figure 8.

In order to reach the expression that describes this mechanism, it was considered several steps as a rate-determining (RDS).

One of the steps was the CO dissociation (Eq. 4-4), and it was considered that step 4-1, 4-2, 4-3 and 4-10 were in quasi-equilibrium, while the surface oxygen concentration was found from the steady-state approximation. From the expressions derived from this RDS, many of them were eliminated because the least-squares fit of the data resulted in negative kinetic and/or equilibrium constants at all temperatures, or due to the basis of a poor fit to the data.

Reaction	Equation
$H_2(g) + 2\,S \underset{k_{-1}}{\overset{k_1}{\rightleftharpoons}} 2\,H\text{–}S$	(4-1)
$CO_2(g) + 2\,S \underset{k_{-2}}{\overset{k_2}{\rightleftharpoons}} CO\text{–}S + O\text{–}S$	(4-2)
$CO\text{–}S \underset{k_{-3}}{\overset{k_3}{\rightleftharpoons}} CO(g) + S$	(4-3)
$CO\text{–}S + S \underset{k_{-4}}{\overset{k_4}{\rightleftharpoons}} C\text{–}S + O\text{–}S$	(4-4)
$C\text{–}S + H\text{–}S \underset{k_{-5}}{\overset{k_5}{\rightleftharpoons}} CH\text{–}S + S$	(4-5)
$CH\text{–}S + H\text{–}S \underset{k_{-6}}{\overset{k_6}{\rightleftharpoons}} CH_2\text{–}S + S$	(4-6)
$CH_2\text{–}S + H\text{–}S \underset{k_{-7}}{\overset{k_7}{\rightleftharpoons}} CH_3\text{–}S + S$	(4-7)
$CH_3\text{–}S + H\text{–}S \underset{k_{-8}}{\overset{k_8}{\rightleftharpoons}} CH_4\text{–}S + S$	(4-8)
$CH_4\text{–}S \underset{k_{-9}}{\overset{k_9}{\rightleftharpoons}} CH_4(g) + S$	(4-9)
$O\text{–}S + H\text{–}S \underset{k_{-10}}{\overset{k_{10}}{\rightleftharpoons}} OH\text{–}S + S$	(4-10)
$OH\text{–}S + H\text{–}S \underset{k_{-11}}{\overset{k_{11}}{\rightleftharpoons}} H_2O\text{–}S + S$	(4-11)
$H_2O\text{–}S \underset{k_{-12}}{\overset{k_{12}}{\rightleftharpoons}} H_2O(g) + S$	(4-12)

Figure 8: Proposed mechanism of CO_2 methanation by Bartholomew *et al*

Finally the equation reached was the only rate expression that resulted in physically meaningful rate and adsorption equilibrium constants as well as a linear Arrhenius plot for the rate constant k_4.

$$r_{CH_4} = \frac{\left(\frac{K_1 K_2 K_{10} k_4 k_{11}}{2}\right)^{1/2} L^2 P_{CO_2}^{1/2} P_{H_2}^{1/2}}{\left(1 + \left(\frac{2K_2 k_4}{K_1 K_{10} k_{11}}\right)^{1/2} \frac{P_{CO_2}^{1/2}}{P_{H_2}^{1/2}} + \left(\frac{K_1 K_2 K_{10} k_{11}}{2k_4}\right)^{1/2} P_{CO_2}^{1/2} P_{H_2}^{1/2} + \frac{P_{CO}}{K_3}\right)^2} \qquad (14)$$

The conclusions of the study are that the rate of CO_2 hydrogenation on Ni/SiO_2 is quite sensitive to reactant concentrations at low H_2 and CO_2 partial pressures while reaction orders approach zero for H_2 and CO_2 at high reactant concentrations.

Also, addition of CO to the reactants above the equilibrium level causes a significant decrease in the rate of CO_2 hydrogenation apparently as a result of product inhibition, since they both adsorb in the same active sites.

The activation energy for CO dissociation is constant at 94 kJ/mol over the full range of temperature (500-600K).

Another study analyzed was performed by Froment *et al*. [18], at 10 bar and H_2 / CO_2 = 1.

From several reactions which may occur only three were proved by experimental results for steam reforming.

$$CH_4 + H_2O \longrightarrow CO + 3H_2 \quad (15)$$

$$CO + H_2O \longrightarrow CO_2 + H_2 \quad (16)$$

$$CH_4 + 2H_2O \longrightarrow CO_2 + 4H_2 \quad (17)$$

Rate equations were written for the rate-determining step of each of the three global reactions 15, 16 and 17, in terms of the concentration of the adsorbed species.

For reaction 15:

$$r_{15} = \frac{k_1}{P_{H_2}^{2,5}}\left(P_{CH_4}P_{H_2O} - \frac{P_{H_2}^3 P_{CO}}{K_1}\right)/(DEN)^2 \quad (18)$$

For reaction 16:

$$r_{16} = \frac{k_2}{P_{H_2}}\left(P_{CO}P_{H_2O} - \frac{P_{H_2}P_{CO_2}}{K_2}\right)/(DEN)^2 \quad (19)$$

For reaction 17:

$$r_{17} = \frac{k_3}{P_{H_2}^{3,5}}\left(P_{CH_4}p_{H_2O}^2 - \frac{P_{H_2}^4 P_{CO_2}}{K_3}\right)/(DEN)^2 \quad (20)$$

$$\text{DEN} = 1 + K_{CO}P_{CO} + K_{H_2}P_{H_2} + K_{CH_4}P_{CH_4} + K_{H_2O}P_{H_2O}/P_{H_2} \quad (21)$$

Reactions rates for the disappearance of CO_2 and for the formation of CO and CH_4 in the reverse water-gas shift and methanation (CO_2 and H_2 as feed) are obtained from:

$$r'_{CO} = r_{15} - r_{16} \quad (22)$$

$$r'_{CO_2} = -(r_{16} + r_{17}) \quad (23)$$

$$r'_{CH_4} = -(r_{15} + r_{17}) \quad (24)$$

The next figure details the scheme of the mechanism to steam reforming from the equations 15, 16 and 17. Note that the reverse equations lead to the methanation of CO_2.

H_2O	+ L	= O-L	+ H_2		(1)
CH_4	+ L	= CH_4-L			(2)
CH_4-L	+ L	= CH_3-L	+ H-L		(3)
CH_3-L	+ L	= CH_2-L	+ H-L		(4)
CH_2-L	+ O-L	= CH_2O-L	+ L		(21)
CH_2O-L	+ L	= CHO-L	+ H-L		(22)
CHO-L	+ L	= CO-L	+ H-L		(23) r.d.s.; r_1
CO-L	+ O-L	= CO_2-L	+ L		(8) r.d.s.; r_2
CHO-L	+ O-L	= CO_2-L	+ H-L		(25) r.d.s.; r_3
CO-L		= CO	+ L		(7)
CO_2-L		= CO_2	+ L		(10)
2H-L		= H_2-L	+ L		(1-bis)
H_2-L		= H_2	+ L		(1-bis)

Figure 9: Mechanism proposed for steam reforming by Xu and Froment

On the other side, Ibraeva *et al*. [19] realized experiments carried out in the temperature range of 498-543K on a NKM-4A nickel-containing catalyst.

The addition of methane or water to the starting mixture in amounts significantly exceeding those formed during methanation did not lead to a change in reaction rate, which indicates the absence of inhibition of the reaction by its products. In accordance with this, there is the following kinetic equation:

$$r = k_1 P_{CO_2}^{l1} P_{H_2}^{m1} / \left(P_{H_2}^{m2} + k_2 P_{CO_2}^{l2}\right)^n \quad (25)$$

Through some calculations it was showed that the experimental results are best described by:

$$r = k_1 P_{CO_2} P_{H_2}^{0,5} / \left(P_{H_2}^{0,5} + k_2 P_{CO_2}\right) \quad (26)$$

Taking into account the data and analysis made during the study, the mechanism proposed is presented on Figure 10:

1) $H_2 + 2Z = 2HZ,$

2) $CO_2 + Z = CO_2Z,$

3) $CO_2Z + HZ = COOHZ + Z,$

4) $COOHZ + HZ = COHZ + OHZ,$

5) $COHZ + HZ = CHZ + OHZ,$

6) $CHZ + HZ = CH_2Z + Z,$

7) $CH_2Z + HZ = CH_3Z + Z,$

8) $CH_3Z + HZ = CH_4 + 2Z,$

9) $OHZ + HZ = H_2O + 2Z.$

Steps 1 and 2 are fast equilibrium and step 3 is a slow one, and the subsequent step 4-9 can be considered as fast irreversible under these conditions.

Figure 10: Mechanism proposed by Ibraeva *et al* accordingly with the data obtained

In the next article analysed of Gao *et al*, from the Journal RSC Advances [20], it is said that Ni is better for methanation reactions to produce methane as compared with Co and Fe. Unsupported Ni nanoparticles or Raney Ni62 are active for carbon monoxide and carbon dioxide methanation.

Ni supported on Al_2O_3 is one of the most widely studied catalysts in methanation reactions for the production of SNG due to its high performance-cost ratio.

Although Ni catalysts are preferred in catalytic methanation reaction, there still exist some problems, such as carbon deposition, sintering, Ni(CO)4 formation, and sulfur poisoning during SNG production.

Next, it is referred the study of Aldana *et al* [21], where is investigate carbon dioxide methanation mechanism over Ni-based ceria-zirconia catalysts. H_2 was found to dissociate on Ni^0 sites while carbon dioxide was activated on the ceria-zirconia support to form carbonates which could be hydrogenated into formate and further into methoxy species.

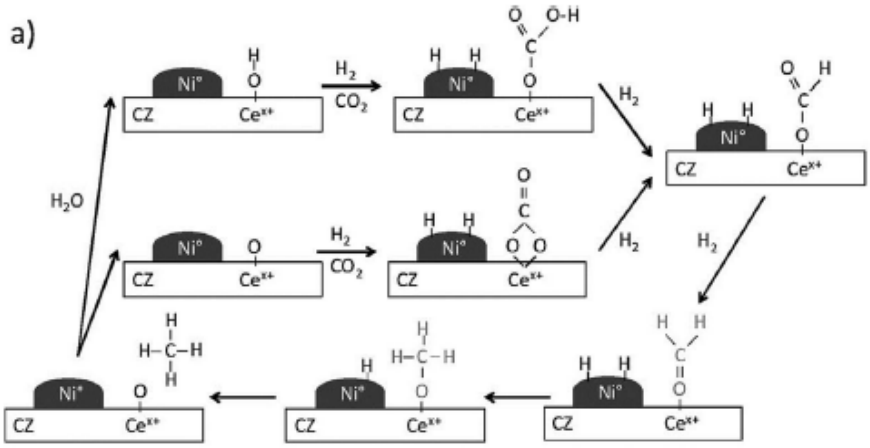

Figure 11: Reaction mechanism proposed on Ni-CZ for carbon dioxide methanation by Aldana *et al*

Another article from the journal Applied Catalysis B: Environmental [22], Koschany *et al* derived LHHW-type rate equations analogously to the methodology of Weatherbee and Bartholomew that recently was also adopted for the methanation of carbon monoxide by Kopyscinski *et al* [23].

The first mechanism assumed considers the cleavage of carbon-oxygen bonds first and subsequent hydrogenation of adsorbed oxygen to water. Hydrogen, carbon dioxide and methane are assumed to adsorb dissociatively.

The second mechanism assumes than occurs first reaction of hydrogen with CO to carbon-hydroxyl COH or formyl HCO, before carbon oxygen bond cleavage.

1: CO_2	+ 2*	⇌	CO* + O*	1: CO_2	+ 2*	⇌ CO*	+ O*
2: H_2	+ 2*	⇌	2 H* +	2: H_2	+ 2*	⇌ 2 H*	+
3: CO*	+ *	⇌	C* + O*	3: CO*	+ H*	⇌ CHO*	+ *
4: C*	+ H*	⇌	CH* + *	4: CHO*	+ *	⇌ CH*	+ O*
5: O*	+ H*	⇌	OH* + *	5: CH*	+ 3H*	⇌ CH_4*	+ 3*
6: OH*	+ H*	⇌	H_2O* + *	6: CH_4*		⇌ CH_4	+ *
7: H_2O*		⇌	H_2O + *	7: O*	+ H*	⇌ OH*	+ *
8: CH*	+ 3H*	⇌	CH_4* + 3*	8: OH*	+ H*	⇌ H_2O*	+ *
9: CH_4*		⇌	CH_4 + *	9: H_2O*		⇌ H_2O	+ *

Figure 12: Mechanism (a) (left) and (b) (right) for derivation of LHHW rate equations by Koschany *et al*

The kinetic rate equations are derived analogously to the methodology of Weatherbee and Bartholomew which has also been adopted by Kopyscinsky *et al*. for the case of CO methanation.

The mechanism (a) considers the cleavage of carbon-oxygen bonds first and subsequent hydrogenation of carbon and carbenes to methane as well as hydrogenation of adsorbed oxygen to water. Hydrogen, carbon dioxide and methane are assumed to adsorb dissociatively.

The mechanism (b) implies that first there is reaction of hydrogen with CO to carbon-hydroxyl COH of formyl HCO, before carbon oxygen bond cleavage.

Exemplarily, the derivation will be presented for mechanism (b) assuming step 3 as rate determining step and treating step 8 as irreversible. The overall reaction rate is equal to the rate of elementary step 3, the formation of the formyl species, which is considered as rate determining step.

$$r = \frac{kP_{CO_2}^{0,5}P_{H_2}^{0,5}\left(1-\frac{P_{CH_4}P_{H_2O}^2}{k_{eq}P_{CO_2}P_{H_2}^4}\right)}{\left(1+\sqrt{K_{H_2}P_{H_2}}+K_{mix}P_{CO_2}^{0,5}+K_{OH}\frac{P_{H_2O}}{P_{H_2}^{0,5}}\right)^2} \quad (27)$$

If instead of hydroxyl water is assumed as most abundant surface intermediate, the last term in the denominator is replaced accordingly:

$$r = \frac{kP_{CO_2}^{0,5}P_{H_2}^{0,5}\left(1-\frac{P_{CH_4}P_{H_2O}^2}{k_{eq}P_{CO_2}P_{H_2}^4}\right)}{\left(1+\sqrt{K_{H_2}P_{H_2}}+K_{mix}P_{CO_2}^{0,5}+K_{H_2O}P_{H_2O}\right)^2} \quad (28)$$

In this article is presented a table with an overview of published models:

Catalyst (Ni wt.%)	T [°C]	p_{max} [bar]	Rate equation	Ref.
Ni/SiO_2 (60)	260–400	1	$r_{CH_4} = \frac{k\left(p_{CO_2}p^2{}_{H_2} - p_{CH_4}p^2{}_{H_2}O/K_{eq}p^2{}_{H_2}\right)}{\left(1+K_{H_2}p^{0.5}H_2+K_{CO_2}p_{CO_2}\right)^5}$	[22]
			$r_{CH_4} = \frac{k\left(p_{CO_2}p^4{}_{H_2} - p_{CH_4}p^2{}_{H_2}O/K_{eq}\right)}{\left(1+K_{H_2}p^{0.5}H_2+K_{CO_2}p_{CO_2}\right)^9}$	
Ni/SiO_2 (60)	280–400	30	$r_{CH_4} = \frac{kp_{CO_2}p^4{}_{H_2}}{\left(1+K_{H_2}p_{H_2}+K_{CO_2}p_{CO_2}\right)^5}$	[19]
Ni/Cr_2O_3 (62)	160–180	1	$r_{CH_4} = kp^{0.5}{}_{CO_2}$	[23]
Ni/Al_2O_3 (28)	200–230	1	$r_{CH_4} = \frac{kp_{CO_2}}{1+K_{CO_2}p_{CO_2}}$	[24]
Ni/SiO_2 (3)	227–327	0.16	$r_{CH_4} = \frac{kp^{0.5}_{CO_2}p^{0.5}_{H_2}}{\left(1+K_1p^{0.5}_{CO_2}p^{0.5}_{H_2}+K_2p^{0.5}_{CO_2}/p^{0.5}_{H_2}+K_3p_{CO}\right)^2}$	[20]
Ni/SiO_2 (58)	275–320	17	$r_{CH_4} = kp^{0.66}_{CO_2}p^{0.21}_{H_2}$	[25]
			$r_{CH_4} = \frac{kp_{CO_2}p_{H_2}}{\left(1+K_{H_2}p_{H_2}+K_{CO_2}p_{CO_2}\right)}$	
Ni	250–350	n.a.	$r_{CH_4} = \frac{kp_{H_2}p^{1/3}_{CO_2}}{1+K_{CO_2}p_{CO_2}+K_{H_2}p_{H_2}+K_{H_2O}p_{H_2O}}$	[26]
$Ni/La_2O_3/Al_2O_3$ (17)	240–320	1	$r_{CH_4} = \frac{kp^{1/2}_{H_2}p^{1/3}_{CO_2}}{\left(1+K_{H_2}p^{1/2}_{H_2}+K_{CO_2}p^{1/2}_{CO_2}+K_{H_2O}p_{H_2O}\right)^2}$	[27]
$Ni/MgAl_2O_4$ (15)	300–400	10	$r_1 = \frac{k_1}{p^{2.5}_{H_2}}\frac{p_{H_2O}p_{CH_4} - \frac{p^3_{H_2}p_{CO}}{k_1}}{\left(1+K_{CO}p_{CO}+K_{H_2}p_{H_2}+K_{CH_4}p_{CH_4}+K_{H_2O}p_{H_2O}/p_{H_2}\right)^2}$	[28]
			$r_2 = \frac{k_2}{p_{H_2}}\frac{p_{H_2O}p_{CO} - \frac{p_{H_2}p_{CO_2}}{k_2}}{\left(1+K_{CO}p_{CO}+K_{H_2}p_{H_2}+K_{CH_4}p_{CH_4}+K_{H_2O}p_{H_2O}/p_{H_2}\right)^2}$	
			$r_3 = \frac{k_3}{p^{3.5}_{H_2}}\frac{p^2_{H_2O}p_{CH_4} - \frac{p^4_{H_2}p_{CO_2}}{k_3}}{\left(1+K_{CO}p_{CO}+K_{H_2}p_{H_2}+K_{CH_4}p_{CH_4}+K_{H_2O}p_{H_2O}/p_{H_2}\right)^2}$	

Figure 13: Overview of published models presented by Koschany et *al*

One important step in the mechanism of the methanation of CO_2 is the reverse water-gas shift reaction (RWGS) where the CO_2 is mixed with H_2 to give CO and H_2O.

In the first article analysed [24] a kinetic study has been made of the reverse water-gas shift reaction. For the reaction of carbon dioxide and hydrogen Bradford's mechanism takes the form:

$$H_2 + M \xrightarrow{k_3} 2H + M \quad \text{initiation} \qquad (6)$$

$$H + CO_2 \underset{k_5}{\overset{k_4}{\rightleftharpoons}} OH + CO \quad \text{propagation} \qquad (7)$$

$$OH + H_2 \underset{k_7}{\overset{k_6}{\rightleftharpoons}} H + H_2O \quad \text{propagation} \qquad (8)$$

$$2H + M \xrightarrow{k_8} H_2 + M \quad \text{termination} \qquad (9)$$

Figure 14: Mechanism to RWGS proposed by Bradford where M is any molecule in the gaseous phase

Considering stationary-state concentration of hydroxyl radicals and equal rates of chain initiation and termination, the measured reaction rate is:

$$\frac{d[H_2O]}{dt} = k_3^{1/2} k_8^{-1/2} [H_2]^{1/2} \times \frac{k_4 k_6 [CO_2][H_2] - k_5 k_7 [CO][H_2O]}{k_6[H_2] + k_5[CO]} \qquad (29)$$

When applied to the experiments the expression can be reduced to:

$$\frac{d[H_2O]}{dt} = \frac{k_3^{1/2} k_8^{-1/2} k_4 [H_2]^{1/2} [CO_2]}{1 + k_5 k_6^{-1} [CO]/[H_2]} \qquad (30)$$

On the study of Grenoble *et al*. [25], it is proposed a mechanism where there is adsorption on the support (S) and on the metal (M) site of the catalyst.

With bifunctional reactions over supported metal catalysts, the question arises as to whether the metal-support interface is the active center.

One way to know this was to vary the dispersion of the metal component and then compare the turnover rates for the catalysts.

To be consistent with the experimental observations, a reaction sequence had to account for both the role of the metal and the role of the support.

$$CO + M \overset{k_{CO}}{\leftrightarrow} CO - M \qquad (31)$$

$$H_2O + S \overset{k_2}{\leftrightarrow} H_2O - S \qquad (32)$$

$$CO - M + H_2O - S \overset{k_F}{\leftrightarrow} F - S + M \qquad (33)$$

$$F - S + M \xrightarrow{k_{WGS}} F - M + S \qquad (34)$$

$$F - M \xrightarrow{fast} CO_2 + H_2O + M \qquad (35)$$

It was assumed Langmuir adsorption isotherms for CO on metal sites and H_2O on support sites.

The decomposition of the formic acid-metal complex is rapid relative to its formation on the metal surface by migration from the support. It is also evident that the transport to and the adsorption of formic acid onto the metal are essentially irreversible due to its rapid decomposition.

With these observations, a kinetic model was developed:

$$r = kP_{CO}^{X} P_{H_2O}^{(1-X)/2} \tag{36}$$

In the article of Wheeler *et al*. [26], the mechanism on a noble metal is assumed to consist of elementary steps as such as the following sequence:

(1) $CO + M \rightleftharpoons CO\text{–}M,$
(2) $H_2O + M \rightleftharpoons H_2O\text{–}M,$
(3) $H_2O\text{–}M + M \rightleftharpoons OH\text{–}M + H\text{–}M,$
(4) $OH\text{–}M + M \rightleftharpoons H\text{–}M + O\text{–}M,$
(5) $2OH\text{–}M \rightleftharpoons H_2O\text{–}M + O\text{–}M,$
(6) $CO\text{–}M + O\text{–}M \rightleftharpoons CO_2\text{–}M + M,$
(7) $CO_2 + M \rightleftharpoons CO_2\text{–}M,$
(8) $H_2 + 2M \rightleftharpoons 2H\text{–}M.$

Figure 15: Mechanism to WGS on a noble metal by Wheeler *et al*

Steps 1, 2, 7 and 8 are adsorption and desorption steps while steps 3, 4, 5 and 6 are surface reaction steps.

With Langmuir isotherms for all species, the rate becomes

$$r'' = \frac{k_f'' K_{CO} K_{H_2O} P_{CO} P_{H_2O} - k_b'' K_{CO_2} K_{H_2} P_{CO_2} P_{H_2}}{(1 + K_{CO} P_{CO} + K_{H_2O} P_{H_2O} + K_{CO_2} P_{CO_2} + K_{H_2} P_{H_2})^2} \tag{37}$$

In case the reaction occurs in a catalyst with presence of ceria, the rate is presumably greater than on the noble metals alone because H_2O can adsorb on ceria rather than being blocked by a surface saturated with CO. The mechanism is the following:

(1) $CO + M \rightleftharpoons CO\text{–}M,$
(2) $H_2O + Ce \rightleftharpoons H_2O\text{–}Ce,$
(3) $H_2O\text{–}Ce \rightleftharpoons O\text{–}Ce + H_2,$
(4) $CO\text{–}M + O - Ce \rightleftharpoons CO_2\text{–}Ce + M,$
(5) $CO_2\text{–}Ce \rightleftharpoons CO_2 + Ce.$

Figure 16: Mechanism to WGS in the presence of ceria by Wheeler *et al*

Accordingly with the dissertation of Callaghan [27] about kinetics of water-gas shift reaction, the formations of carbon blocks the catalyst sites causing catalyst deactivation and an increase in the pressure drop across the bed caused by plugging or fouling of the reactor.

About the catalyst (nickel supported on α-alumina), alumina support plays an intricate role in the reaction mechanism because of the effect of the acid/base groups on the supports.

Recording Froment *et al*, the following assumptions were made in order to develop a model to describe the experimental results:

(1) H_2O reacts with Ni, yielding OS and $H_{2(g)}$

(2) CH_4 is adsorbed onto surface Ni, and reacts with OS or dissociates to form chemisorbed radicals

(3) The concentration of carbon-containing radicals are much lower than the total concentration of the active sites

(4) Adsorbed atomic oxygen oxidizes the carbon-containing radical

(5) Formed hydrogen directly releases to the gas phase and/or is in equilibrium with hydrogen-containing radicals

Thermodynamic analysis suggests that those which form CO and CO_2 directly from CH_4 are not likely.

Callaghan afirmas that the results of several of these investigations suggest that the WGS reaction largely occurs via three mechanisms: 1) the formate mechanism, 2) the redox mechanism and 3) the carbonate mechanism.

1) Formate mechanism

It is said the study of Campbell and Daube explores the WGS reaction in terms of a formate mechanism on copper, given in the next figure, where S represents a surface site.

Formate Reaction Mechanism	
$CO + S \leftrightarrows CO{\cdot}S$	(s_1)
$H_2O + S \leftrightarrows H_2O{\cdot}S$	(s_2)
$H_2O{\cdot}S + S \leftrightarrows OH{\cdot}S + H{\cdot}S$	(s_3)
$CO{\cdot}S + OH{\cdot}S \leftrightarrows HCOO{\cdot}S + S$	(s_5)
$HCOO{\cdot}S \leftrightarrows CO_2 + H{\cdot}S$	(s_{20})
$2H{\cdot}S \leftrightarrows H_2 + 2{\cdot}S$	(s_{18})
$CO + H_2O \leftrightarrows CO_2 + H_2$	*(OR)*

Figure 17: Mechanism proposed based on formate mechanism by Campbell and Daube

Van Herwijnen and De Jong applied their rate equation to data from a catalyst $Cu/ZnO/Cr_2O_3$, suggesting that the oxidation by water is the rate determining step assessing several potential WGS models developed by other researchers.

Research Group	Rate Expression
Campbell, et al. [36]	$r = \frac{kP_{CO}P_{H_2O}}{\left(1 + K_1P_{CO} + K_2P_{H_2O} + K_3P_{CO_2} + K_4P_{H_2}\right)^2}(1-\beta)$
Moe [68]	$r = kP_{CO}P_{H_2O}(1-\beta)$
Shchibrya, et al. [69]	$r = \frac{kP_{H_2O}P_{CO}}{AP_{H_2O} + P_{CO_2}}(1-\beta)$
Kul'kova-Temkin [70]	$r = kP_{CO}\left(\frac{P_{H_2O}}{P_{H_2}}\right)^{\frac{1}{2}}(1-\beta)$
Goodridge-Quazi [71]	$r = kP_{CO}^{a}P_{H_2O}^{b}P_{CO_2}^{e}P_{H_2}^{d}$

where $\beta = \frac{P_{CO_2}P_{H_2}}{KP_{CO}P_{H_2O}}$

Figure 18: Table with several kinetic models from Callaghan's dissertation

For the case of the RWGS reaction, experimental data with only CO_2 and H_2 in the feed were collected by van Herwijinen and De Jong and the rate equation may be written by

$$\bar{r} = \frac{kx_{CO_2}(1 - x_{CO_2})}{1 + Kx_{CO_2}(1 - x_{CO_2}) + Bx_{CO_2}} \tag{38}$$

The experimental data indicate that the maximun rate occurs when x_{CO_2}>> 0,5, therefore, B is a negative constant.

$$\bar{r} = \frac{kP_{CO_2}P_{H_2}}{1 + K_{CO_2.H_2}P_{CO_2}P_{H_2} + K_{H_2}P_{H_2}} \tag{39}$$

After fitting the measured rates and optimization, the rate of the reverse WGS reaction is given in moles/g.s by:

$$\bar{r} = \frac{4.26 \times 10^5 \exp\left(-\frac{23000}{k_BT}\right)P_{CO_2}P_{H_2}}{1 + 40_{CO_2.H_2}P_{CO_2}P_{H_2} + 3.66 \times 10^{-6}\exp\left(-\frac{13100}{k_BT}\right)P_{H_2}} \tag{40}$$

2) Redox mechanism

This mechanism was studied by Temkin [28], wherein the key surface intermediate of interest is adsorbed atomic oxygen.

Two-Step Redox Reaction Mechanism	
$H_2O + S \leftrightarrows O{\cdot}S + H_2$	(s_{27})
$O{\cdot}S + CO \leftrightarrows CO_2 + S$	(s_{28})
$CO + H_2O \leftrightarrows CO_2 + H_2$	(OR)

Figure 19: Mechanism based on redox mechanism proposed by Temkin

Where the experimental data is represented by the following equation, where k has the units $sec^{-1}atm^{-1}$:

$$\bar{r} = \frac{kP_{CO}P_{H_2O}}{\chi P_{H_2O} + P_{CO_2}} \tag{41}$$

$$\log \chi = -\frac{8800}{4.57T} + 2{,}31 \tag{42}$$

$$\log k = -\frac{34000}{4.57T} + 10{,}3 \tag{43}$$

Another mechanism was proposed by Ovesen *et al* on a Cu catalyst, where it was assumed that the steps 3, 4 and 6 were rate-limiting.

Redox Reaction Mechanism	
$H_2O + S \leftrightarrows H_2O{\cdot}S$	(s_2)
$H_2O{\cdot}S + S \leftrightarrows OH{\cdot}S + H{\cdot}S$	(s_3)
$2OH{\cdot}S \leftrightarrows H_2O{\cdot}S + O{\cdot}S$	(s_{10})
$OH{\cdot}S + S \leftrightarrows O{\cdot}S + H{\cdot}S$	(s_6)
$2H{\cdot}S \leftrightarrows H_2 + 2S$	(s_{18})
$CO + S \leftrightarrows CO{\cdot}S$	(s_1)
$CO{\cdot}S + O{\cdot}S \leftrightarrows CO_2{\cdot}S + S$	(s_4)
$CO_2{\cdot}S \leftrightarrows CO_2 + S$	(s_{15})
$CO + H_2O \leftrightarrows CO_2 + H_2$	(OR)

Figure 20: Different redox mechanism proposed by Ovensen *et al*

3) Carbonate mechanism

This mechanism was proposed by Lund et al and is presented in the next table:

Carbonate Reaction Mechanism*	
$CO + 2O{\cdot}S \leftrightarrows CO_3{\cdot}S_2$	(s_{23})
$CO_3{\cdot}S_2 \leftrightarrows CO_3{\cdot}S + S$	(s_{24})
$CO_3{\cdot}S \leftrightarrows CO_2 + S$	(s_{25})
$H_2O + S \leftrightarrows H_2O{\cdot}S$	(s_2)
$H_2O{\cdot}S + O{\cdot}S \leftrightarrows 2OH{\cdot}S$	(s_{10})
$2OH{\cdot}S \leftrightarrows 2O{\cdot}S + H_2$	(s_{26})
$H_2O{\cdot}S + S \leftrightarrows OH{\cdot}S + H{\cdot}S$	(s_3)
$2H{\cdot}S \leftrightarrows H_2 + 2S$	(s_{18})
$CO + H_2O \leftrightarrows CO_2 + H_2$	(OR)

Figure 21: Carbonate Reaction Mechanism proposed by Lund *et al*

In the next figure it is presented all the possible reactions that have been investigated by many researchers and resumed in Callaghan's dissertation.

s_1	$CO + S \leftrightarrows CO{\cdot}S$	s_{21}	$CO{\cdot}S + O{\cdot}S \leftrightarrows CO_2 + 2S$	s_{41}	$H_2 + M \rightarrow 2H + M$
s_2	$H_2O + S \leftrightarrows H_2O{\cdot}S$	s_{22}	$H_2 + O{\cdot}S \leftrightarrows H_2O{\cdot}S$	s_{42}	$H + CO_2 \leftrightarrows OH + CO$
s_3	$H_2O{\cdot}S + S \leftrightarrows OH{\cdot}S + H{\cdot}S$	s_{23}	$CO + 2O{\cdot}S \leftrightarrows CO_3{\cdot}S_2$	s_{43}	$OH + H_2 \leftrightarrows H + H_2O$
s_4	$CO{\cdot}S + O{\cdot}S \leftrightarrows CO_2{\cdot}S + S$	s_{24}	$CO_3{\cdot}S_2 \leftrightarrows CO_3{\cdot}S + S$	s_{44}	$2H + M \rightarrow H_2 + M$
s_5	$CO{\cdot}S + OH{\cdot}S \leftrightarrows HCOO{\cdot}S + S$	s_{25}	$CO_3{\cdot}S \leftrightarrows CO_2 + S$	s_{45}	$O_2 + 2S \leftrightarrows 2O{\cdot}S$
s_6	$OH{\cdot}S + S \leftrightarrows O{\cdot}S + H{\cdot}S$	s_{26}	$2OH{\cdot}S \leftrightarrows 2O{\cdot}S + H_2$	s_{46}	$OH + S \leftrightarrows OH{\cdot}S$
s_7	$CO{\cdot}S + OH{\cdot}S \leftrightarrows CO_2{\cdot}S + H{\cdot}S$	s_{27}	$H_2O + S \leftrightarrows O{\cdot}S + H_2$	s_{47}	$H + S \leftrightarrows H{\cdot}S$
s_8	$HCOO{\cdot}S + S \leftrightarrows CO_2{\cdot}S + H{\cdot}S$	s_{28}	$O{\cdot}S + CO \leftrightarrows CO_2 + S$	s_{48}	$O + S \leftrightarrows O{\cdot}S$
s_9	$HCOO{\cdot}S + O{\cdot}S \leftrightarrows CO_2{\cdot}S + OH{\cdot}S$	s_{29}	$CO_2 + O{\cdot}S \leftrightarrows CO_3{\cdot}S$	s_{49}	$COOH + S \leftrightarrows COOH{\cdot}S$
s_{10}	$H_2O{\cdot}S + O{\cdot}S \leftrightarrows 2OH{\cdot}S$	s_{30}	$HCOO{\cdot}S + H{\cdot}S \leftrightarrows CO{\cdot}S + H_2O{\cdot}S$	s_{50}	$COOH{\cdot}S + S \leftrightarrows CO{\cdot}S + OH{\cdot}S$
s_{11}	$H_2O{\cdot}S + H{\cdot}S \leftrightarrows OH{\cdot}S + H_2{\cdot}S$	s_{31}	$CO{\cdot}S + H_2O \leftrightarrows HCOOH{\cdot}S$	s_{51}	$COOH{\cdot}S + S \leftrightarrows CO_2{\cdot}S + H{\cdot}S$
s_{12}	$OH{\cdot}S + H{\cdot}S \leftrightarrows O{\cdot}S + H_2{\cdot}S$	s_{32}	$HCOOH{\cdot}S \leftrightarrows HCOOH + S$	s_{52}	$COOH{\cdot}S + H{\cdot}S \leftrightarrows CO{\cdot}S + H_2O{\cdot}S$
s_{13}	$HCOO{\cdot}S + OH{\cdot}S \leftrightarrows CO_2{\cdot}S + H_2O{\cdot}S$	s_{33}	$2OH{\cdot}S \leftrightarrows H_2O + O{\cdot}S$	s_{53}	$COOH{\cdot}S + O{\cdot}S \leftrightarrows CO_2{\cdot}S + OH{\cdot}S$
s_{14}	$HCOO{\cdot}S + H{\cdot}S \leftrightarrows CO_2{\cdot}S + H_2{\cdot}S$	s_{34}	$HCOOH{\cdot}S \leftrightarrows H_2{\cdot}S + CO_2$	s_{54}	$COOH{\cdot}S + OH{\cdot}S \leftrightarrows CO_2{\cdot}S + H_2O{\cdot}S$
s_{15}	$CO_2{\cdot}S \leftrightarrows CO_2 + S$	s_{35}	$HCOOH \leftrightarrows H_2 + CO_2$	s_{55}	$HCOO + 2S \leftrightarrows HCOO{\cdot}S_2$
s_{16}	$H{\cdot}S + H{\cdot}S \leftrightarrows H_2{\cdot}S + S$	s_{36}	$HCOOH \leftrightarrows H_2O + CO$	s_{56}	$HCOO{\cdot}S_2 \leftrightarrows CO_2{\cdot}S + H{\cdot}S$
s_{17}	$H_2{\cdot}S \leftrightarrows H_2 + S$	s_{37}	$2HCOOH \leftrightarrows HCOH + H_2O + CO_2$	s_{57}	$HCOO{\cdot}S_2 + O{\cdot}S \leftrightarrows CO_2{\cdot}S + OH{\cdot}S + S$
s_{18}	$2H{\cdot}S \leftrightarrows H_2 + 2S$	s_{38}	$HCOO{\cdot}S + H{\cdot}S \leftrightarrows H_2COO{\cdot}S + S$	s_{58}	$HCOO{\cdot}S_2 + OH{\cdot}S \leftrightarrows CO_2{\cdot}S + H_2O{\cdot}S + S$
s_{19}	$H_2O{\cdot}S + S \leftrightarrows O{\cdot}S + H_2{\cdot}S$	s_{39}	$H_2COO{\cdot}S + 4H{\cdot}S \leftrightarrows CH_3OH + H_2O + 5S$	s_{59}	$H_2 + O{\cdot}S + S \leftrightarrows H{\cdot}S + OH{\cdot}S$
s_{20}	$HCOO{\cdot}S \leftrightarrows CO_2 + H{\cdot}S$	s_{40}	$H_2O + 2S \leftrightarrows OH{\cdot}S + H{\cdot}S$	s_{60}	$HCOOH{\cdot}S \leftrightarrows HCOO{\cdot}S + H{\cdot}S$

All possible reactions for WGS investigated by many researchers

At the end of this research an 18-step mechanism is comprised of the previous elementary reaction steps and the overall reaction (OR). So the proposed mechanism for WGS reaction proposed by Callaghan is:

s_1: $$6CO + 6S \leftrightarrows 6CO.S$$

s_2: $$6H_2O + 6S \leftrightarrows 6H_2O.S$$

s_3: $$5H_2O.S + 5S \leftrightarrows 5OH.S + 5H.S$$

s_4: $$CO.S + O.S \leftrightarrows CO_2.S + S$$

s_5: $$4CO.S + 4OH.S \leftrightarrows 4HCOO.S + 4S$$

s_6: $$2OH.S + 2S \leftrightarrows 2O.S + 2H.S$$

s_7: $$CO.S + O.S \leftrightarrows CO_2.S + S$$

s_8: $$HCOO.S + S \leftrightarrows CO_2.S + H.S$$

s_9: $$HCOO.S + O.S \leftrightarrows CO_2.S + OH.S$$

s_{10}: $$H_2O.S + O.S \leftrightarrows 2OH.S$$

s_{11}: $$H_2O.S + H.S \leftrightarrows OH.S + H_2.S$$

s_{12}: $$2OH.S + 2H.S \leftrightarrows 2O.S + 2H_2.S$$

s_{13}: $$HCOO.S + OH.S \leftrightarrows CO_2.S + H_2O.S$$

s_{14}: $$HCOO.S + H.S \leftrightarrows CO_2.S + H_2.S$$

s_{15}: $$6CO_2.S \leftrightarrows 6CO_2 + 6S$$

s_{16}: $$H.S + H.S \leftrightarrows H_2.S + S$$

s_{17}: $$5H_2.S \leftrightarrows 5H_2 + 5S$$

s_{18}: $$2H.S \leftrightarrows H_2 + 2S$$

OR $$6CO + 6H_2O \leftrightarrows 6CO_2 + 6H_2$$

Figure 23: Mechanism proposed for WGS by Callaghan composed by 18 steps

Byron Smith *et al*. [29] made a review of the water-gas shift reaction kinetics, where the dissertation of Callaghan is refered. In this article is presented the activation energies of the mechanisms proposed in Figure 23.

Elementary Step	Ko Adsorption/desorption(1/atm s) Surface reaction (1/s)	Ea (kcal/mol)
CO + S ↔ CO.S	1.5 x 10^6	0
H_2O + S ↔ H_2O.S	1.0 x 10^6	0
H_2O.S + S ↔ OH.S +H.S	1.0 x 10^{13}	25.4
CO.S + O.S ↔ CO_2.S + S	1.0 x 10^{13}	10.7
CO.S + OH.S ↔ HCOO.S + S	1.0 x 10^{13}	0
OH.S + S ↔ O.S + H.S	1.0 x 10^{13}	15.5
CO.S + OH.S ↔ CO_2.S + H.S	1.0 x 10^{13}	0
HCOO.S + S ↔ CO_2.S + H.S	1.0 x 10^{13}	1.4
HCOO.S + O.S ↔ CO_2.S + OH.S	1.0 x 10^{13}	4
H_2O.S + O.S↔ 2OH.S	1.0 x 10^{13}	29
H_2O.S + H.S ↔ OH.S + H_2.S	1.0 x 10^{13}	26.3
OH.S + H.S ↔ O.S + H_2.S	1.0 x 10^{13}	1.3
HCOO.S + OH.S ↔ CO_2.S + H_2O.S	1.0 x 10^{13}	0.9
HCOO.S + H.S ↔ CO_2.S + H_2.S	1.0 x 10^{13}	14.6
CO_2.S ↔ CO_2 + S	4.0 x 10^{12}	5.3
H.S + H.S ↔ H_2.S + S	1.0 x 10^{13}	15.3
H_2.S ↔ H_2 + S	6.0 x 10^{12}	5.5
H.S + H.S ↔ H_2 + 2S	6.0 x 10^{12}	15.3

(S is the vacant site and X.S is the adsorbed X species)

Figure 24: Activation energies of the mechanism proposed by Callaghan

The authors affirm there are a number of kinetic expressions published about the kinetics of WGS but, in general, the associative mechanism is represented by the Langmuir Hinshlewood model and the Eley – Rideal type model.

The most commonly used models are listed out in the next figure:

Model	*Kinetic Expression*
High Temperature Shift *[Ref. Twigg (1989)]*	
Kodama et al.	$r = \frac{k\left[[CO][H_2O] - \frac{[CO_2][H_2]}{K}\right]}{(1 + K_{CO}[CO] + K_{H_2O}[H_2O] + K_{CO_2}[CO_2] + K_{H_2}[H_2])}$
Hulburt - Vasan	$r = \frac{k[H_2O]}{1 + K[H_2O]/[H_2]}$
Langmuir Hinshelwood Model	$r = \frac{kK_{CO}K_{H_2O}\left[[CO][H_2O] - \frac{[CO_2][H_2]}{K}\right]}{(1 + K_{CO}[CO] + K_{H_2O}[H_2O] + K_{CO_2}[CO_2] + K_{H_2}[H_2])^2}$
Oxidation Reduction Model	$r = \frac{k_1k_2\{[CO][H_2O] - [CO_2][H_2]/K\}}{k_1[CO] + k_2[H_2O] + k_{-1}[CO_2] + k_{-2}[H_2]}$
Bohlboro et al.	$r = kP^a_{CO}P^b_{H2O}P^c_{CO2}P^{\ d}_{H2}$
Low Temperature Shift *[Ref. Van Herwijnen and De Jong (1980)]*	
Campbell et al.	$r = k\frac{P_{CO}P_{H_2O}(1-\beta)}{(1 + K_{CO}P_{CO} + K_{H_2O}P_{H_2O} + K_{CO_2}P_{CO_2} + K_{H_2}P_{H_2})^2}$
Shchibrya et al.	$r = \frac{kP_{H_2O}P_{CO}(1-\beta)}{AP_{H_2O} + P_{CO_2}}$
Moe	$r = kP_{CO}P_{H2O}(1-\beta)$
Kulkova and Temkin	$r = kP_{CO}\left(\frac{P_{H_2O}}{P_{H_2}}\right)^{0.5}(1-\beta)$
Goodgidge and Quazi	$r = kP^a_{CO}P^b_{H2O}P^c_{CO2}P^{\ d}_{H2}$

Figure 25: A several kinetic models proposed by many researchers for WGS reaction resumed by Byron Smith *et al*

Ang *et al*. [30] performed a study of the reaction kinetics on Ni/5K/CeO_2 trough the effect of partial pressures of reactants and products (CO, H_2O, CO_2 and H_2) on the kinetic rate of the WGS reaction at 400ºC.

After getting the reaction orders with respect to the components, a power rate law was proposed:

$$r = Aexp\left(\frac{E_a}{RT}\right)[P_{CO}]^{0.19}\left[P_{H_2O}\right]^{0.58}\left[P_{CO_2}\right]^{-0.15}\left[P_{H_2}\right]^{-0.51}(1-\beta) \qquad (44)$$

where

$\left(\beta = \frac{[CO_2][H_2]}{[CO][H_2O]K_{eq}}\right)$ and $K_{eq} = exp\left(\frac{4577.8}{T} - 4.33\right)$

The mechanism that fitted better the kinetic law is based on a redox reaction:

$$CO + s_1 \overset{K_1}{\leftrightarrow} CO \cdot s_1 \qquad (10.i)$$

$$H_2O + s_2 \overset{K_2}{\leftrightarrow} H_2O \cdot s_2 \qquad (10.ii)$$

$$H_2O \cdot s_2 \overset{K_3}{\leftrightarrow} H \cdot s_1 + OH \cdot s_2 \qquad (10.iii)$$

$$s_1 + OH \cdot s_2 \overset{K_4}{\leftrightarrow} H \cdot s_1 + O \cdot s_2 \qquad (10.iv)$$

$$CO \cdot s_1 + O \cdot s_2 \overset{K_5}{\leftrightarrow} CO_2 \cdot s_1 + s_2 (RDS) \qquad (10.v)$$

$$CO_2 \cdot s_1 \overset{K_6}{\leftrightarrow} CO_2 + s_1 \qquad (10.vi)$$

$$H \cdot s_1 + H \cdot s_1 \overset{K_7}{\leftrightarrow} H_2 + 2s_1. \qquad (10.vii)$$

Figure 26: Redox reaction mechanism proposed by Ang *et al*

Then, Mohsenzadeh *et al* [31], studied nine elementary steps, where occurs water dissociation, direct path to CO oxidation to CO_2, the carboxyl path and the formate path, and finally formation of hydrogen.

$$H_2O \rightleftharpoons OH + H \quad \text{(s1)}$$
$$OH \rightleftharpoons O + H \quad \text{(s2)}$$
$$CO + O \rightleftharpoons CO_2 \quad \text{(s3)}$$
$$CO + OH \rightleftharpoons COOH \quad \text{(s4)}$$
$$COOH \rightleftharpoons CO_2 + H \quad \text{(s5)}$$
$$CO + H \rightleftharpoons CHO \quad \text{(s6)}$$
$$CHO + O \rightleftharpoons HCOO \quad \text{(s7)}$$
$$HCOO \rightleftharpoons CO_2 + H \quad \text{(s8)}$$
$$H + H \rightleftharpoons H_2 \quad \text{(s9)}$$

The results indicate that the Ni(110) surface has the lowest barrier for water dissociation (steps 1 and 2), formyl formation (step 6), formate dissociation (step 8) and H_2 formation (step 9), and that the lowest barrier for CO oxidation to CO_2 (step 3) is on the Ni(100) surface. Also, H_2O, OH, HCOO, CO_2 and H_2 bind strongest to the Ni(110) surface while COOH, CHO, CO, O and H bind strongest to the Ni(100) surface.

From [22] it can be extracted the mechanism relative to the water-gas shift reaction:

Redox mechanism	Associative mechanism
CO + * ↔ CO*	CO + * ↔ CO*
H2O + * ↔ H2O*	H2O + * ↔ H2O*
H2O* + * ↔ OH* + H*	H2O* + * ↔ OH* + H*
OH* + * ↔ O* + H*	**CO* + OH* ↔ COOH* + ***
CO* + O* ↔ CO2* + *	**COOH* + * ↔ H* + CO2***
CO2* ↔ CO2 + *	CO2* ↔ CO2 + *
2H* ↔ H2 + 2*	2H* ↔ H2 + 2*

Figure 27: Two proposed mechanisms to WGS where * is a vacant site and X* is the absorbed specie

The kinetics of the water gas shift reaction has been also studied by Froment *et al* [18], and they propose the following kinetic model with the respective thermodynamic values.

$$r = k\frac{P_{CO}P_{H_2O}P_{H_2}^{-1}\left(1 - \frac{P_{CO_2}P_{H_2}}{KP_{CO}P_{H_2O}}\right)}{(1 + K_{CO}P_{CO} + K_{H_2}P_{H_2} + K_{CH_4}P_{CH_4} + K_{H_2O}\,P_{H_2O}/P_{H_2})} \quad (45)$$

With k in $kg.kg_{cat}^{-1}.h^{-1}.bar^{-1}$:

$$k = 1.955 \times 10^6 exp\left(\frac{67.13 \times 10^3}{RT}\right) \quad (46)$$

Several references will be also indicated about the values of the heat adsorption of hydrogen and carbon dioxide in nickel catalysts, in order to confirm the results obtained in this report.

The first one, D. Brennan and F.H. Hayes [32] obtained a heat adsorption of hydrogen, near the saturation, of 21kJ/mol. They affirm this value is in accordance with other references as Beeck, Wahba and Kemball, Rideal and Sweet, and Klemperer and Stone, where it was verified heat adsorptions of 125 to 167kJ/mol initially, reaching values of 75kJ/mol near the saturation.

In the report of C.H. Bartholomew [33], it is showed several studies of adsorption of hydrogen in nickel based catalysts with a range of 61 to 130kJ/mol; however these values decrease to around 42kJ/mol in the study of hydrogen adsorption on Nickel (100) single-crystal face of Tomasz Panczyk et al [34].

In the last report analyzed to adsorption of hydrogen, James T. Richardson et al [35] made a review on previous studies citing again Sweet and Rideal with values of 104 to 134kJ/mol and Christmann et al with 59 to 92kJ/mol.

To the heat adsorption of CO_2 on nickel, Sheng-Guang Wang et al [36] realized experiments in Nickel (100) and they obtained values of 34 to 71kJ/mol, considering non dissociative adsorption which is in accordance with the doctoral thesis of Michele Rizzi [37], whose also consider non dissociative adsorption, that report values between 28 and 64 kJ/mol.

H.J Freund [38] and Takao Kwan et al [39] considered CO_2 dissociation into adsorbed CO and O on a Ni surface, but their values differ from each other: 34 and 92kJ/mol, respectively.

A. L. Cabrera et al [40] studied the adsorption of carbon monoxide on nickel and cobalt foils and they obtained a heat adsorption for CO of 17kJ/mol and 33-63kJ/mol, in the molecular and dissociate state, respectively.

In the other side, M. McD. Baker *et al* [41] realized experiences at θ=0.74 and at saturation and they obtained the values of 146.3 and 18.8 kJ/mol, respectively. In this article, it is mentioned Beeck [42] obtained the same value of 146.3 kJ/mol for θ=0.85.

2. Catalyst characterization

In this work it was used an industrial powder catalyst named “Octolyst”, provided by CEA sited in Grenoble. It was known the catalyst was composed by Ni aluminate which had undergone a pretreatment under H_2 at low temperature which extracts a fraction of Ni out of the structure leading to a system Ni / $NiAl_2O_4$ / Al_2O_3. It was necessary to characterize it in order to know its structure and the optimal conditions of work. Several techniques were implemented as temperature programmed reduction with hydrogen (TPR-H_2), chemisorptions with H_2, N_2 physisorption and x-ray diffraction (XRD).

Initially the catalyst was divided in several fractions depending on their particle size comprised in a range of 500-315, 315-200, 200-125, 125-100, 100-50 e 50-25 μm. It was determined that the average diameter of the initial sample was around 290 μm. The apparent density was determined for the fraction with highest and smallest diameter with the following values obtained of 0.78 and 0.50, respectively.

2.1 Temperature Programmed Reduction

Several experiments of temperature programmed reduction with hydrogen (TPR-H_2) were realized to determine the behaviour of the catalyst during reduction.

For that, a well known portion of catalyst was exposed to a flow of a reducing gas mixture (H_2-Ar) with 10% (vol) of hydrogen while the temperature was increased linearly. The rate of reduction was continuously followed by measuring the composition of the gas at the outlet of the reactor.

The nickel reducible is present in a structure of nickel oxide and nickel alumina. The reduction of nickel present in nickel oxide can be described by

$$NiO + H_2 \rightarrow Ni^0 + H_2O \qquad (47)$$

In the first experiment, the temperature was increased until 900ºC with a ramp of 15.0ºC/min. The results showed in Figure 28 suggest a reduction of all the nickel in nickel oxide around 340ºC. The second peak suggests a reduction of the nickel present in $NiAl_2O_3$ around 560ºC.

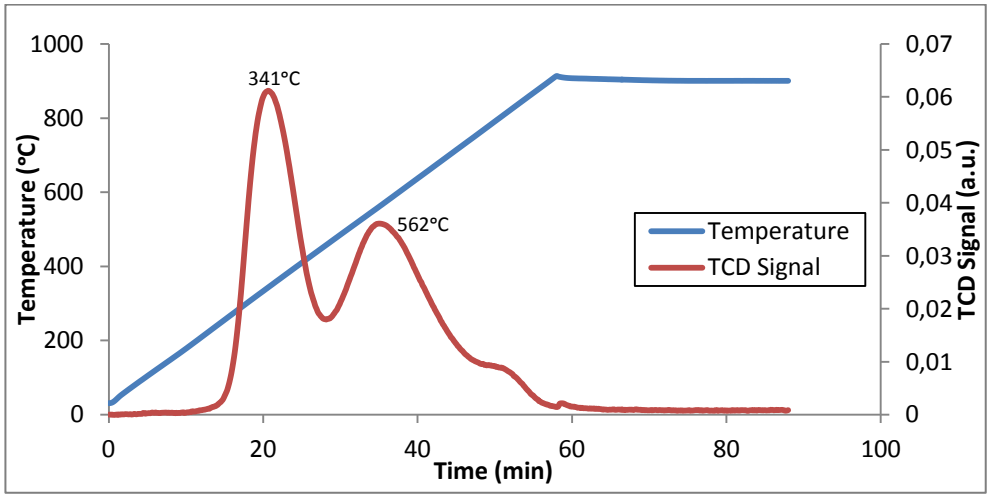

Figure 28: Profile of temperature and TCD Signal during the reduction till 900ºC

Knowing the quantity of hydrogen consumed during analyse, it is possible to know the quantity of nickel reducible in the sample, taking into account the stoichiometry of the reaction 1:1. The value obtained is around 14% (g/g_{cat}). However, as it is observed in the Figure 28, only 47.5% of nickel is present in nickel oxide, calculated by the ratio of the area of the first peak with the total area of the two peaks.

In order to confirm this conclusion, a second experiment was realized. In this case the reduction was made in two parts: first increasing the temperature 5ºC/min until 400ºC and maintain during one hour; the second, after cool down the reactor under a flow of hydrogen, increasing the temperature at 15ºC/min until 900ºC.

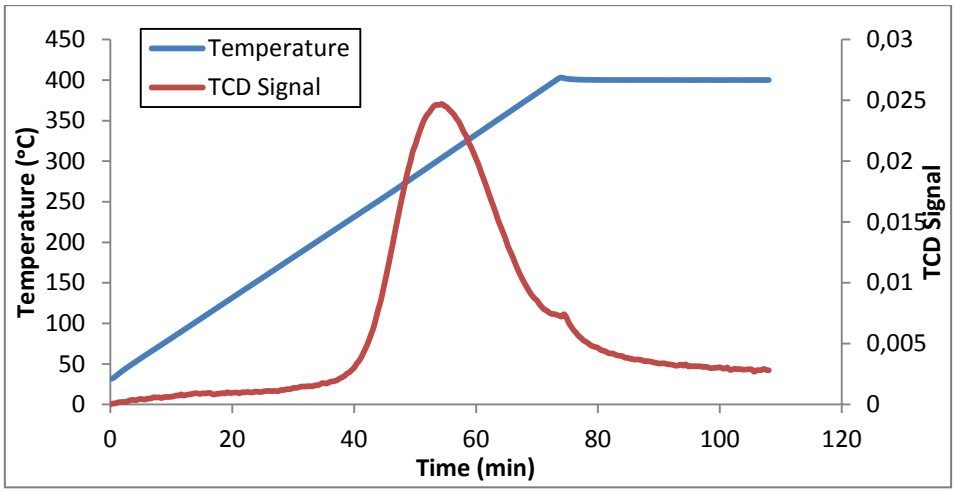

Figure 29: Profile of temperature and TCD Signal during the experiment for the first part of the reduction at 400ºC

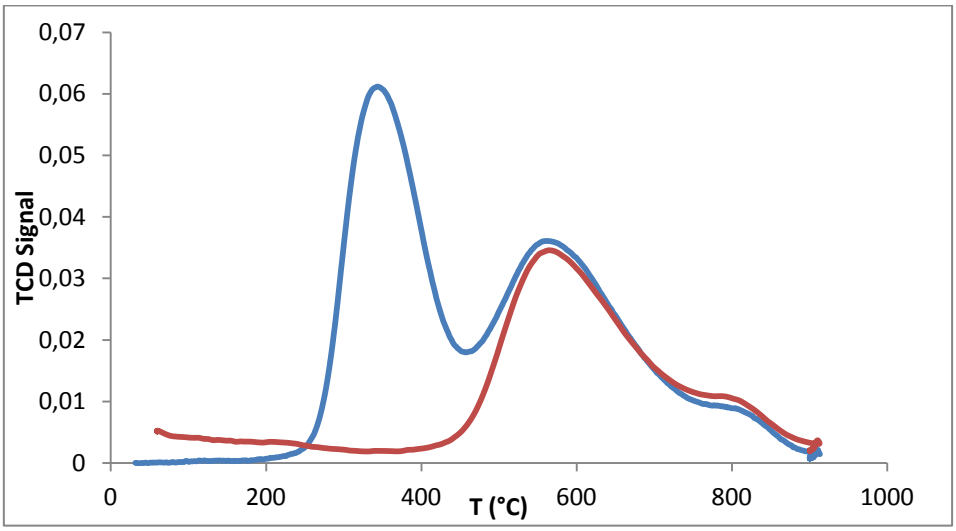

Figure 30: Comparison of the profile TCD Signal in function of temperature of continuously reduction till 900ºC ( ) and reduction till 900ºC after pre-reduction at 400ºC ( )

As it is observed in Figure 29 and Figure 30, all the nickel present in NiO is reduced at 400ºC, as no peak appears during the second part of the reduction at 900ºC, indicating there was no nickel present in the form of NiO to be reduced. Taking into account the total quantity of hydrogen consumed during the first stage of reduction (Figure 29), it is obtained 7.8% of Ni in

the sample, about half of the previous experiment. This result is in accordance with the previous observations because it was determined that around 50% of the nickel reducible is present in nickel oxide. The quantity of hydrogen consumed during all the reduction also showed to be similar to the first experiment. Finally, a third reduction was realized until 500ºC during one hour.

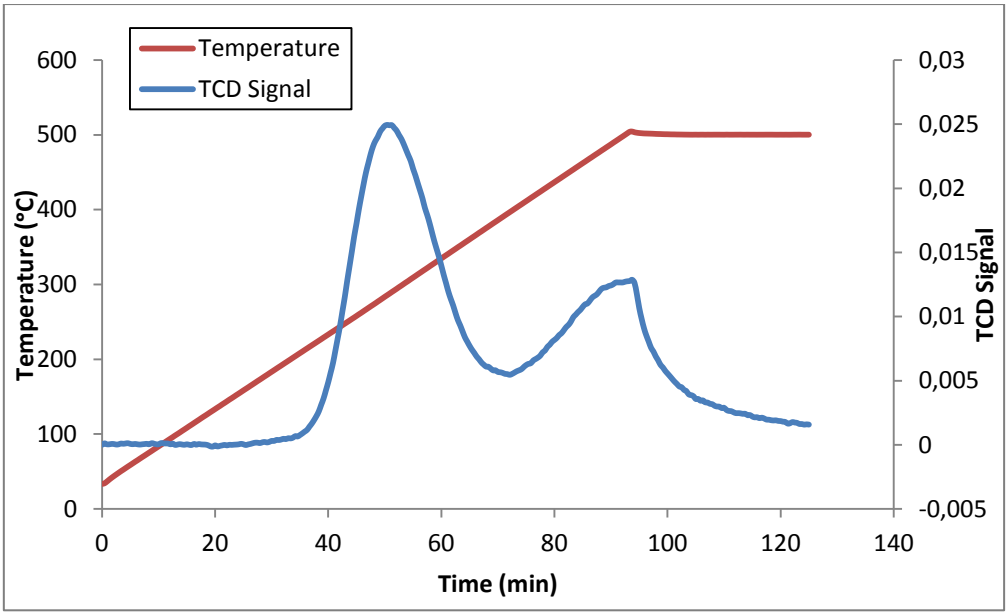

Figure 31: Profile of temperature and TCD Signal during the reduction till 500ºC

Once again it is observed that all the nickel present in nickel oxide is reduced at 400ºC. After this temperature occurs the reduction of around 47% of the Ni present in $NiAl_2O_3$, and in this case the reducible nickel is around 11.0%.

As it is possible to observe a stable reduction at 500ºC during one hour and it is not expected a reaction temperature higher than this value, it was decided a temperature of reduction before any catalytic test of 500ºC during one hour and with an increase of the temperature of 5ºC/min.

2.2 Chemisorption

One of the most important characteristics of the catalyst is its metal dispersion that it is directly connected to the number of active sites and, consequently, the activity of the catalyst.

This dispersion is evaluated by measuring chemisorption of H_2 or CO through the formation of an irreversibly adsorbed monolayer. For that, it was used the pulse technique where the adsorbate gas is injected as successive small pulses of known volume into the flow of the inert gas.

Two experiments were made: in the first analyze, the sample of catalyst was reduced at 400ºC during one hour with a gas mixture of 10% H_2-Ar, being cooled down under Argon only until 60ºC where a sequence of 20 pulses of 500µL each (10%H_2-Ar) were injected. Then, the sample was heated until 900ºC under a flow of Argon; in the second one, the first stage of reduction occurred at 500ºC.

Plotting the quantity of hydrogen adsorbed for each pulse, as shown in Figure 32, it is possible to observe that after the seventh pulse (for 400ºC) and ninth pulse (for 500ºC), the quantity does not change which indicates that the chemisorption of the gas occurred in all nickel reduced.

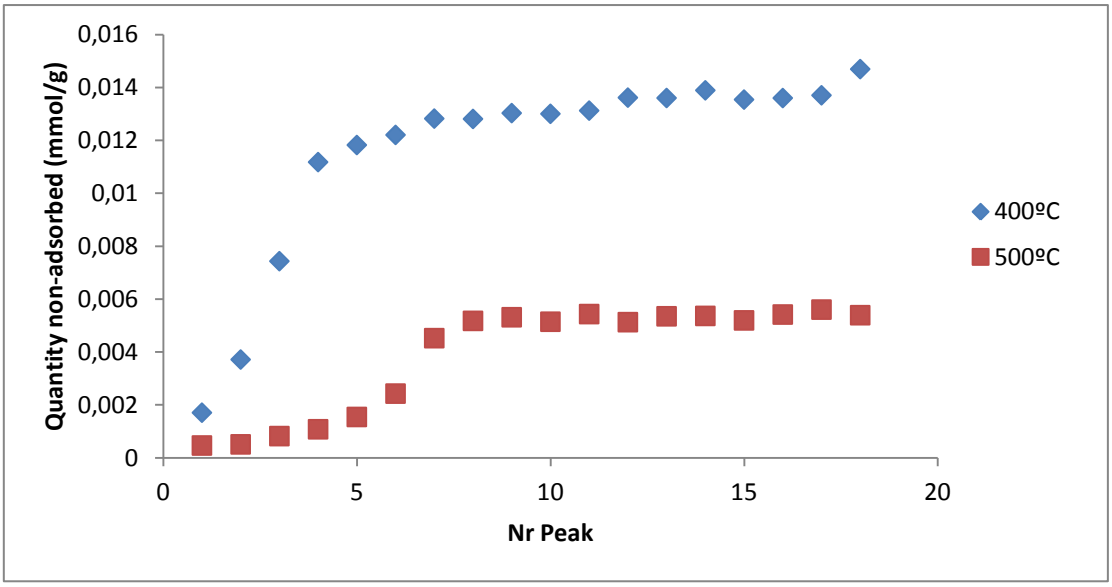

Figure 32: Quantity of hydrogen non-adsorbed in each pulse in the two experiments of chemisorption

Knowing the quantity of hydrogen injected in each time (0.020362 mmol/g), through the plot is taken the quantity of hydrogen consumed in each pulse. The necessary amount to saturate the surface, i.e., the amount of Ni present in the surface, taking into account that only one atom of hydrogen is adsorbed to each atom of nickel, will be two times the sum of the total quantity of hydrogen consumed in all the pulses.

$$H_2\ consumed\ in\ pulse\ i = H_{2,loop} \times \left(1 - \frac{peak\ i}{peak\ of\ saturation}\right) \quad (48)$$

The dispersion can then be calculated as the ratio of the quantity of nickel in the surface with the quantity of nickel reduced present in the catalyst (determined by the reduction).

$$\%Dispersion = \frac{Amount\ Ni\ in\ the\ surface}{Amount\ of\ Ni\ reduced} \quad (49)$$

In this case the catalyst has a dispersion of around 8% and 5% for samples reduced at 400ºC and 500ºC, respectively.

Another calculation realized was the particle size of nickel, d, through the surface area and the volume of an atom of nickel.

$$S_{Ni^0} = Ni_{surface} \times N_A \times \sigma_{Ni} \quad (50)$$

$$V_{Ni^0} = \frac{m_{Ni^0}}{\rho_{Ni^0}} \quad (51)$$

As it is considered a particle as a cube, the volume of the particle is d^3 and the surface area is $5 \times d^2$, so then it is possible to calculate the particle size by

$$d = 5 \times \frac{V_{Ni^0}}{S_{Ni^0}} \quad (52)$$

It was obtained the value of 10.6 nm and 16.7 nm for the samples reduced at 400ºC and 500ºC, respectively.

Remembering the empirical equation $d \times dispersion \approx 0.8$, the results obtained are valid.

2.3 N_2 physisorption

The Brunauer-Emmet-Teller (BET) theory consists on adsorption of gas molecules to determine the surface area of the sample of catalyst and its pore diameter.

In this case, the isotherms were traced by following the quantity of nitrogen adsorbed with the increase of the relative pressure as the reverse operation (desorption of the gas when the relative pressure decreases).

The isotherms can be linearized by

$$\frac{(P/P^0)}{[V_m.(1-P/P^0)]} = \frac{1}{n_m.C} + \left[\frac{(C-1)}{n_m.C}\right].\left(\frac{P}{P^0}\right) \quad (53)$$

Where V_m is the quantity of nitrogen adsorbed, n_m is the monolayer capacity and C an empirical constant.

The surface area can be calculated by the capacity of the monolayer obtained from the slope and interception of the previous equation, by the Avogadro Number, N, and by the molecular cross-sectional area, σ_N, (0,162 nm^2 for N_2) [43].

$$S_{BET} = n_m.N.\sigma_N \quad (54)$$

Assuming that near the relative pressure close to 1, the pores are fulfilled with liquid nitrogen, it is possible to determine their volume, V_{pore}, with the volume of liquid nitrogen at 77K (34.65 cm^3/mol). The pore diameter, d_{pore}, can then be calculated through

$$d_{pore} = \frac{4 \times V_{pore}}{a_{BET}} \quad (55)$$

The measurement of the BET surface was realized in the fraction with biggest and smallest particle size and the in a sample reduced with the reduction treatment chosen. The isotherms obtained are represented in the next figure.

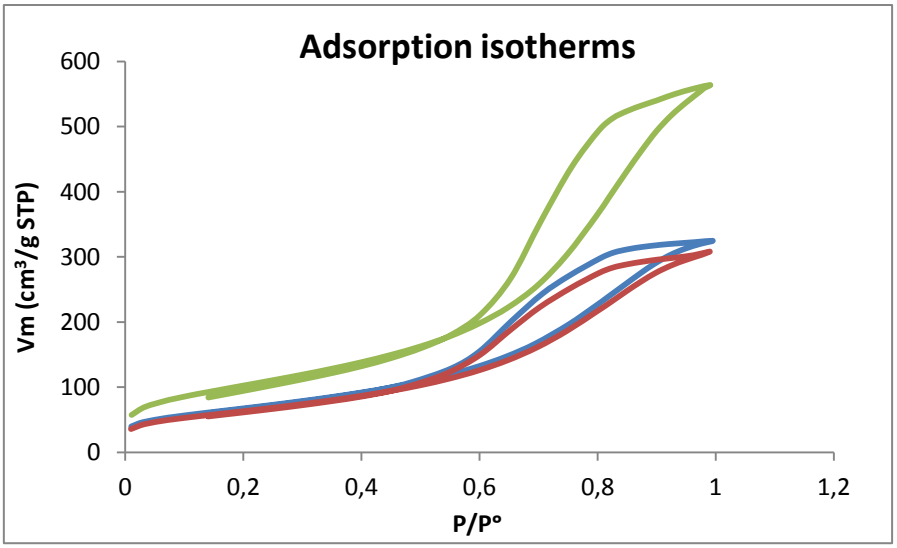

Figure 33: Isotherms obtained for the fraction 500 – 315 µm (—), 50 – 25 µm (—) and to the fraction 200 – 125 µm after the reduction treatment (—)

As it is possible to observe a hysteresis loop appears near the relative pressure of 0.554. This is a signature for mesoporous materials since molecules get adsorbed layer by layer (fill higher energy sites near pore wall then low energy sites away from wall). When molecules accumulated on two opposing walls get close enough to each other they collapse into a thermodynamically lower energy state. This process is called capillary condensation. After reducing pressure during desorption, it is needed a higher gradient of chemical potential (or equivalently pressure drop) to pull the adsorbed molecules out of their sites. Taking the values of N_2 adsorbed in the linear zone of relative pressure (before the hysteresis – between 0.05 and 0.4) and applying the equation 54, a surface areas of 246 and 231 m^2/g were obtained to the fraction of 500-315 and 50-25 µm, respectively, and a average pore diameter of 8.0 nm and pore volume of 0.50 cm^3/g for both. As expected the values obtained are similar for both samples, since these are characteristics of the internal structure and it is not influenced by the particle size.

It is also important to observe the influence of the reduction treatment in the structure of the catalyst. For that, a sample was reduced until 500ºC during one hour at 5ºC/min, and cooled down under hydrogen, to be analyzed in N_2 physisorption.

In this case, the structural properties were modified: the surface area was increased to 370 m^2/g, the average pore diameter to 9 nm and the pore volume for 0.90 cm^3/g. This is due to the removal of nickel from the nickel alumina structure leading to the formation of γ-Al_2O_3 that occurs during the reduction between 400 and 500ºC.

2.4 X-Ray Diffraction

X-Ray Diffraction is a non-destructive technique widely used to reveal detailed information about the chemical composition and crystallographic structure of a solid material.

A crystal lattice is a regular three-dimensional distribution (cubic, rhombic, etc.) of atoms arranged in space to form a series of parallel planes separated from another by a distance, d, which varies according to the nature of the material. In any crystal, these planes exist in a number of different orientations, each with its own specific d-spacing.

When a monochromatic X-ray beam with wavelength λ is projected onto a crystalline material at an angle θ, diffraction occurs only when distance travelled by the rays reflected form successive planes differs by a complete number n of wavelengths (Bragg's Law).

$$n\lambda = 2d(hkl)\ sin\theta \tag{56}$$

By varying the angle θ, the Bragg's Law (equation 56) conditions are satisfied by different d-spacings in polycrystalline materials. Plotting the angular positions and intensities of the resultant diffracted peaks of radiation produces a pattern, which is characteristic of the sample. Where a mixture of different phases is present, the resultant diffractogram is formed by addition of the individual patterns.

The equipment used was Bruker AXS D8 Advance. The analyses were performed with a source of x-rays of cooper (λ=1,5418Å) and a detector LynxEye (filter of Nickel that allows the passage of the kα of cooper). The angle 2θ was varied between 15 and 75º, with a step of 0.012º and with 0.05 sec per step. The diffractograms were processed with the software EVA by Brunker and compared with data base ICDD. Then, the crystallite sizes, s, were calculated using the equation Scherrer, that correlates it with the full width at half maximum-intensity (FWHM), B, a constant K, the wavelength of the x-radiation employed, λ, and the angular position of the peak maximum, θ.

$$s = \frac{K\lambda}{Bcos\theta} \tag{57}$$

The constant K depends on the definitions of crystallite size and broadening, the shape of the crystallites and the reflection being examined. Ideally, the constant should be adjusted according with the characteristics of the crystallites, but there is no practical use as far as catalyst are concerned and the value of K should be taken as 0.9. [43]

In order to evaluate the efficiency of the reduction, four samples with the range size of 500-315 μm were used: no reduction, reduction at 400ºC during one hour, reduction at 500ºC during one hour and reduction at 500ºc during two hours, whose results are presented next.

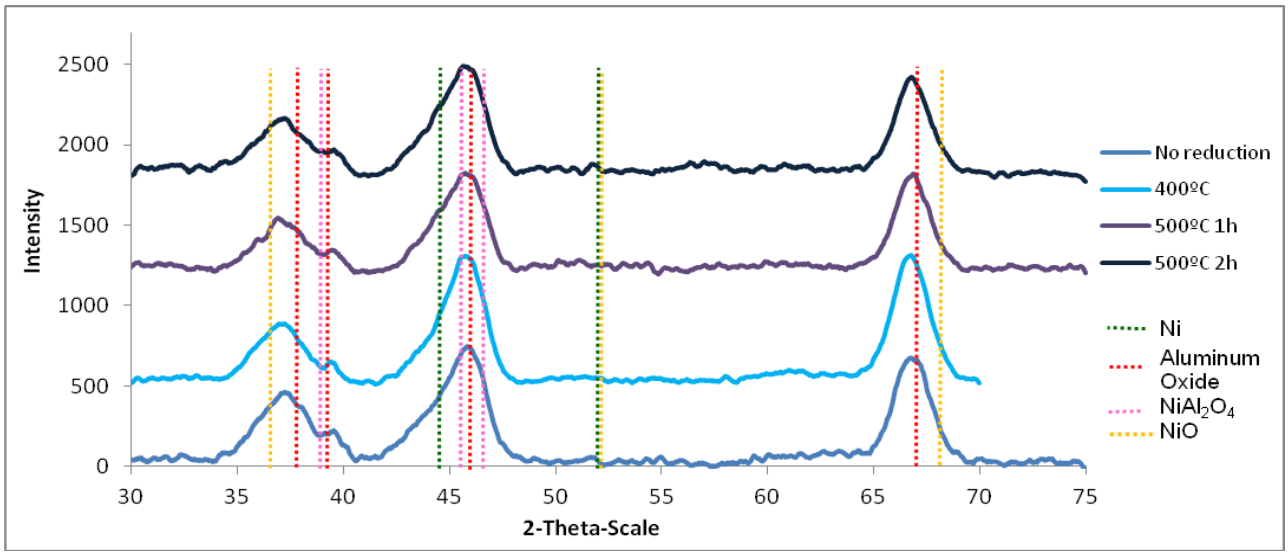

Figure 34: Results of XRD for all samples with the respectively standard pattern for the compounds

It is observed that the original catalyst is constituted by $NiAl_2O_4$, Al_2O_3 and NiO. According to the results realized in TPR, initially there is a reduction of Ni present in nickel oxide and therefore Ni present in the structure alumina. It is possible to observe at 35 – 40º a contribution to the peak of NiO, aluminium oxide and nickel alumina. The presence of aluminium oxide is due to the preparation of the catalyst: it is known the producer performed a pre-reduction of the catalyst, extracting particles of nickel from the structure nickel alumina, and by oxidation, the formation of NiO.

After the reduction, particles of metallic nickel are formed and should show the pattern presented in green in the previous figure. This peak is included in the wide peak of aluminium oxide and nickel alumina, but it is possible to observe the formation of a shoulder at 44º in the reductions at 500ºC.

In order to estimate the crystallites' size of Ni, an analysis was made only between 40 and 53º, to the sample reduced at 500ºC during two hours.

Taking into account that the peaks of the patterns are symmetric, the axis of symmetry taken correspond to the angles of the standard pattern (44,5º to Ni and 46º to AlO). First it was drawn the peak of aluminium oxide, taking the original values between 46 and 50º, then the values of the left side were calculated in order to produce a symmetric peak. The peak of nickel was calculated by subtraction of the original values with the ones calculated for aluminium oxide, adjusting to obtain a symmetric peak. This adjustment is due to a small contribution of nickel alumina, as it is possible to observe in the Figure A-5 in the annexes.

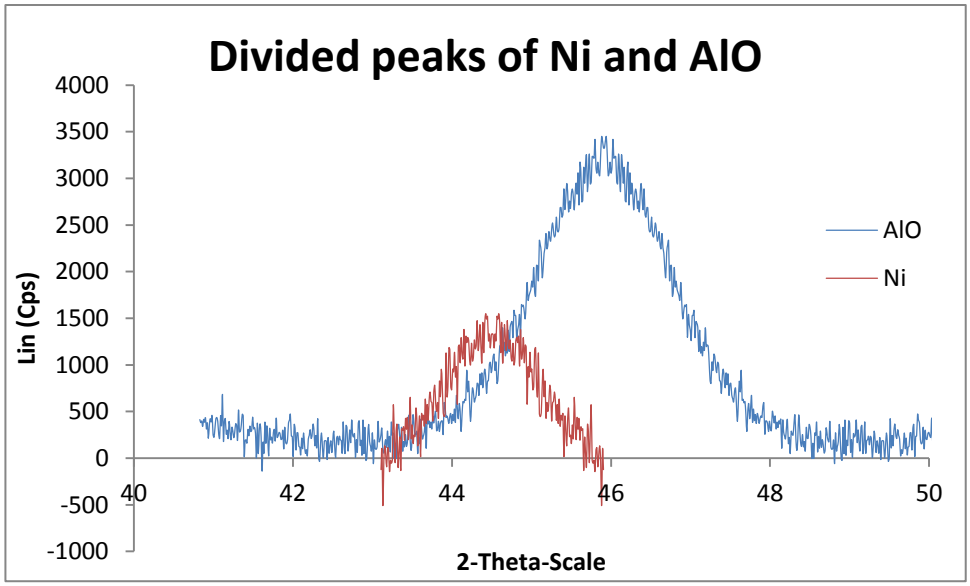

Figure 35: Division of the peak in order to calculate the crystallite size

Through the equation 57, and taking into account the peak of Ni, it was determined a crystallite size of around 6.1 nm.

Comparing this value with the one obtained from chemisorption at 500ºC (16.7 nm), it can be concluded this method may not have been very accurate, maybe due to the difficulty in separating the peaks because of the noise produced by the apparatus. Also, as it was referred, there is a contribution of nickel alumina in the wide peak that was not taken into account.

3. Experimental Setup

The catalytic tests were performed in an experimental setup of stainless steel at atmospheric pressure. The supply of nitrogen, carbon dioxide, carbon monoxide, hydrogen, methane and argon is made from individual bottles (1) with mass flow controllers Brooks SLA 5850E (2) connected to an electronic apparatus Brooks 0254. The gas flow leaves the debit regulators in a pipeline to a mixture pipe (3). A three way valve allows the measurement of the flow, a bypass or a flow to the reactor. A pressure indicator (4) was placed before this valve to permit the measurement of the pressure in the reactor. The flow enters in a glass reactor (5) with an inner diameter of 0.3 cm and a length of 30 cm. The catalyst is placed in a fixed bed between two pieces of quartz wool, since this component has a good thermal conductivity and acts as an inert to the reaction. The reactor is heated by an electrical resistance (6) in thermal contact with the reactor and isolated from the outside with quartz wool. The temperature is controlled by a regulator PID Minicor. The thermocouple of regulation was placed in contact with the resistance and other thermocouple was placed at the exit of the catalytic bed and it is defined as reaction temperature. A second valve is placed after the outlet of the reactor to allow its isolation. The effluent flows through a cold trap (7) to condense the water formed in the reaction. (Some photos can be seen in annexes).

The effluent is transferred to an online micro-chromatographer in gas phase Agilent M200H (8), equipped with two columns: a column molecular sieve of 5Å (MS5A) at 110ºC for separation of H_2, N_2, CO and CH_4 (vector gas: Argon); the other column is poraplot U (PPU) at 45ºC for the separation of the common peak, CH_4 and CO_2 (vector gas: Helium). The detection is made by thermal conductivity. The retention times (in sec) in the module A are: H_2 49.15; N_2 73.84; CH_4 95.57; CO 125.59. In the module B are: common peak (N_2, H_2, CO) 25.10; CH_4 27.80; CO_2 52.50.

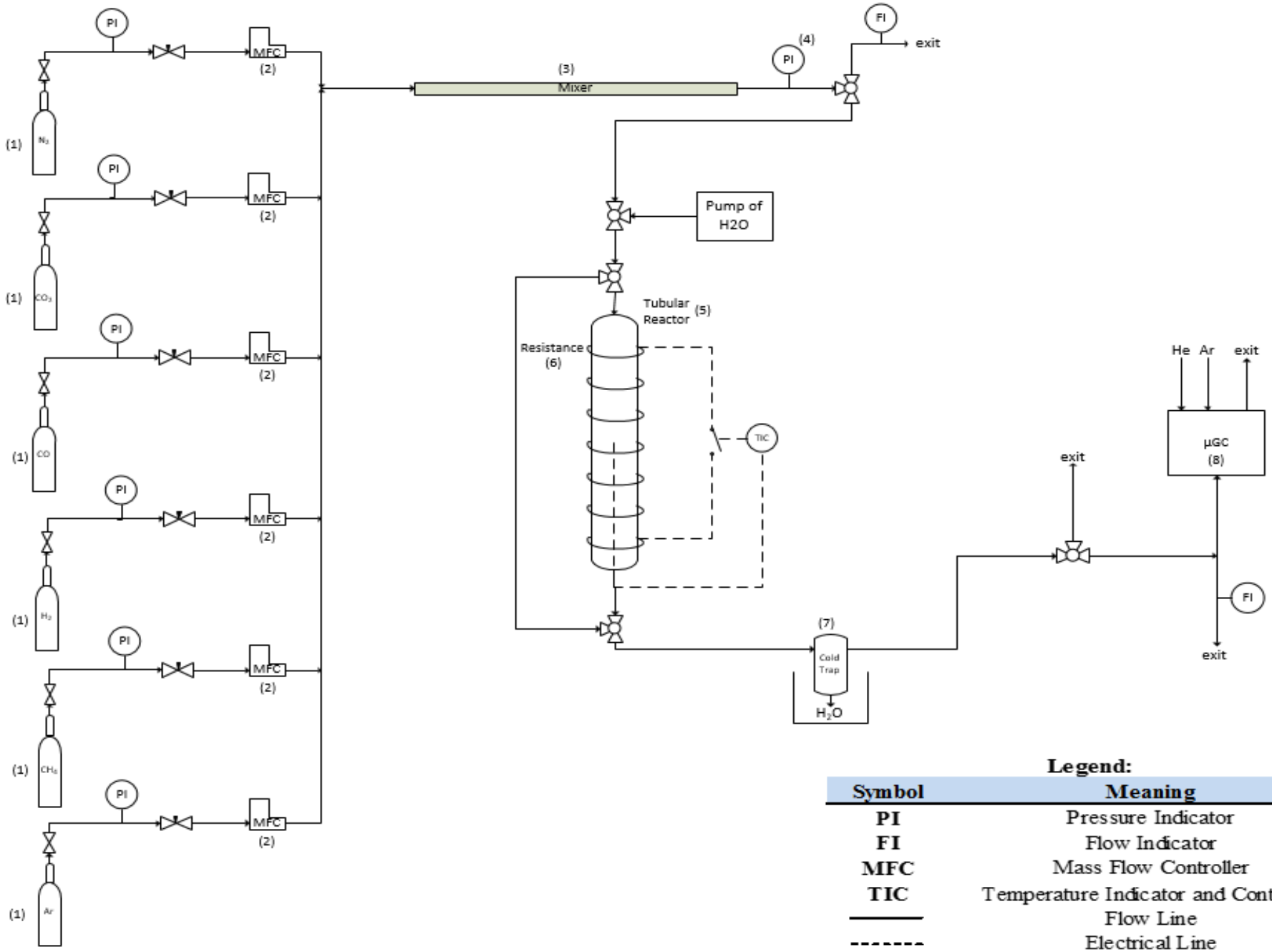

Legend:

Symbol	Meaning
PI	Pressure Indicator
FI	Flow Indicator
MFC	Mass Flow Controller
TIC	Temperature Indicator and Controller
———	Flow Line
- - - - - - -	Electrical Line

4. Kinetic Modeling

Before any catalytic test, the catalyst was reduced at 5ºC/min until 500ºC during one hour with a flow of around 50 mL/min of 10%H_2-N_2, as decided previously. The catalytic bed was fixed by quartz wool and composed by the sample of catalyst dispersed in SiC. This material allows the uniformity of temperature to maintain isothermal conditions and the quantity used was determined in order to have a height of the catalytic bed three times higher than the inner diameter of the reactor, in order to allow a plug flow. All the catalytic tests were performed at atmospheric pressure, measured before the entrance on the reactor.

4.1 External and Internal Limitations

Initially it was investigated the presence of limitations to external diffusion. For that, the reactor was loaded with a specific mass and catalytic tests were made. Then it was loaded with a different mass and the total flow was change to maintain the space velocity, GHSV, at 189000 h^{-1}. With the same composition of gases, catalytic test were realized.

By plotting the formation rate of methane (by CO_2 methanation) and the formation rate of CO (by reverse water-gas shift) for the different masses of catalyst in function of time, it is possible to evaluate the existence of any limitation to external diffusion.

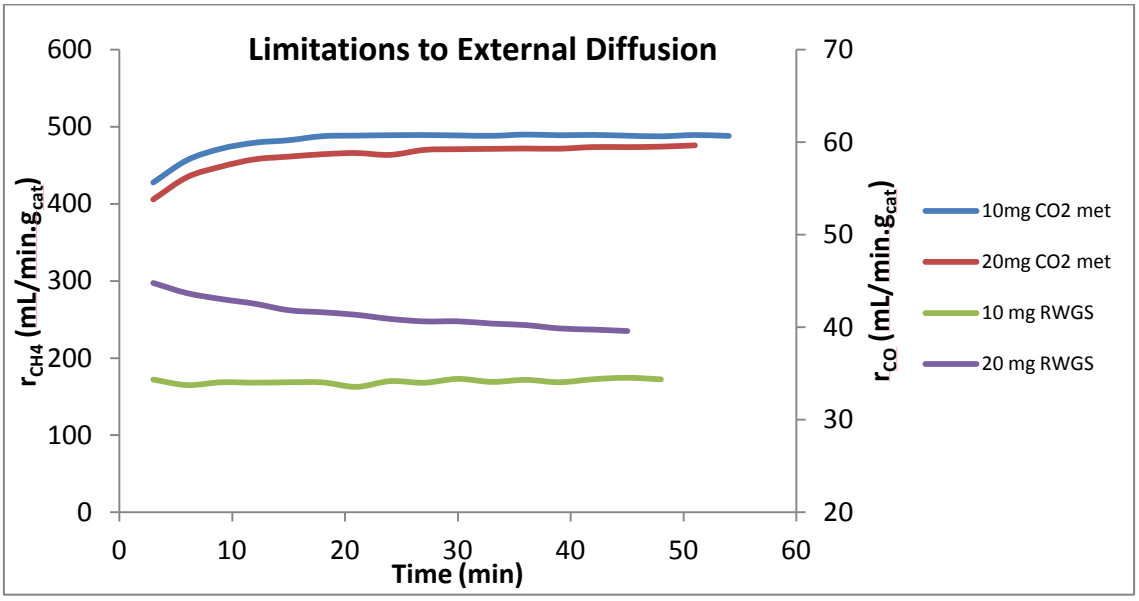

Figure 36: Formation rates of methane and CO at 400ºC for 10 and 20 mg of catalyst at 400ºC

The existence of limitations to external diffusion is characterized by an increasing of the formation rate of methane and CO when the mass of catalyst is higher. This is due to the increase of the flow rate and consequently the turbulence in the catalytic bed, i.e., a thinner stagnation film is formed that permits a better access of the molecules to the surface of the catalyst. As it is observed on the graph above, the formation rate of methane is very stable at 400ºC and it has not limitations to external diffusion. However, it is not the case for the

formation of CO. As the two reactions are connected it can be concluded that the difference might be due to some instability associated to the equipment and to the scale presented (much lower than the rate formation of methane) and not derived from limitations to external diffusion.

Next, it was investigated the presence of limitations to internal diffusion by realizing catalytic tests with the same mass of one of the previous experiments but with three different particle size, maintaining the space velocity, GHSV, of 176400 h^{-1} at 350ºC. An evidence of the existence of limitations to internal diffusion is an increase of the formation rate of the products with the decrease of the particle size, as it permits a better access of the molecules to the inner active sites. Plotting the formation rate in order of time for methane and carbon monoxide at different particles size, it was possible to verify that although the formation rate of methane and CO seems to be affected by change of particle size of the catalyst, it occurs in the opposite way of the expected one, i.e., it is not observed an increase of the formation rate with smaller particle sizes. It can then be concluded that the difference is due to some instability associated to the equipments (observed previously) and there are no limitations to internal diffusion.

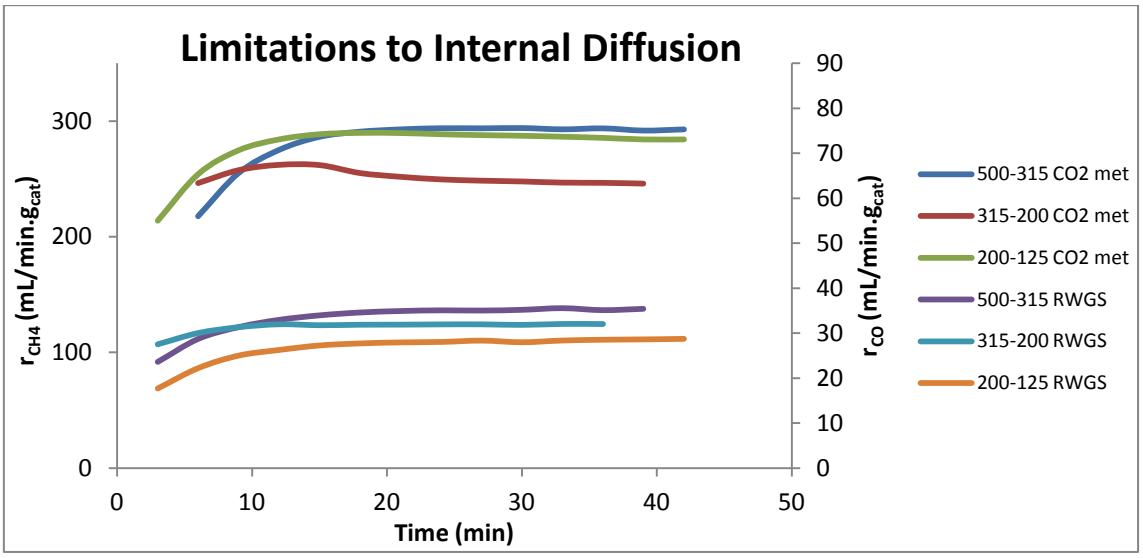

Figure 37: Formation rates of methane and CO with 10mg of catalyst with different particle sizes at 350ºC

Taking into account that, in order to not have effect of the wall in the reactor, the inner diameter of the reactor should be ten to twenty times higher than the particle size of the catalyst, it was decided the catalytic tests would be performed in the fraction of 200-125 µm. A smaller fraction could not be chosen as that would imply a big pressure drop in the catalytic bed.

4.2 Influence of CO_2 on CO_2 methanation

As it was concluded that the catalyst is not affected by limitations to external and internal diffusions, the catalytic tests were started. Initially it was tested the influence of CO_2 in the reaction of methanation and in the reaction of reverse water-gas shift. For that it is important to have a conversion around 20% or less to assure no influences of the thermodynamic equilibrium and to guarantee no formation of heavier hydrocarbons. During this experiment two

reactions occur: CO_2 methanation and reverse water-gas shift. From the formation of CO it can occur also CO methanation, but it was admitted that all methane formed comes from CO_2 methanation only, as the formation of CO is limited by the low conversion.

After some experiments to settle a low conversion, it was chosen a mass of catalyst of 2mg, a gas hourly space velocity (GHSV) of $1.90x10^6$ h^{-1} and a variation of temperature between 400 and 325ºC. Then, the flow of CO_2 was changed, and all the other components were kept constant. In order to have the same total flow in all experiments, the difference caused by decreasing the flow of CO_2 was compensated by Argon. The partial pressure of CO_2 was maintained low (less than 0.23 bar and the ratio H_2/CO_2 varied between 3 and 6.7.

By plotting the formation rate of methane and CO in function of the partial pressure of CO_2 it is possible to observe its influence in the reactions.

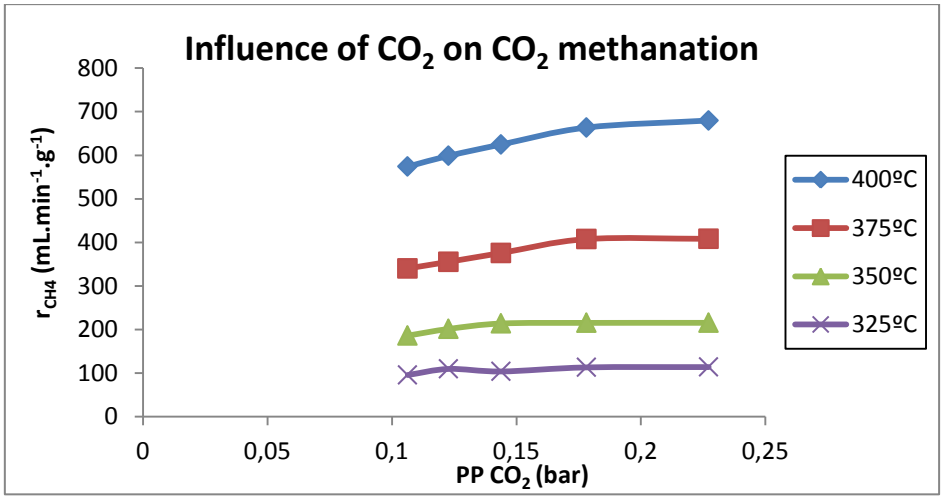

Figure 38: Influence of CO_2 on formation rate of methane at four different temperatures

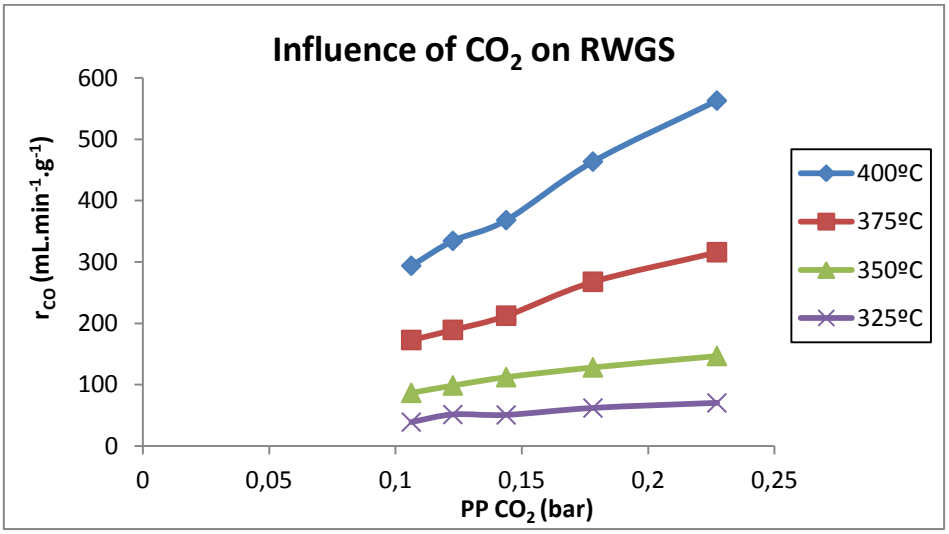

Figure 39: Influence of CO_2 on formation rate of CO at four different temperatures

At these partial pressures, it is possible to observe a weak influence of CO_2 in methanation of CO_2 as the formation rate of methane decreases slightly with the decrease of the partial pressure of CO_2. However, a strong influence it is observed in the reverse water-gas shift

reaction. In order to confirm these results, a second experiment was realized with a lower partial pressure of CO_2 and H_2, but approximately the same ratio, with compensation with Ar.

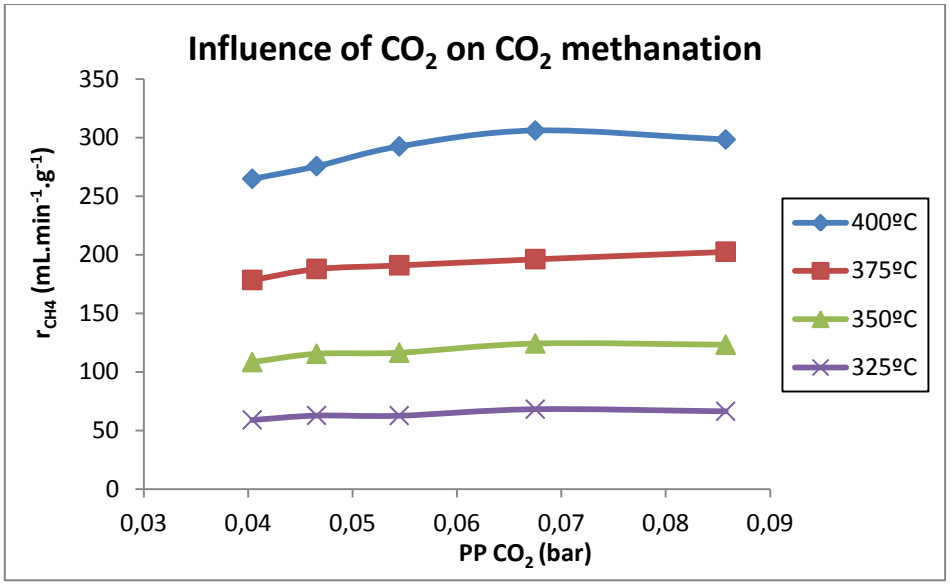

Figure 40: Influence of CO_2 on formation rate of methane at lower partial pressures of CO_2 and H_2

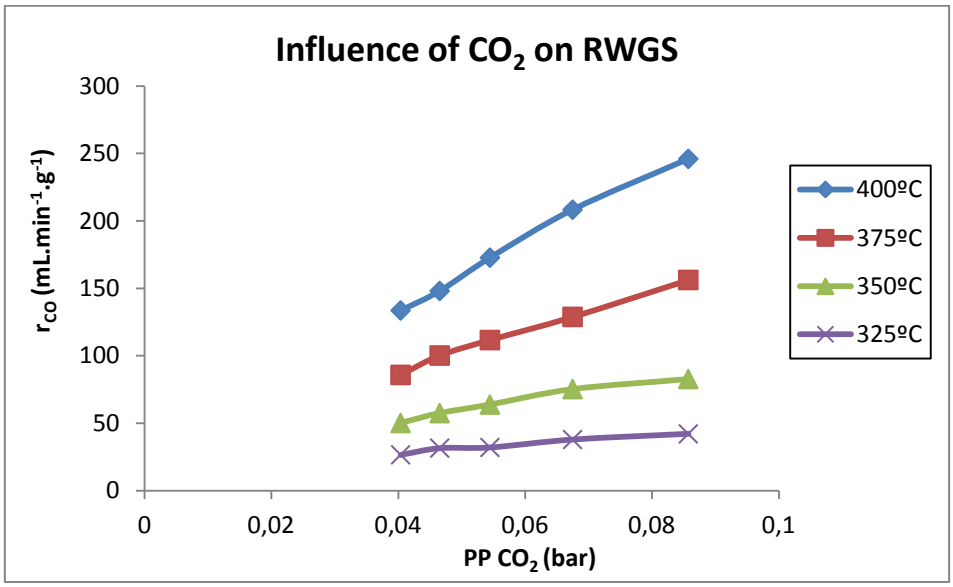

Figure 41: Influence of CO_2 on formation rate of CO at lower partial pressures of CO_2 and H_2

The influence of carbon dioxide on the reaction presents a similar behaviour in both cases with different partial pressures and it is also observed a similar formation of CO and CH_4.

The next step was ascertaining the influence of H_2 in the same reactions. For that, it was followed the same procedure, but this time the partial pressure of CO_2 was kept constant, and H_2 was varied compensating the total flow by addition of Argon.

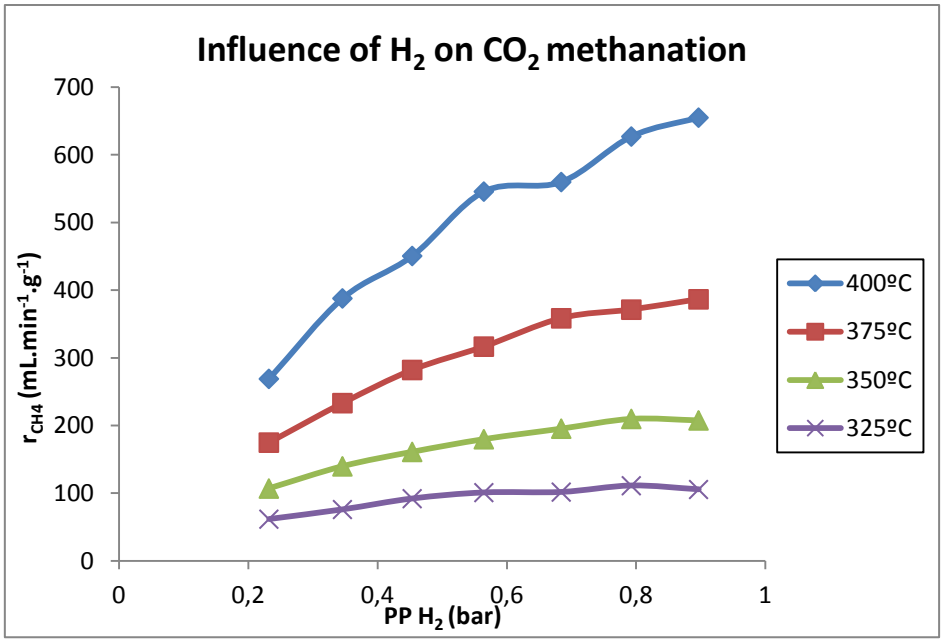

Figure 42: Influence of H_2 on formation rate of methane at four different temperatures

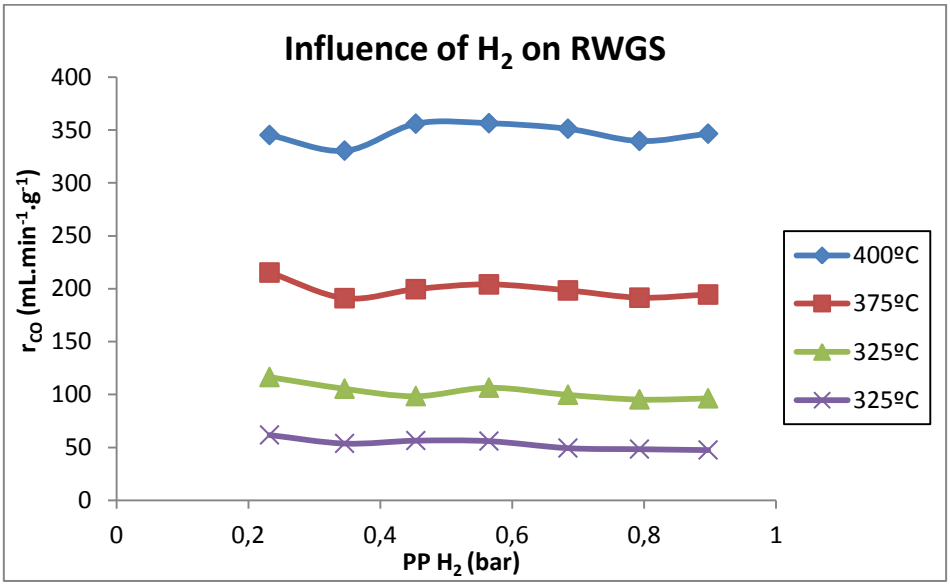

Figure 43: Influence of H_2 on formation rate of CO at four different temperatures

It is possible to observe a strong increasing of the formation rate of methane with the increase of the partial pressure of hydrogen, however, in Figure 43 it is obviously a non-influence of hydrogen in the formation rate of CO, what indicates no coverage of the surface by H_2 as it acts as a “cleaner” of the oxygen from the surface, if it is considered a redox mechanism, as strongly suggested in literature.

As one of the objectives of this internship is to find a kinetic model for the reaction in study, the results obtained were tested in the models reviewed in the first part of this report (Table 1), where some will be presented and discussed and the remaining are presented in appendice.

First it was tested the model of Bartholomew *et al* [17] in its original equation.

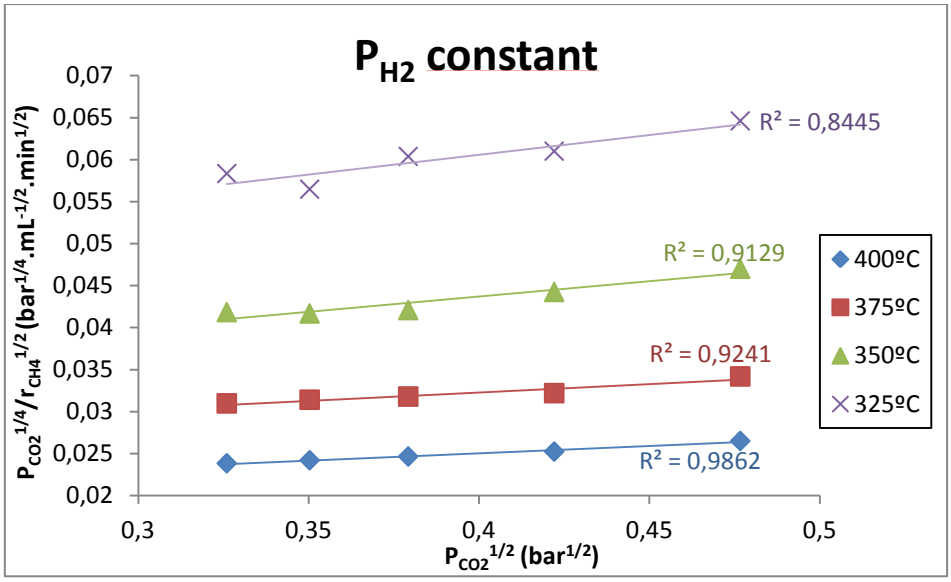

Figure 44: Test of the experimental results in the model of Bartholomew *et al* with P_{H2} constant

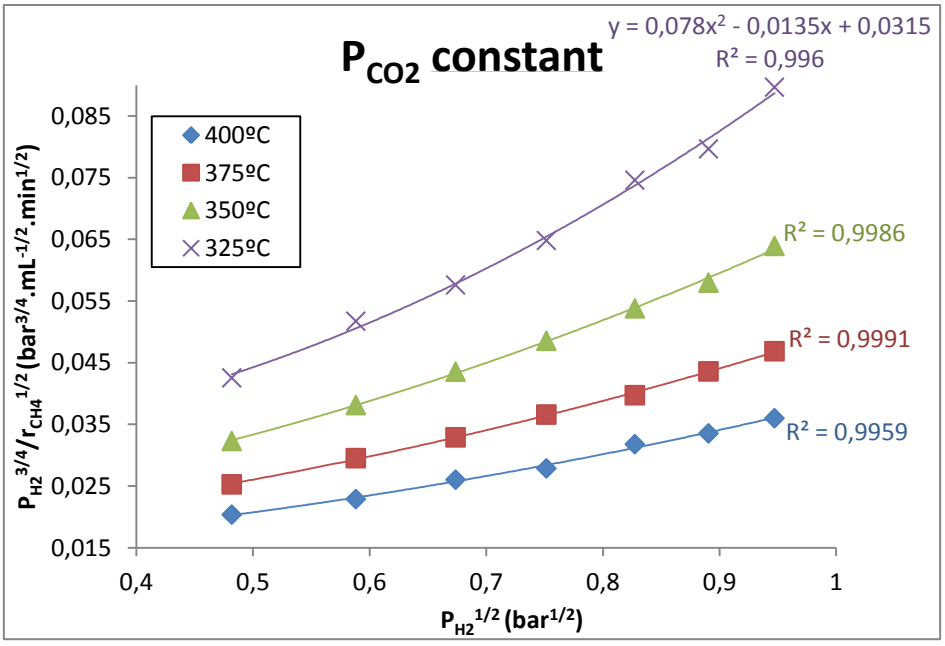

Figure 45: Test of the experimental results in the model of Bartholomew *et al* with P_{CO2} constant

From Figure 45 it is observed the experimental results cannot be described by this model as there is a negative parameter. A negative parameter would imply that some adsorption or kinetic constants were negative, what it is not possible. One possibility is considering this parameter equal to zero, and for that it is necessary neglect the term $1 + \frac{P_{CO}}{K_3}$, and plotting P_{H2} in function of $\frac{P_{H_2}^{3/4}}{r_{CH_4}^{1/2}}$

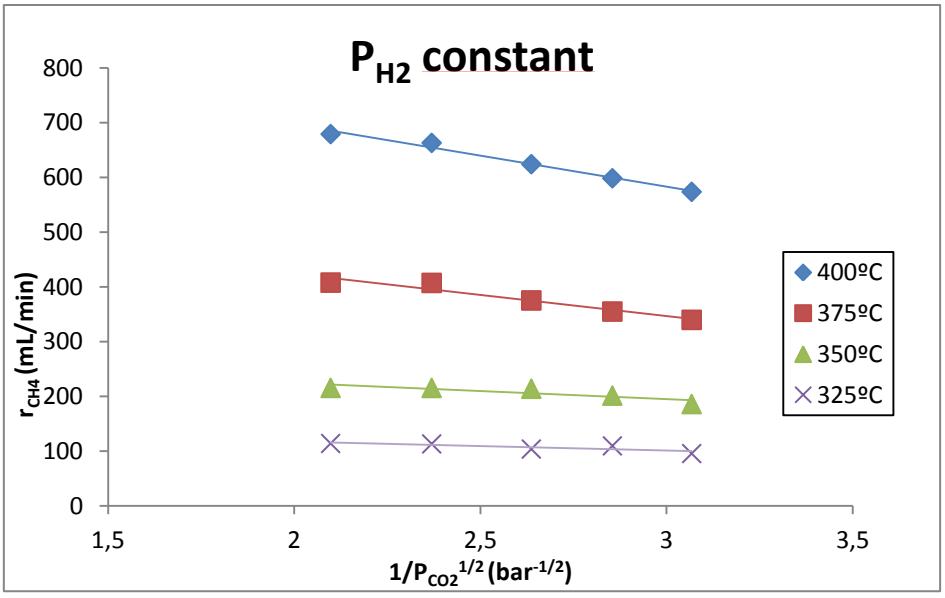

Figure 46: Test of the modified model of Bartholomew *et al* with P_{H2} constant

With this alteration, it is obtained a negative slope in the cases when the partial pressure of hydrogen is kept constant and, due to the explanation given previously, this model was excluded.

The next model here presented is the model of Xu and Froment [18] that affirms no adsorption of CO_2 in the active sites of the catalyst.

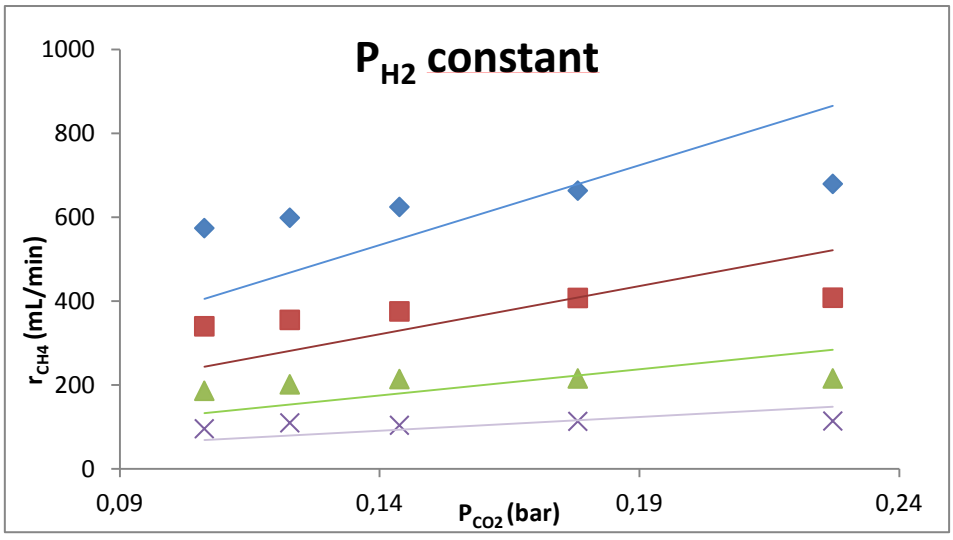

Figure 47: Test of the model of Xu and Froment with P_{H2} constant

In this case it is affirmed a linear regression between the partial pressure of CO_2 and the formation rate of methane, what implies an interception equal to zero when the partial pressure of hydrogen is kept constant, whereby it is possible to also exclude this model.

The last model here represented belongs to Wheeler *et al* [26] where molecular adsorption of CO_2, H_2, CO and H_2O occurs. This model was developed for WGS reaction but it is here tested for CO_2 methanation.

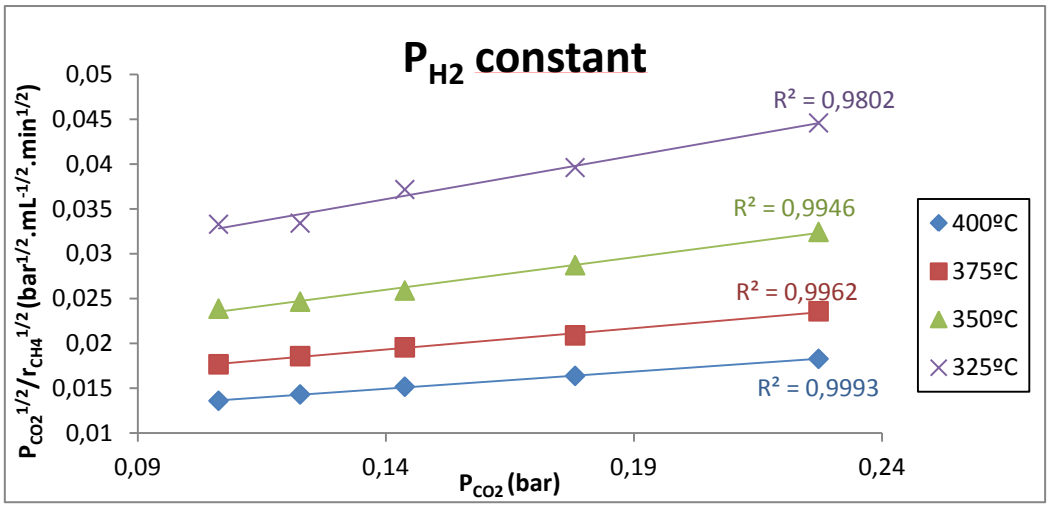

Figure 48: Test of the model of Wheeler *et al* with P_{H2} constant

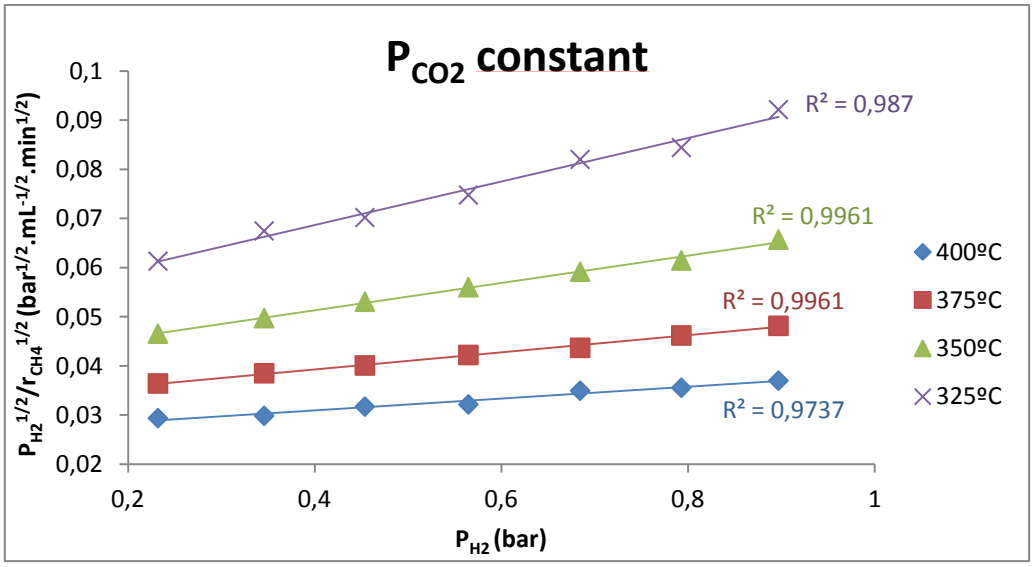

Figure 49: Test of the model of Wheeler *et al* with P_{CO2} constant

It is showed a very good fit of the experimental results in the model, however, it was also tested the other forms of adsorption. This means it was tested the dissociative adsorption of CO_2 without adsorption of H_2, the dissociative adsorption of CO_2 with non-dissociative adsorption of H_2 and the opposite, and finally dissociative adsorption of both that is translated for a square root in the adsorption constant and in the partial pressure of the respective component (Table 2). For all the cases, through the values of slope and interception for both graphs, and knowing the partial pressure of CO_2 and H_2, the heat adsorption of CO_2 and H_2 were calculated and compared with the literature. It was also calculated the kinetic constant of the reaction. The model that best described the data and showed values close to the literature was the original non-dissociative adsorption of CO_2 and H_2. The other components were not taking into account as their formation was limited and therefore no influence in the kinetics.

$$r_{CH_4} = \frac{kK_{CO_2}K_{H_2}P_{CO_2}P_{H_2}}{\left(1 + K_{CO_2}P_{CO_2} + K_{H_2}P_{H_2}\right)^2} \quad (58)$$

Table 1: Models from literature tested for experiments with CO_2 methanation

#Equation	Equation of the model	$P_{H_2}constant$	$P_{CO_2}constant$
Eq. 14 (Bartholomew et al, *Journal of Catalysis*, 1982)	$r_{CH_4} = \frac{\left(\frac{K_1K_2K_{10}k_4k_{11}}{2}\right)^{1/2} L^2 P_{CO_2}^{1/2} P_{H_2}^{1/2}}{\left(1 + \left(\frac{2K_2k_4}{K_1K_{10}k_{11}}\right)^{1/2} \frac{P_{CO_2}^{1/2}}{P_{H_2}^{1/2}} + \left(\frac{K_1K_2K_{10}k_{11}}{2k_4}\right)^{1/2} P_{CO_2}^{1/2} P_{H_2}^{1/2} + \frac{P_{CO}}{K_3}\right)^2}$	$\frac{P_{CO_2}^{1/4}}{r_{CH_4}^{1/2}} = a.P_{CO_2}^{1/2} + b$	$\frac{P_{H_2}^{3/4}}{r_{CH_4}^{1/2}} = a.P_{H_2} + b.P_{H_2}^{1/2} + c$
Eq. 19 (Xu and Froment, *AIChE Journal*, 1989)	$r_{14} = \frac{k_2}{P_{H_2}}\left(P_{CO}P_{H_2O} - \frac{P_{H_2}P_{CO_2}}{K_2}\right)/(DEN)^2$	$r_{CO} = a.P_{CO_2}$	$\frac{1}{r_{CO}^{1/2}} = a.P_{H_2} + b$
Eq. 20 (Xu and Froment, *AIChE Journal*, 1989)	$r_{15} = \frac{k_3}{P_{H_2}^{3,5}}\left(P_{CH_4}p_{H_2O}^2 - \frac{P_{H_2}^4 P_{CO_2}}{K_3}\right)/(DEN)^2$	$r_{CH_4} = a.P_{CO_2} + b$	$\frac{P_{H_2}^{1/4}}{r_{CH_4}^{1/2}} = a.P_{H_2} + b$
Eq. 26 (Ibraeva et al, *Theor. Exp. Chem.*, 1991)	$r = k_1P_{CO_2}P_{H_2}^{0,5}/\left(P_{H_2}^{0,5} + k_2P_{CO_2}\right)$	$\frac{1}{r_{CH_4}} = a.\frac{1}{P_{CO_2}} + b$	$\frac{1}{r_{CH_4}} = a.\frac{1}{P_{H_2}^{1/2}} + b$
Eq. 28 (Koschany, F. et al, *Applied Catalysis B: Envir.*, 2016)	$r = \frac{kP_{CO_2}^{0,5}P_{H_2}^{0,5}\left(1 - \frac{P_{CH_4}P_{H_2O}^2}{k_{eq}P_{CO_2}P_{H_2}^4}\right)}{\left(1 + \sqrt{K_{H_2}P_{H_2}} + K_{mix}P_{CO_2}^{0,5} + K_{H_2O}P_{H_2O}\right)^2}$	$\frac{P_{CO_2}^{1/4}}{r_{CH_4}^{1/2}} = a.P_{CO_2}^{1/2} + b$	$\frac{P_{H_2}^{1/4}}{r_{CH_4}^{1/2}} = a.P_{H_2}^{1/2} + b$
Eq. 37 (Wheeler, C., *Journal of Catalysis*, 2004)	$r'' = \frac{k_f''K_{CO}K_{H_2O}P_{CO}P_{H_2O} - k_b''K_{CO_2}K_{H_2}P_{CO_2}P_{H_2}}{(1 + K_{CO}P_{CO} + K_{H_2O}P_{H_2O} + K_{CO_2}P_{CO_2} + K_{H_2}P_{H_2})^2}$	$\frac{P_{CO_2}^{1/2}}{r_{CH_4}^{1/2}} = a.P_{CO_2} + b$	$\frac{P_{H_2}^{1/2}}{r_{CH_4}^{1/2}} = a.P_{H_2} + b$
Eq. 39 (Callaghan, C.A., Worcester Polytechnic Institute, 2006)	$\bar{r} = \frac{kP_{CO_2}P_{H_2}}{1 + K_{CO_2.H_2}P_{CO_2}P_{H_2} + K_{H_2}P_{H_2}}$	$\frac{1}{r_{CH_4}} = a.\frac{1}{P_{CO_2}} + b$	$\frac{1}{r_{CH_4}} = a.\frac{1}{P_{H_2}} + b$

Table 2: Modified Wheeler et at models for the experiments with CO_2 methanation

	Proposed Model	$P_{H_2} constant$	$P_{CO_2} constant$
Diss. Ads. of CO_2	$r_{CH_4} = \frac{kK_{CO_2}P_{CO_2}^{1/2}P_{H_2}}{\left(1 + K_{CO_2}P_{CO_2}^{1/2}\right)^2}$	$\frac{P_{CO_2}^{1/4}}{r_{CH_4}^{1/2}} = a.P_{CO_2}^{1/2} + b$	$r_{CH_4} = a.P_{H_2}$
Non-Diss. Ads. of CO_2 and H_2	$r_{CH_4} = \frac{kK_{CO_2}K_{H_2}P_{CO_2}P_{H_2}}{\left(1 + K_{CO_2}P_{CO_2} + K_{H_2}P_{H_2}\right)^2}$	$\frac{P_{CO_2}^{1/2}}{r_{CH_4}^{1/2}} = a.P_{CO_2} + b$	$\frac{P_{H_2}^{1/2}}{r_{CH_4}^{1/2}} = a.P_{H_2} + b$
Diss. Ads. for CO_2 and Non-Diss. Ads. for H_2	$r_{CH_4} = \frac{kK_{CO_2}{}^{1/2}K_{H_2}P_{CO_2}{}^{1/2}P_{H_2}}{\left(1 + K_{CO_2}{}^{1/2}P_{CO_2}{}^{1/2} + K_{H_2}P_{H_2}\right)^2}$	$\frac{P_{CO_2}^{1/4}}{r_{CH_4}^{1/2}} = a.P_{CO_2}^{1/2} + b$	$\frac{P_{H_2}^{1/2}}{r_{CH_4}^{1/2}} = a.P_{H_2} + b$
Non-Diss. Ads. for CO_2 and Diss. Ads. for H_2	$r_{CH_4} = \frac{kK_{CO_2}K_{H_2}{}^{1/2}P_{CO_2}P_{H_2}{}^{1/2}}{\left(1 + K_{CO_2}P_{CO_2} + K_{H_2}{}^{1/2}P_{H_2}{}^{1/2}\right)^2}$	$\frac{P_{CO_2}^{1/2}}{r_{CH_4}^{1/2}} = a.P_{CO_2} + b$	$\frac{P_{H_2}^{1/4}}{r_{CH_4}^{1/2}} = a.P_{H_2}{}^{1/2} + b$
Diss. Ads. of CO_2 and H_2	$r_{CH_4} = \frac{kK_{CO_2}{}^{1/2}K_{H_2}{}^{1/2}P_{CO_2}{}^{1/2}P_{H_2}{}^{1/2}}{\left(1 + K_{CO_2}{}^{1/2}P_{CO_2}{}^{1/2} + K_{H_2}{}^{1/2}P_{H_2}{}^{1/2}\right)^2}$	$\frac{P_{CO_2}^{1/4}}{r_{CH_4}^{1/2}} = a.P_{CO_2}^{1/2} + b$	$\frac{P_{H_2}^{1/4}}{r_{CH_4}^{1/2}} = a.P_{H_2}{}^{1/2} + b$

This model was also tested for the reaction of Reverse Water-Gas Shift, and it was observed a good fit of the data in the model. However, the kinetic parameters calculated differ a lot from the ones calculated from CO_2 methanation and as the catalyst is the same and the reactions are linked, it is necessary to presente a new model that gives similar values for the constant

The redox mechanism is largely accepted among the studies found in literature, whereby it will be the starting point for the kinetic model of this reaction. It is observed in Figure 43 there is no influence of hydrogen, what means this compound only acts to remove the atom of oxygen adsorbed by the active site from CO_2, as exemplified next:

$$CO_2 + X \overset{k_{CO_2}}{\longleftrightarrow} CO + OX$$

$$H_2 + OX \overset{k_{H_2}}{\longleftrightarrow} H_2O + X$$

The model that describes this mechanism assumes the reduction of CO_2 as a rate

$$r_{CO} = \frac{k_{CO_2} P_{CO_2} k_{H_2} P_{H_2}}{\left(k_{CO_2} P_{CO_2} + k_{H_2} P_{H_2}\right)} \Big/ \left(1 + K_{CO_2} P_{CO_2} + K_{H_2} P_{H_2}\right) \quad (59)$$

determining step and takes into account the number of active sites, as in CO_2 methanation:

As the oxidation of hydrogen to form water is much faster than the reduction of CO_2, the term $k_{CO_2} P_{CO_2}$ in the denominator can be neglected, and consequently the rate reaction will depend only of the pressure of CO_2, what confirms the behaviour explicit in Figure 41 and Figure 43. The kinetic constant of the reduction step will be considered the same for the global reaction.

$$r_{CO} = \frac{k_{RWGS} P_{CO_2}}{\left(1 + K_{CO_2} P_{CO_2} + K_{H_2} P_{H_2}\right)} \quad (60)$$

This model was tested by plotting the $r_{CO} \times DEN$ (denominator) using the adsorption constants calculated from the study of CO_2 methanation in function of the partial pressure of CO_2.

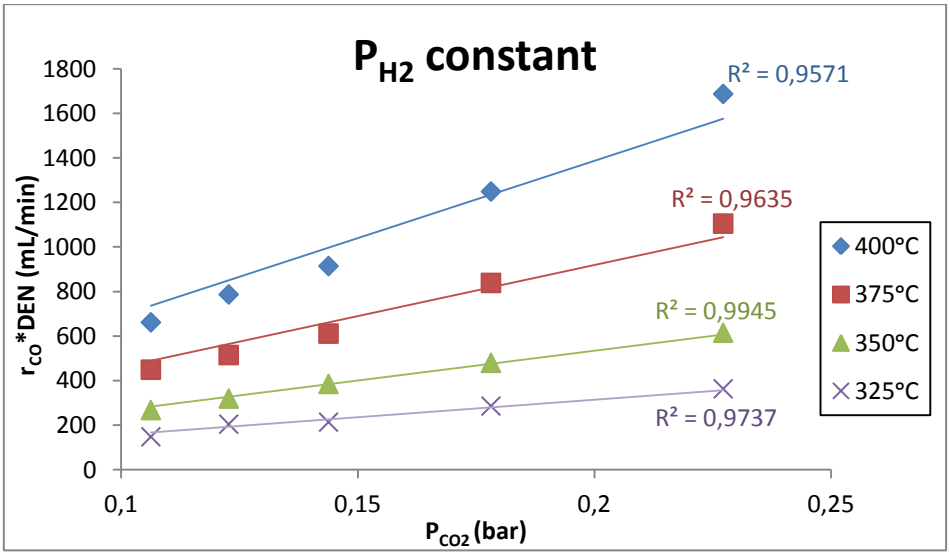

Figure 50: Test of the proposed redox model for RWGS with P_{H2} constant

4.3 Influence of CO on CO methanation

The CO methanation is an important reaction to study since it occurs due the formation of CO from the reverse water-gas shift reaction. For that, the next step was verifying the influence of CO and H_2 in the reaction of methanation of CO. Again, the partial pressure of CO and H_2 was varied separately compensating with Argon.

In this case there is a small contribution of the reaction of water-gas shift, but it can be neglected, as the formation of H_2O is limited.

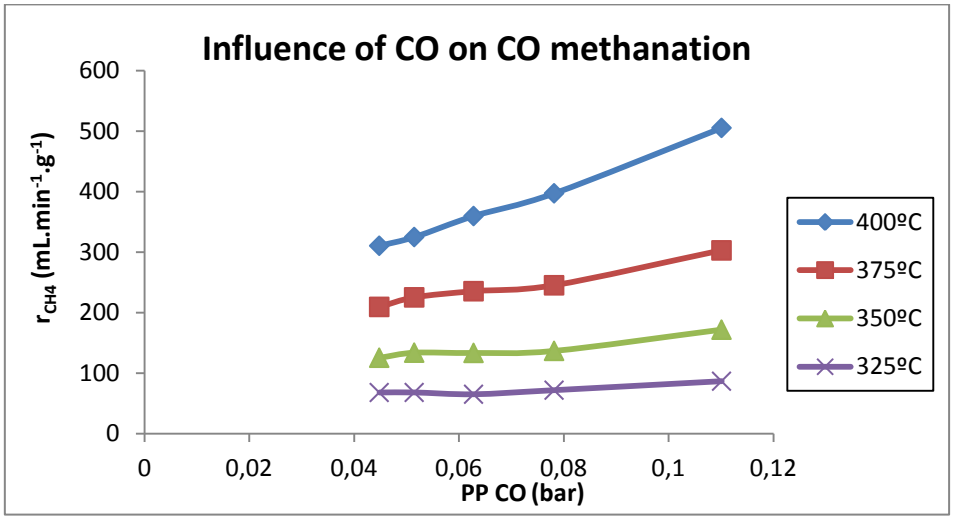

Figure 51: Influence of CO on the formation rate of CH_4 at four different temperatures

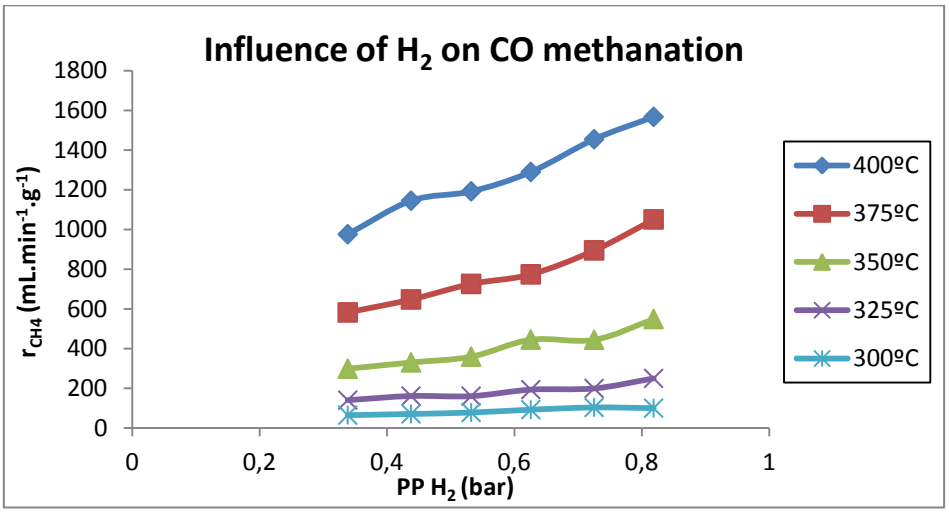

Figure 52: Influence of H_2 on the formation rate of CH_4 at four different temperatures

It is possible to observe an important influence of the two reactants in the formation rate of methane, what implies both compounds are present in the rate determining step. It was admitted a model similar to Wheeler's used in CO_2 methanation. It was also tested the nature of adsorption of the compounds, where the equations are presented in Table 3. The model that best described the experimental data is the one that admits molecular adsorption of CO and hydrogen (being in accordance with the conclusion from CO_2 methanation in the case of the

nature of adsorption of hydrogen). The kinetic parameters were also calculated in the same way as CO_2 methanation, and the values obtained for hydrogen are similar for the ones obtained previously.

$$r_{CH_4} = \frac{kK_{CO}K_{H_2}P_{CO}P_{H_2}}{\left(1 + K_{CO}P_{CO} + K_{H_2}P_{H_2}\right)^2} \quad (61)$$

Table 3: Adapted Wheeler et al models for the experiments with CO methanation

	Proposed Model	$P_{H_2} constant$	$P_{CO} constant$
Diss. Ads. of CO	$r_{CH_4} = \frac{kK_{CO}P_{CO}^{1/2}P_{H_2}}{\left(1+K_{CO}P_{CO}^{1/2}\right)^2}$	$\frac{P_{CO}^{1/4}}{r_{CH_4}^{1/2}} = a.P_{CO}^{1/2} + b$	$r_{CH_4} = a.P_{H_2}$
Non-Diss. Ads. of CO and H_2	$r_{CH_4} = \frac{kK_{CO}K_{H_2}P_{CO}P_{H_2}}{\left(1+K_{CO}P_{CO}+K_{H_2}P_{H_2}\right)^2}$	$\frac{P_{CO}^{1/2}}{r_{CH_4}^{1/2}} = a.P_{CO} + b$	$\frac{P_{H_2}^{1/2}}{r_{CH_4}^{1/2}} = a.P_{H_2} + b$
Diss. Ads. for CO and Non-Diss. Ads. for H_2	$r_{CH_4} = \frac{kK_{CO}^{1/2}K_{H_2}P_{CO}^{1/2}P_{H_2}}{\left(1+K_{CO}^{1/2}P_{CO}^{1/2}+K_{H_2}P_{H_2}\right)^2}$	$\frac{P_{CO}^{1/4}}{r_{CH_4}^{1/2}} = a.P_{CO}^{1/2} + b$	$\frac{P_{H_2}^{1/2}}{r_{CH_4}^{1/2}} = a.P_{H_2} + b$
Non-Diss. Ads. for CO and Diss. Ads. for H_2	$r_{CH_4} = \frac{kK_{CO}K_{H_2}^{1/2}P_{CO}P_{H_2}^{1/2}}{\left(1+K_{CO}P_{CO}+K_{H_2}^{1/2}P_{H_2}^{1/2}\right)^2}$	$\frac{P_{CO}^{1/2}}{r_{CH_4}^{1/2}} = a.P_{CO} + b$	$\frac{P_{H_2}^{1/4}}{r_{CH_4}^{1/2}} = a.P_{H_2}^{1/2} + b$
Diss. Ads. of CO and H_2	$r_{CH_4} = \frac{kK_{CO}^{1/2}K_{H_2}^{1/2}P_{CO}^{1/2}P_{H_2}^{1/2}}{\left(1+K_{CO}^{1/2}P_{CO}^{1/2}+K_{H_2}^{1/2}P_{H_2}^{1/2}\right)^2}$	$\frac{P_{CO}^{1/4}}{r_{CH_4}^{1/2}} = a.P_{CO}^{1/2} + b$	$\frac{P_{H_2}^{1/4}}{r_{CH_4}^{1/2}} = a.P_{H_2}^{1/2} + b$

4.4 Influence of CH_4

After observing the influence of CO_2, H_2 and CO, it was verified the influence of CH_4 in the reaction of methanation of CO_2 (and consequently reverse water-gas shift) and methanation of CO. For that, it was performed experiments with only CO_2 and H_2, and only CO and H_2 at the inlet. It was chosen conditions near the stoichiometric one for both cases and it was introduced different amounts of methane at the inlet of the reactor decreasing the flow of Argon to maintain the total flow constant as all the other flows were kept constants. The inlet flow of methane was high enough to be always higher than the one formed by the reactions.

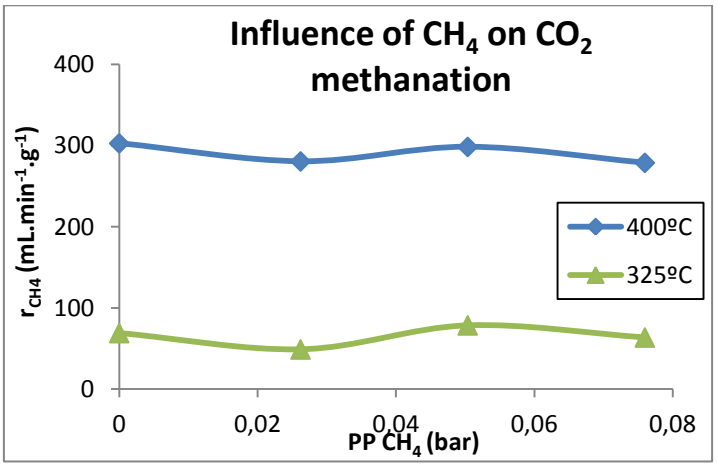

Figure 53: Influence of methane in the methanation of CO_2 at two different temperatures

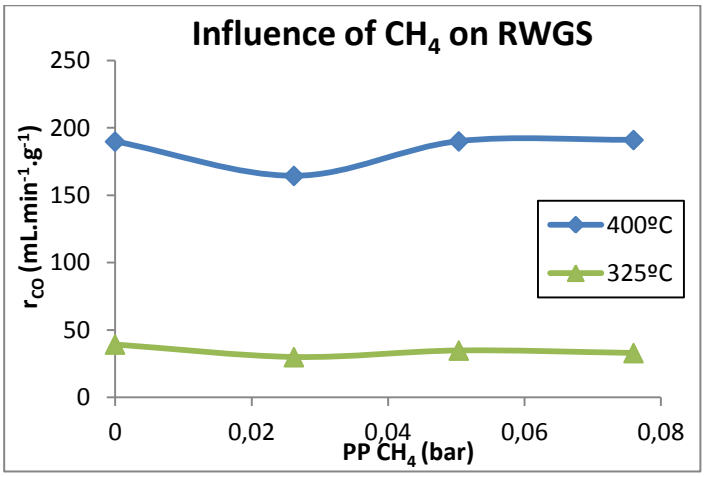

Figure 54: Influence of methane in the reaction of reverse water-gas shift

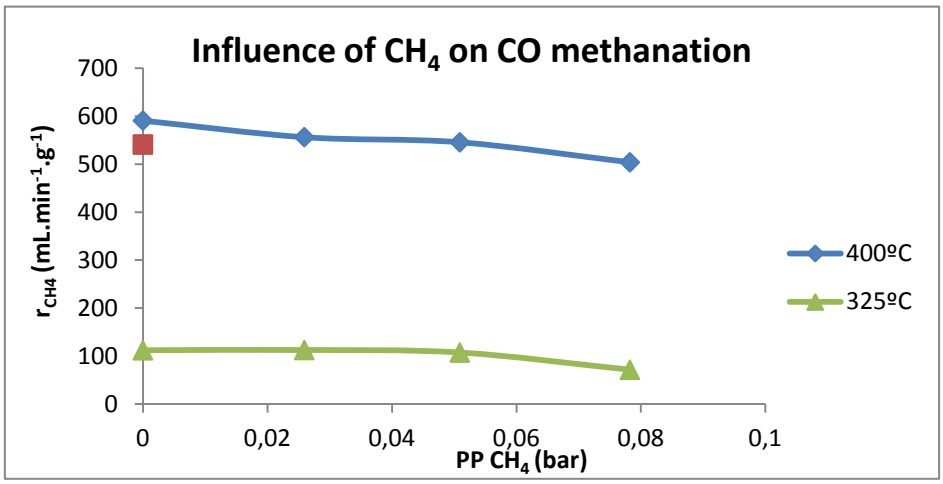

Figure 55: Influence of methane in the methanation of CO at two different temperatures with repetition of one experiment (red point)

The oscillatory character of the Figure 53 and Figure 54 shows no influence of methane in CO_2 methanation and reverse water-gas shift. However, it is observed a slight decrease of the formation rate of methane in CO methanation that may indicate influence of this component. The experiment at 400ºC and no methane (red point) was repeated and it indicated a formation rate near the experiment with highest partial pressure of methane. Then, it can be concluded

that the catalyst suffered some deactivation during the experiment and there is no influence of methane in the reaction.

It can be concluded the models proposed for the three reactions are also validated by these experiments since it doesn't consider adsorption of methane in the active sites.

4.5 Influence of H_2O

Finally it was observed the influence of the last product: water. For this case, it was performed separately CO_2 and CO methanation with different inlet flows of water vapour at three different temperatures. As what happened to methane, the inlet flow of water was high enough to be always higher than the one formed by the reactions.

The results in Figure 56, Figure 57 and Figure 58 show a considerable influence of this component in the reaction which leads to the conclusion that water is adsorbed in the active sites of the catalyst, reducing the accessibility of the mainly reactants to those.

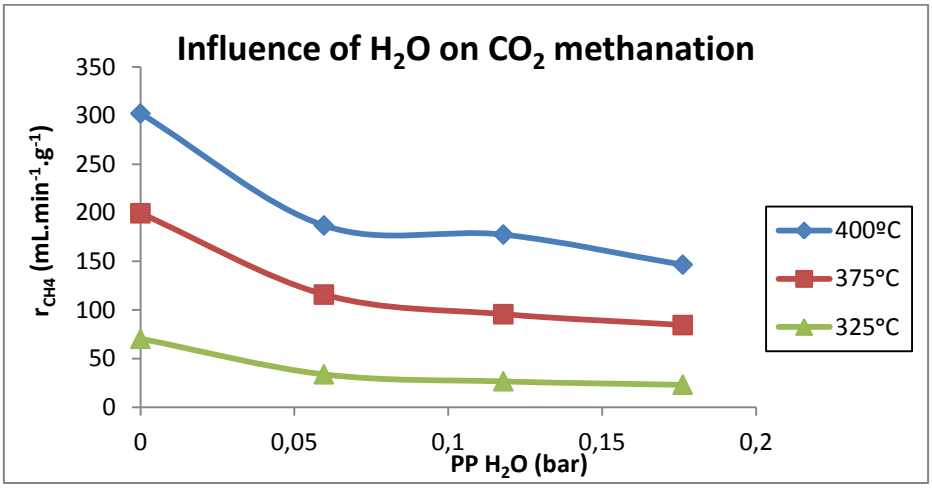

Figure 56: Influence of water in the reaction of CO_2 methanation at three different temperatures

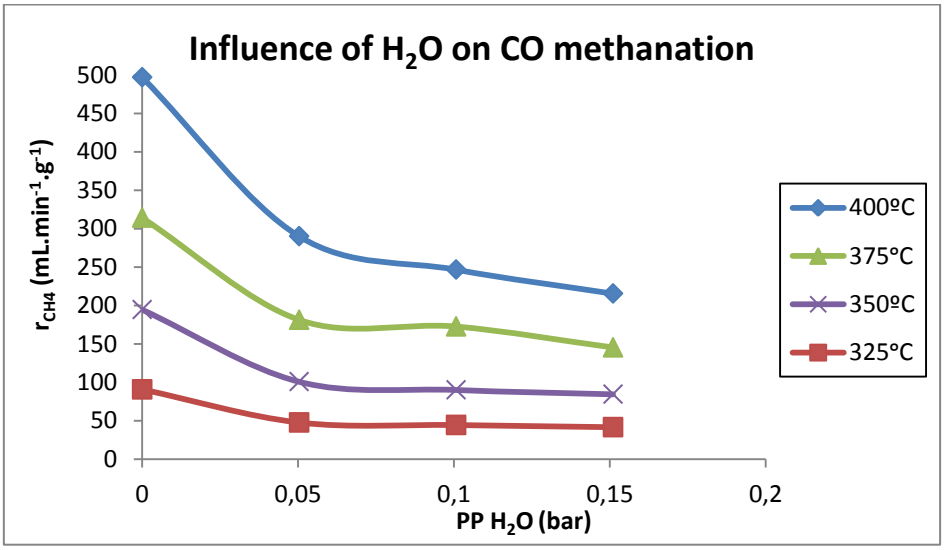

Figure 57: Influence of water in the reaction of CO methanation at four different temperatures

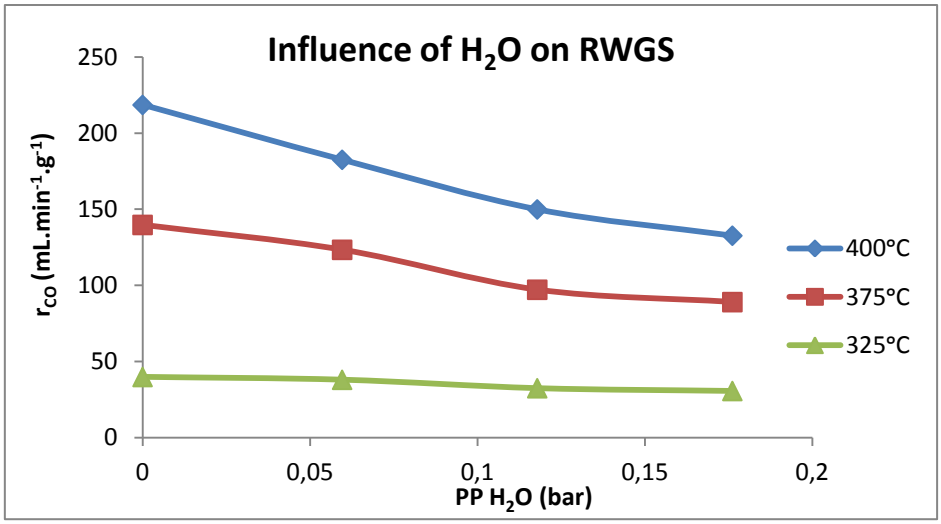

Figure 58: Influence of water in the reverse water-gas shift at three different temperatures

In order to determine the heat adsorption of water in the catalyst, it was analyzed the fitting of the data in the model of Wheeler *et al* proposed for CO_2 and CO methanation (equation 62) and also with a small alteration (dissociative adsorption of water – equation 63).

$$r_{CH_4} = \frac{A}{\left(B + K_{H_2O}P_{H_2O}\right)^2} \tag{62}$$

$$r_{CH_4} = \frac{A}{\left(B + K_{H_2O}^{1/2}P_{H_2O}^{1/2}\right)^2} \tag{63}$$

This assumption is made considering the main reaction is CO_2 methanation (and CO methanation for the respective case), so the parameters A and B are the ones belonged to the model of each reaction, for example B is the balance to the active sites $(1 + K_{CO_2}P_{CO_2} + K_{CO}P_{CO} + K_{H_2}P_{H_2})$. It was showed a better fit of the experimental data for the model that described dissociative adsorption of water.

Concerning the reverse water-gas shift reaction, the same method was applied (being A and B the parameters belonged to the model) and there was an accordance with the nature of the adsorption of water – dissociative (equation 64).

$$r_{CO} = \frac{A}{\left(B + K_{H_2O}^{1/2}P_{H_2O}^{1/2}\right)^2} \tag{64}$$

So finally it is possible to propose a modified model of Wheeler *et al* for CO_2 methanation (equation 65) and CO methanation (equation 66) and a redox model for RWGS (equation 67) described by

$$r_{CH_4} = \frac{k_{CO_2 met} K_{CO_2} K_{H_2} P_{CO_2} P_{H_2}}{\left(1 + K_{CO_2} P_{CO_2} + K_{CO} P_{CO} + K_{H_2} P_{H_2} + K_{H_2O}^{1/2} P_{H_2O}^{1/2}\right)^2} \quad (65)$$

$$r_{CH_4} = \frac{k_{COmet} K_{CO} K_{H_2} P_{CO} P_{H_2}}{\left(1 + K_{CO_2} P_{CO_2} + K_{CO} P_{CO} + K_{H_2} P_{H_2} + K_{H_2O}^{1/2} P_{H_2O}^{1/2}\right)^2} \quad (66)$$

$$r_{CO} = \frac{k_{RWGS} P_{CO_2}}{\left(1 + K_{CO_2} P_{CO_2} + K_{CO} P_{CO} + K_{H_2} P_{H_2} + K_{H_2O}^{1/2} P_{H_2O}^{1/2}\right)} \quad (67)$$

For each set of experiments it was possible to calculate the constant adsorption of the components and the respective kinetic constant of the reaction for each temperature. As both constants follow the Arrhenius Law it is possible to calculate the heat adsorption, the activation energy and the pre-exponential factor. The results are presented in the next table.

Table 4: Kinetic parameters calculated from experimental data at low conversion

	CO_2	CO	H_2	H_2O	CO_2 methanation	CO methanation	RWGS
Qads (kJ/mol)	27.38 (28 – 92)*	58.91 (33 – 62)*	43.80 (37 – 48)*	62.91 (48)*	-	-	-
K_0 (bar^{-1})	4.62×10^{-2}	1.16×10^{-4}	3.33×10^{-4}	2.54×10^{-5} ($bar^{-1/2}$)	-	-	-
Ea (kJ/mol)	-	-	-	-	96.94	118.97	72.55
k_0 (mol/min.g)	-	-	-	-	7.36×10^{6}	1.00×10^{9}	1.25×10^{5}

* - Values found in literature

4.6 Adjustment of the kinetic parameters

All the experiments presented until now in this report were performed with a conversion lower than 20% to assure no influence of the products in the kinetics and to guarantee the reactions occur far from the thermodynamic equilibrium.

To conclude this work, it was necessary to evaluate the prediction of the conversion and flow rates of the reactions given by the models proposed, not only at lower conversions but also near the thermodynamic equilibrium. For that, experiments at three different temperatures were realized in order to simulate a plug flow reactor:

- it was established 3mg of mass of catalyst with a flow rate at the inlet of around 110 mL/min in order to have low conversation;
- the flow rate was decreased to other three values, maintaining the composition, what implies a higher conversion;

- after, the mass of catalyst was increased to 12 mg and the experiments were performed with the same previous inlet flows. In this case, the conversion of the reactants is even higher and it is expected to reach the thermodynamic equilibrium.

With these data, it was calculated the equivalent mass of each case for a reference flow of 100 mL/min. This means:

$$m_{equiv} = m_{exp} \times \frac{FR_{exp}}{100} \tag{68}$$

Where m_{equiv} is the equivalent mass, m_{exp} is the experimental mass (3 or 12 mg) and FR_{exp} is the experimental inlet flow.

By plotting the experimental conversion and/or the flow rates at the outlet of the reactor obtained in function of the equivalent mass, it is observed a behaviour of a plug flow reactor.

To evaluate the models proposed in the sections above, they were also simulated, in an excel file at the same three temperatures, in an isothermal plug flow reactor considering an inlet flow of 100 mL/min, a composition equal to the experiments and a mass of catalyst equal to the biggest equivalent mass of the experimental results. For that it was taken into account 500 small CSTR reactor in series, each one isothermal. The flows of the components at the outlet of each small reactor were calculated through a mass balance, taking into account that the formation/consumption of the components were given by the models presented previously. The kinetic constants used were the ones calculated during the kinetic study. The outlet of one small reactor was considered to be the inlet of the next one, and again the mass balance was performed to determine the outlet flow of the new reactor, and so on.

Plotting the behaviour of the conversion and the flows of the compounds at the outlet of each small CSTR reactors in function of the accumulated mass (that can be correlated with the length of the catalytic bed) and comparing with the experimental data obtained it is possible to observe if the models proposed describe well the behaviour of the reaction in study.

First, it was performed individually CO_2 and CO methanation and then an equimolar mixture of both at the inlet with the same composition of the experimental tests. As the conversion is significantly higher at the biggest mass of catalyst, it is important to consider all the reactions studied (including the reverse ones). For example:

$$r_{CO_2met} = \frac{k_{CO_2met} K_{CO_2} P_{CO_2} K_{H_2} P_{H_2} \left(1 - \frac{P_{H_2O}^2 P_{CH_4}}{P_{H_2}^3 K_{CO_2met}}\right)}{\left(1 + K_{CO_2} P_{CO_2} + K_{CO} P_{CO} + K_{H_2} P_{H_2} + K_{H_2O}^{1/2} P_{H_2O}^{1/2}\right)^2} \tag{69}$$

Initially, there was not a perfect fit of the models with the experimental data, so it was performed an adjustment of the kinetic constants by the method of least squares, i.e, the outlet flows of the components and the conversion obtained from the models should be equal to the ones obtained experimentally. The values obtained are presented in the next table.

Table 5: Final values of the kinetic constants

	CO_2	CO	H_2	H_2O	CO_2 methanation	CO methanation	RWGS
Qads (kJ/mol)	56.8 (28 – 92)*	121.4 (33 – 62)*	105.1 (37 – 48)*	94.4 (48)*	-	-	-
K_0 (bar^{-1})	$4.7x10^{-6}$	$2.9x10^{-9}$	$4.3x10^{-10}$	$7.6x10^{-7}$ ($bar^{-1/2}$)	-	-	-
Ea (kJ/mol)	-	-	-	-	242.4	144.0	94.3
k_0 (mol/min.g)	-	-	-	-	$1.1x10^{21}$	$1.9x10^{12}$	$1.6x10^{7}$

In the next figures it is presented some examples of the comparison between the experimental data and the behaviour predicted by the models, with the final constants. The remaining results are showed in the appendices.

Only CO_2 at the inlet:

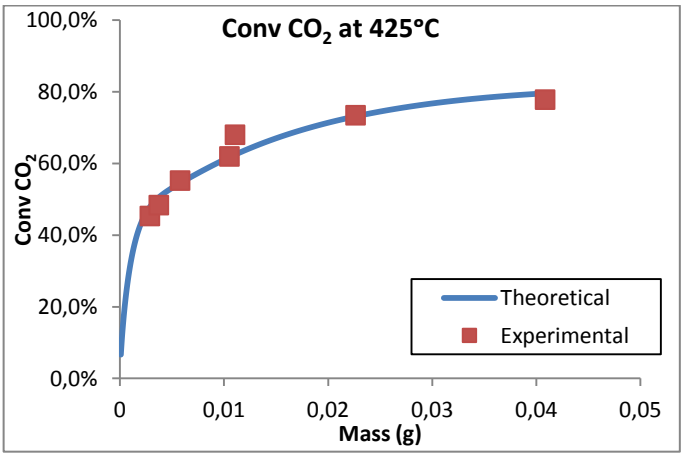

Figure 59: Comparison between the prevision of the conversion of CO_2 at 425ºC by the kinetic model and the experimental results

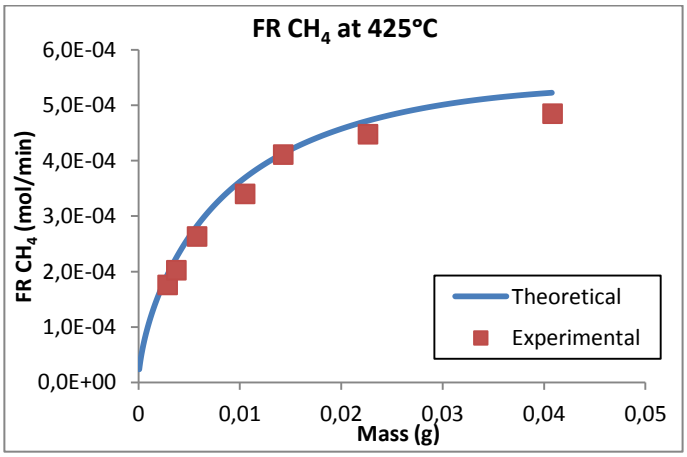

Figure 60: Comparison between the prevision of the flow rate of CH_4 at 425ºC by the kinetic model and the experimental results

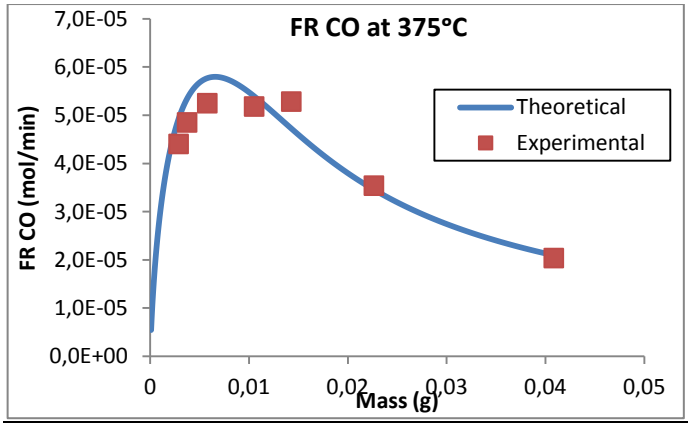

Figure 61: Comparison between the prevision of the flow rate of CO at 375ºC by the kinetic model and the experimental results

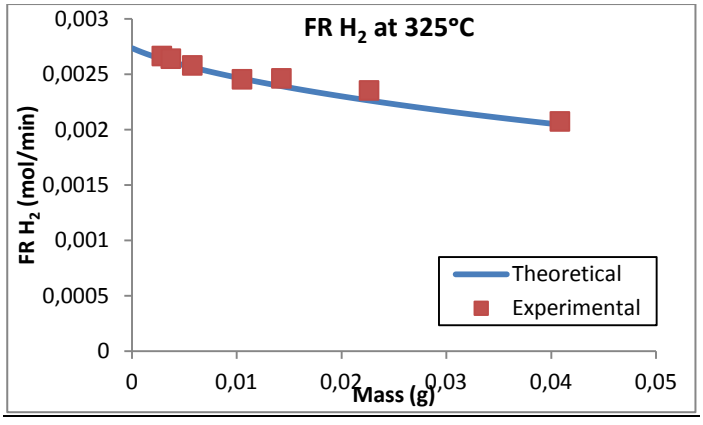

Figure 62: Comparison between the prevision of the flow rate of H_2 at 325ºC by the kinetic model and the experimental results

Only CO at the inlet:

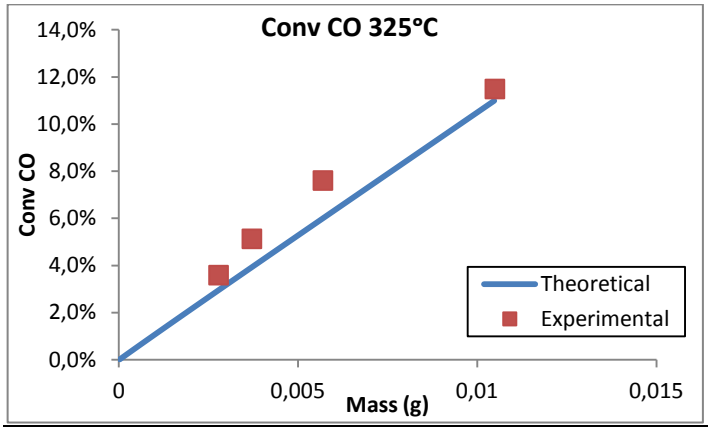

Figure 63: Comparison between the prevision of the conversion of CO at 325ºC by the kinetic model and the experimental results

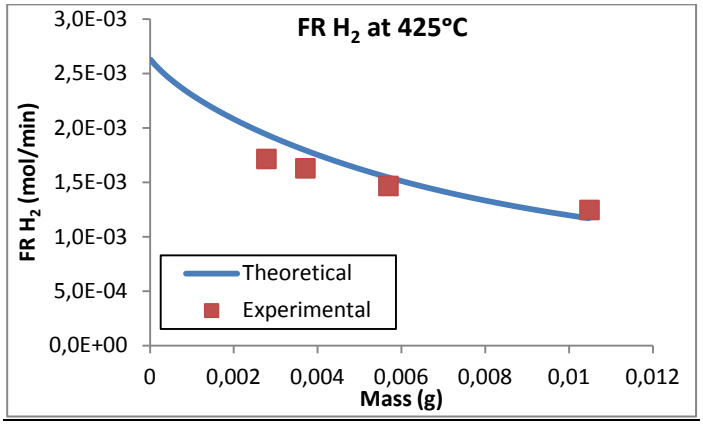

Figure 64: Comparison between the prevision of the conversion of H_2 at 425ºC by the kinetic model and the experimental results

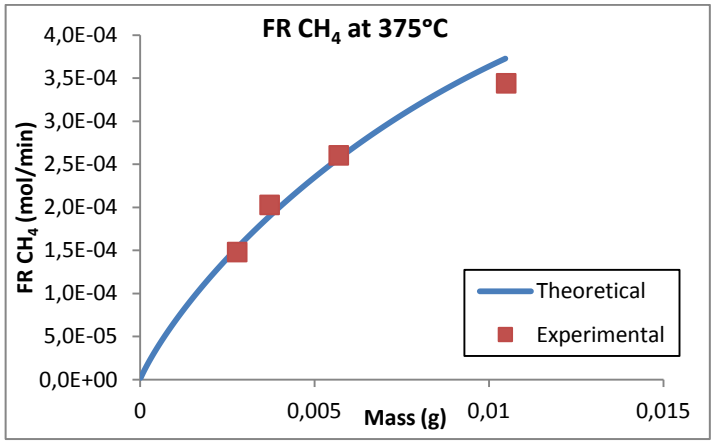

Figure 65: Comparison between the prevision of the flow rate of CH_4 at 375ºC by the kinetic model and the experimental results

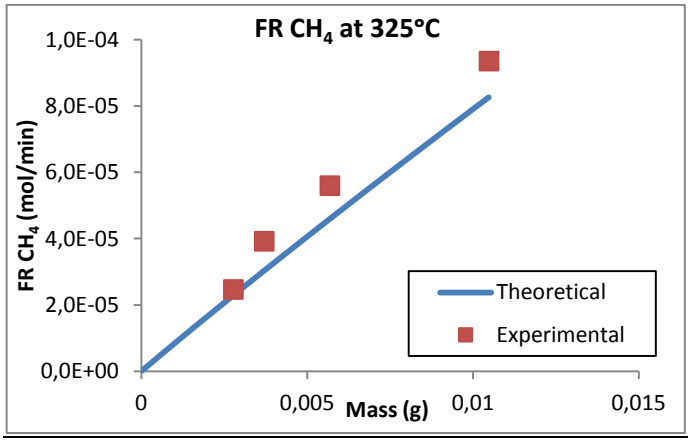

Figure 66: Comparison between the prevision of the flow rate of CH_4 at 325ºC by the kinetic model and the experimental results

Equimolar mixture of CO_2 and CO at the inlet:

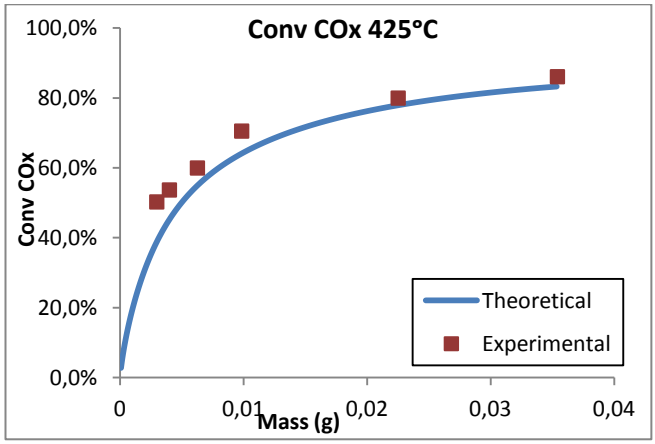

Figure 67: Comparison between the prevision of the conversion of COx at 425ºC by the kinetic model and the experimental results

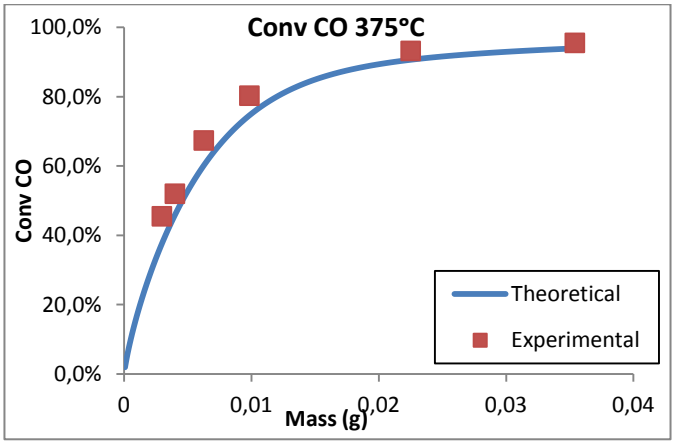

Figure 68: Comparison between the prevision of the conversion of CO at 375ºC by the kinetic model and the experimental results

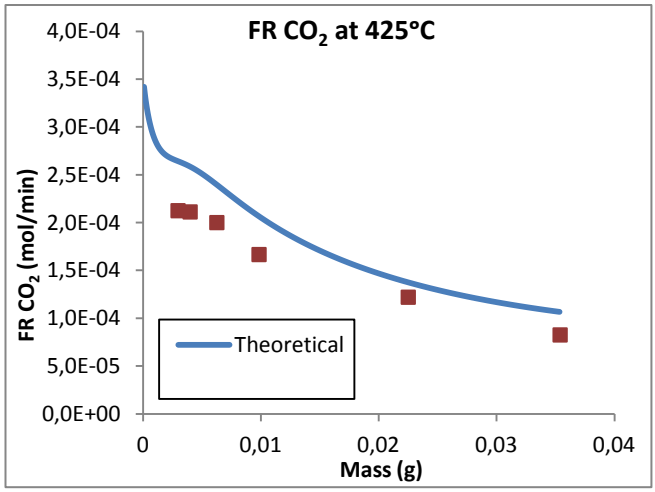

Figure 69: Comparison between the prevision of the flow rate of CO_2 at 425ºC by the kinetic model and the experimental results

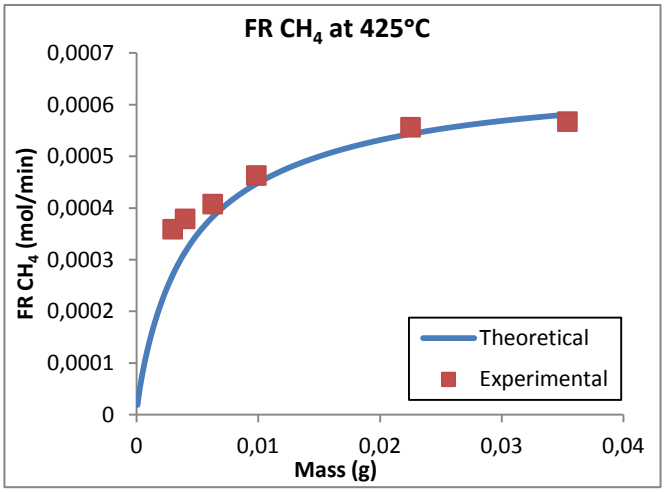

Figure 70: Comparison between the prevision of the flow rate of CH_4 at 425ºC by the kinetic model and the experimental results

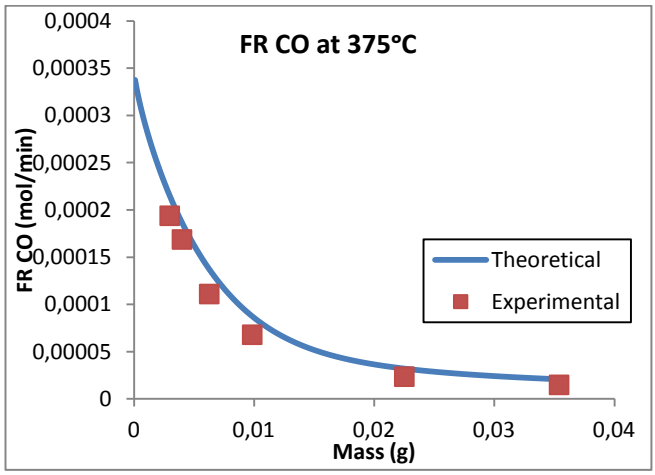

Figure 71: Comparison between the prevision of the flow rate of CO at 375ºC by the kinetic model and the experimental results

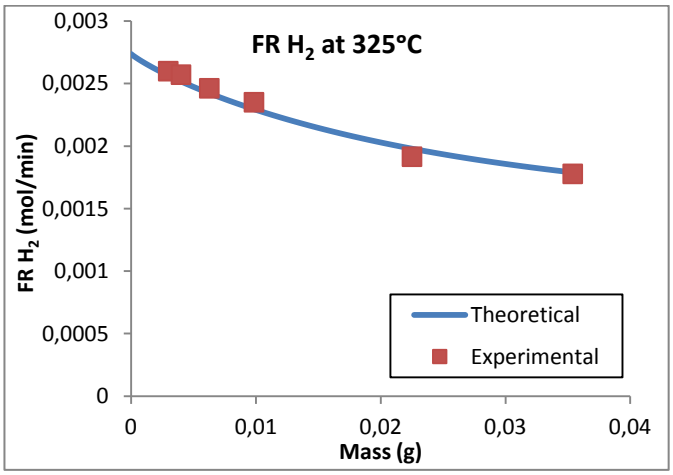

Figure 72: Comparison between the prevision of the flow rate of H_2 at 325ºC by the kinetic model and the experimental results

Before the kinetic studies of CO_2 methanation at low conversion it was assumed the methane formed from CO methanation could be neglected, as the source of CO was the reverse water-gas shift reaction and it was being limited. Through the simulation of the reactor, it was possible to predict this contribution by calculating the amount of methane formed from CO methanation as only CO_2 is present at the inlet.

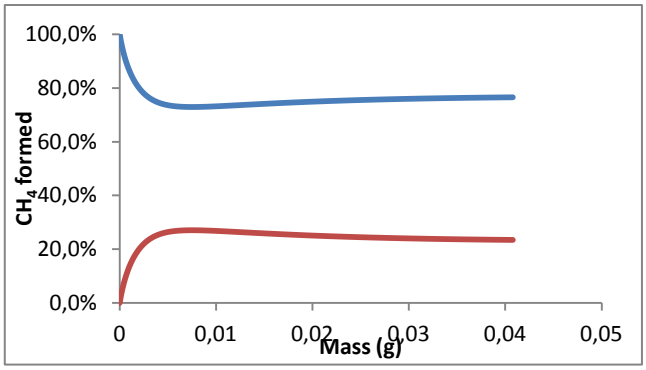

Figure 73: Profile of the amount of methane formed from CO (—) and CO_2 (—) methanation at 425ºC

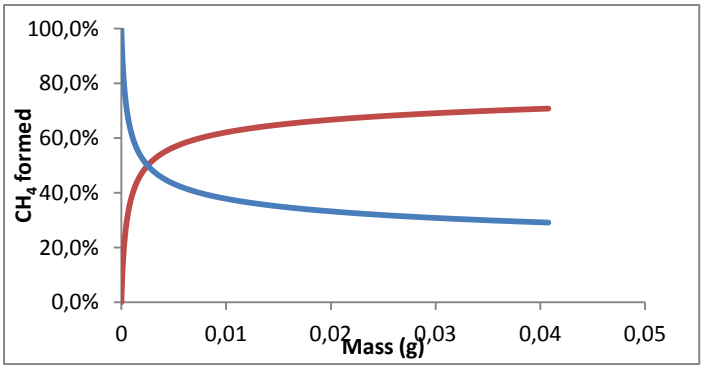

Figure 74: Profile of the amount of methane formed from CO (—) and CO_2 (—) methanation at 325ºC

At the beginning, it was expected that the main part of CO_2 will form methane and only a small part would react to give CO. On the other hand, it was expected the catalyst would perform preferably CO_2 methanation instead of CO methanation. However, it is observed in the previous figures that the contribution of CO for the formation of methane is significant at lower masses, this means at low conversion of CO_2. This can be confirmed by the Figure 61 where it is observed a big increase of the flow rate of CO in the beginning of the catalytic bed and then its fast decrease, suggesting the consumption of CO to form methane. Also it was observed a similar formation of CH_4 and CO in CO_2 methanation. This implies that the assumption made in the beginning is not valid.

In order to have a better perception of the predictability of the models proposed, it was compared the values of the conversions and the yields of methane for CO and CO_2 methanation in parity plots, i.e., the experimental values were represented in function of the ones calculated by the models.

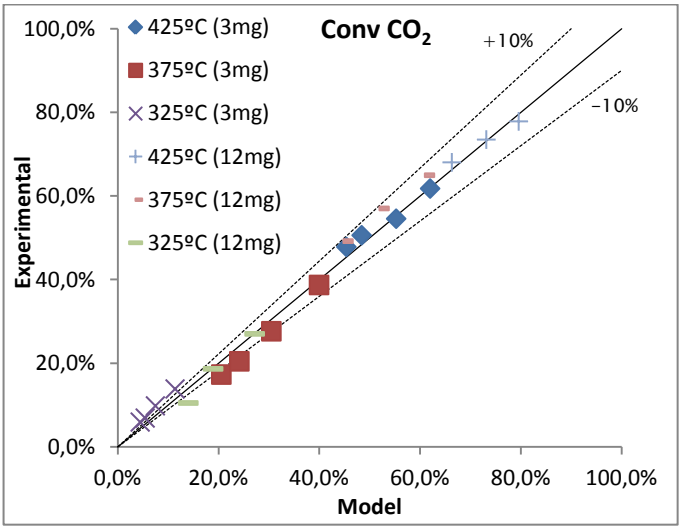

Figure 75: Comparison of the values of conversion of CO_2 with only CO_2 at the inlet

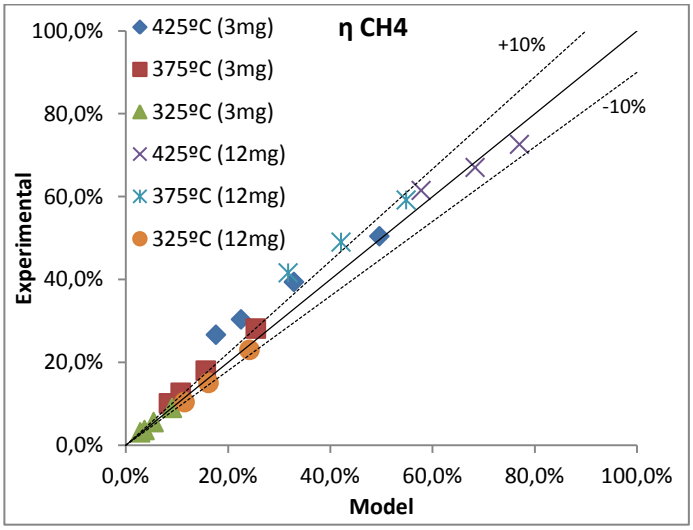

Figure 76: Comparison of the values of the yield of methane with only CO_2 at the inlet

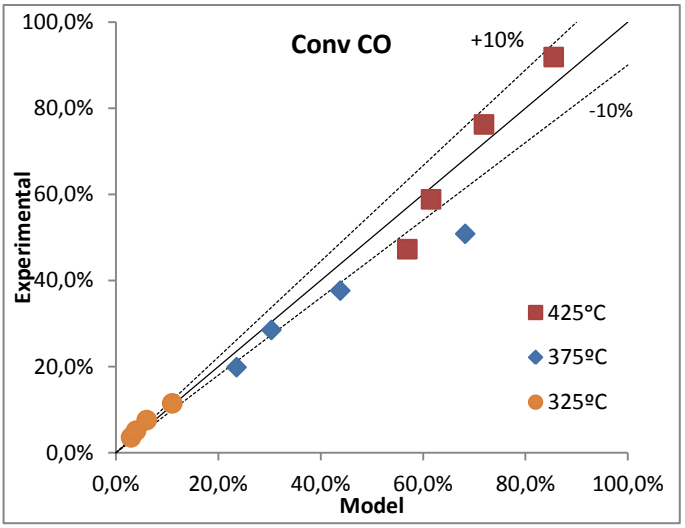

Figure 77: Comparison of the values of conversion of CO with only CO at the inlet

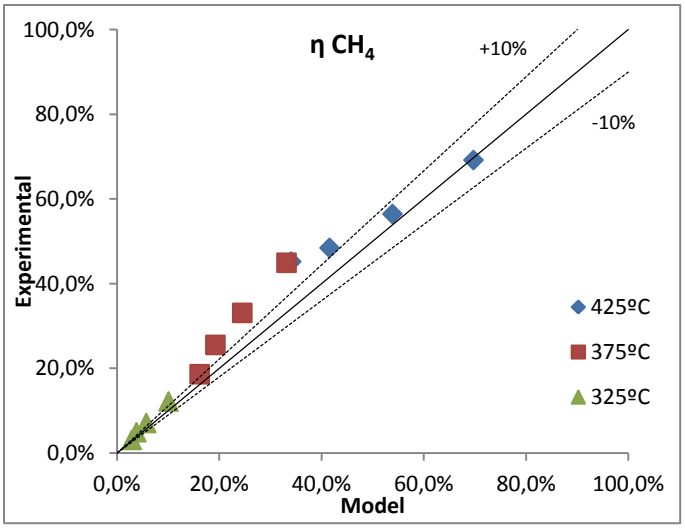

Figure 78: Comparison of the values of the yield of methane with only CO at the inlet

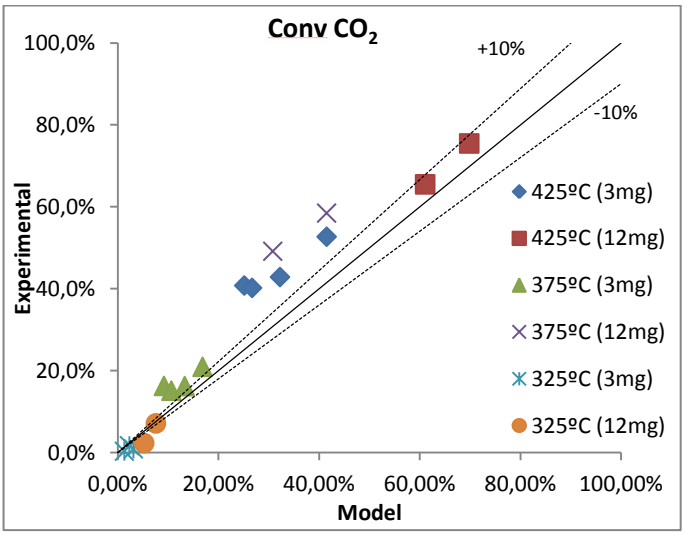

Figure 79: Comparison of the values of conversion of CO_2 with CO_2 and CO at the inlet

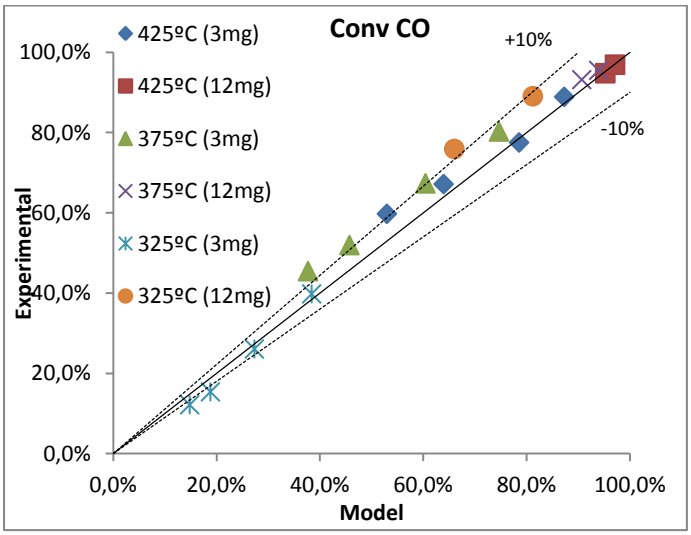

Figure 80: Comparison of the values of conversion of CO with CO_2 and CO at the inlet

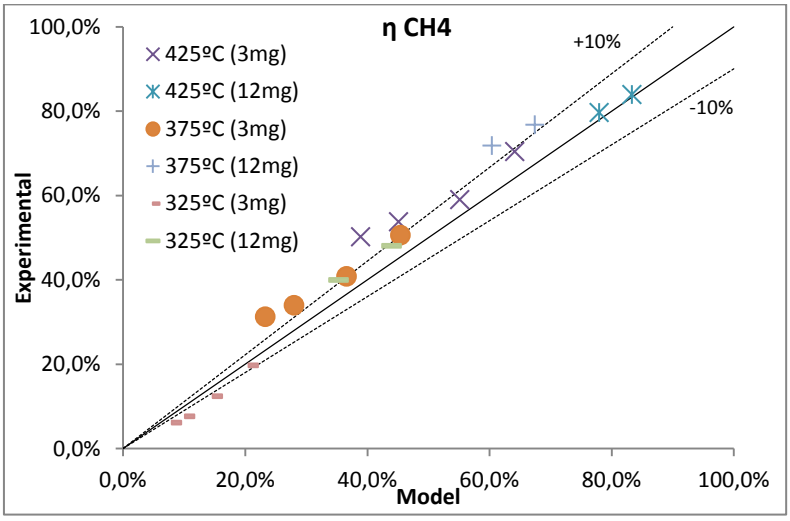

Figure 81: Comparison of the values of yield of methane with CO_2 and CO at the inlet

5. Temperature study

During the experiments, the temperature of the reactor was kept constant by changing the set point of the controller of the oven, in order to maintain the temperature at the outlet in the desired value.

As, in reality, the reactor is polytropic, it was studied the profile of the temperature by an enthalpic balance and assuming heat transfer trough its walls. For that, the temperature of the outlet of each CSTR reactor was calculated considering it as a cylinder and taking into account the thermal conductivity of pirex glass. The kinetic constants were corrected for the temperature of each small reactor.

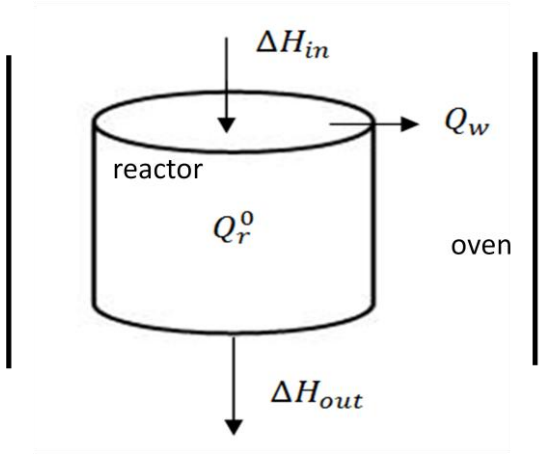

Figure 82: Scheme of the enthalpic balance to the reactor, considering the inlet enthalpy (ΔH_{in}), the outlet enthalpy (ΔH_{out}), the heat released by the reaction (Q_r^0) and the heat transferred through the walls (Q_w)

$$\Delta H_{in} + Q_r^0 = \Delta H_{out} + Q_w \qquad (70)$$

In this study it was not considered the convection inside and outside of the reactor nor even the radial and axial heat transfer of the catalytic bed due to the temperature gradient between the layers. This was admitted since all the experiments were realized with a catalytic bed diluted in SiC. Some examples of the profile temperature are presented next.

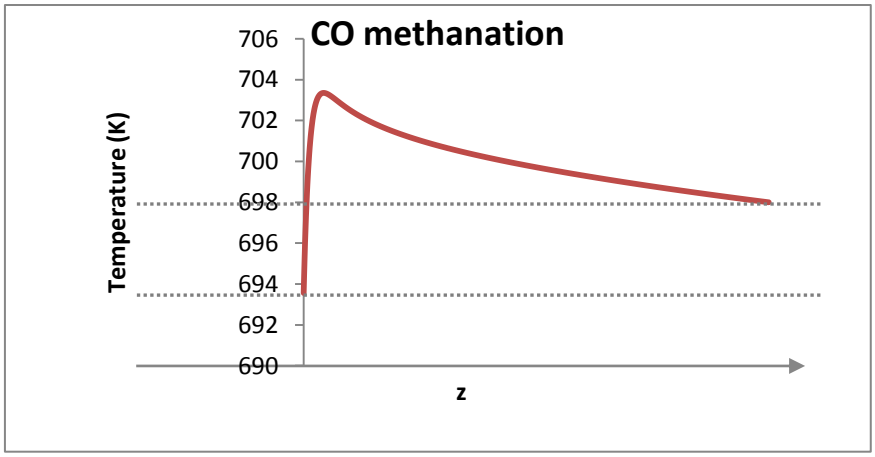

Figure 83: Profile temperature of CO methanation at a conversion of 45% at 425ºC with a low mass

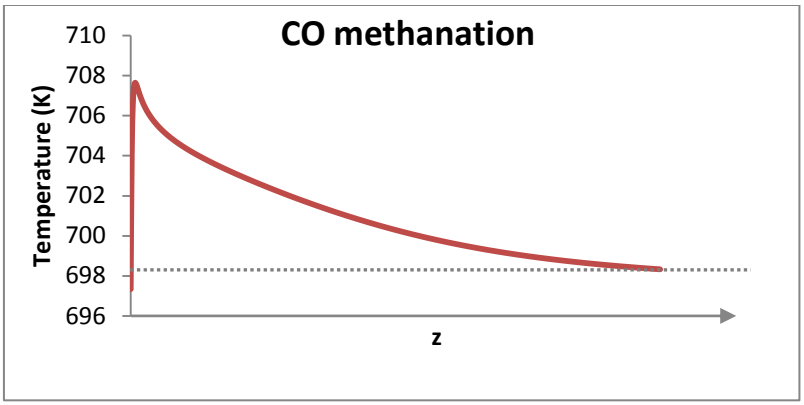

Figure 84: Profile temperature of CO methanation at a conversion of 92% at 425ºC with a high mass

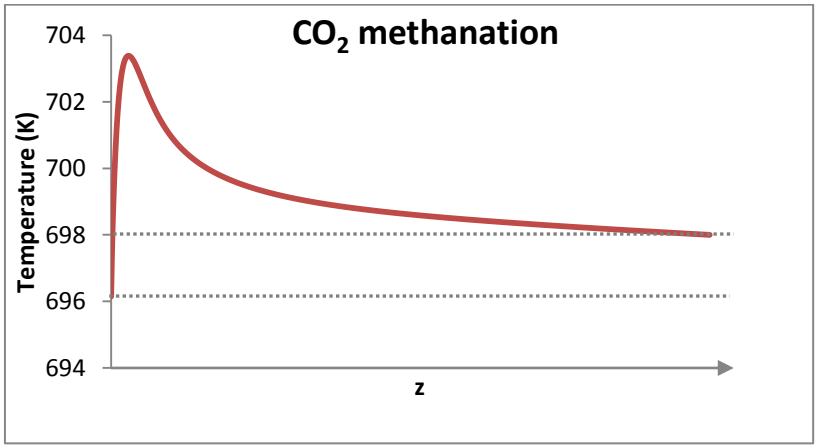

Figure 85: Profile temperature of CO_2 methanation at a conversion of 47% at 425ºC with a low mass

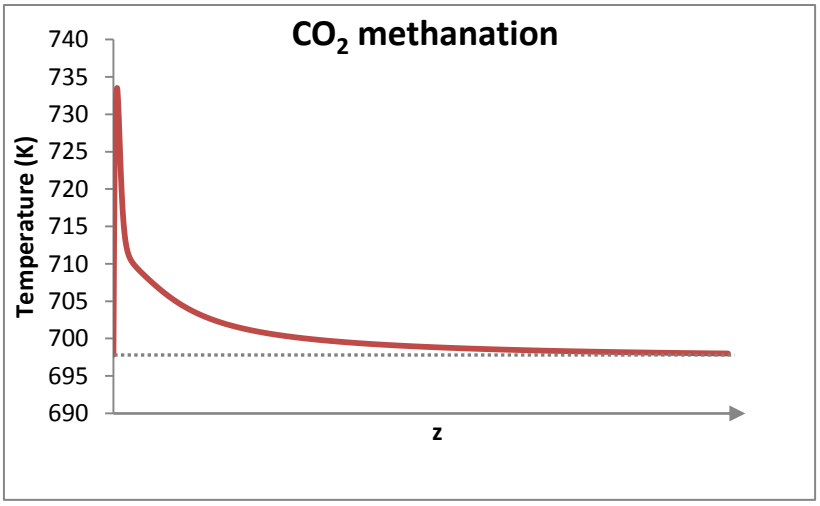

Figure 86: Profile temperature of CO_2 methanation at a conversion of 79% at 425ºC with a high mass

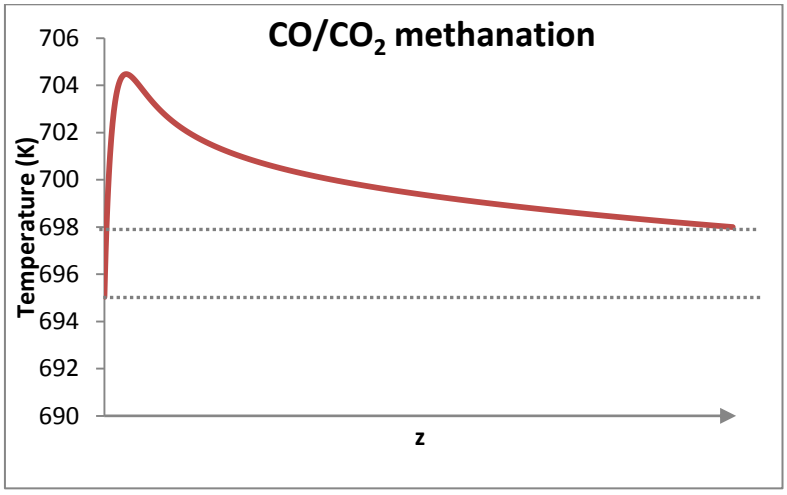

Figure 87: Profile temperature of CO/CO_2 methanation at a conversion of COx of 32% at 425ºC with a low mass

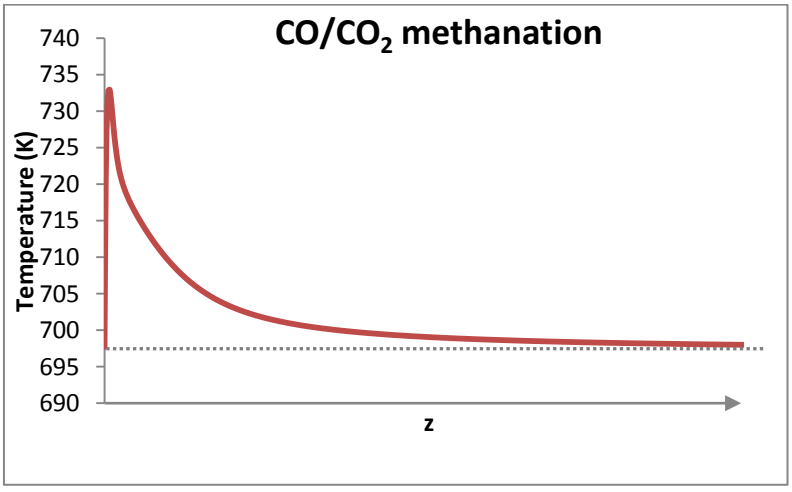

Figure 88: Profile temperature of CO/CO_2 methanation at a conversion of COx of 86% at 425ºC with a high mass

Considering an inlet temperature equal to the one registered during the experiments at the outlet, it was observed this last one was higher than the expected one. So, the inlet temperature was calculated by iterations in order to maintain the value of the exit of the catalytic

bed desired. This difference is inexistent in the experiments with higher catalyst mass and low flow rate and increases to 4ºC for the smallest mass with high flow rate. As it was expected the opposite as the smallest masses have higher dilution in SiC, it can be concluded this difference is due to the reactivity that occurs in all layers of the catalytic bed, i.e., the reactions occur in the beginning of the catalytic bed and the its final layers act as a dispersant of the heat. In the cases where the catalytic bed is small, all the layers are involved in the reaction, and so there is not a good dispersion of the heat. This could be avoided by increasing the amount of SiC of the catalytic bed.

However, the previsions of the isothermal and non-isothermal models are similar (see some examples in annex), possibly due to the presence of SiC. This observation is consistent with the results of the external diffusion limitation test, i.e., it was observed no difference in the reaction rate with the increase of the mass, what means the superheat observed in the first layers of the catalytic bed does not influence the activity of the catalyst.

6. Conclusions

Extended literature review on the studies of CO_2 methanation and reverse water-gas shift allowed to establish the possible mechanisms involved in these reactions and their kinetic models, always taking into account the type of catalyst used and the nature of the active sites.

After some characterization of the industrial catalyst used, to better understand its properties and the adequate treatment of reduction, the kinetic tests were realized. As in the CO_2 methanation also occurs reverse water-gas shift in parallel, and due to this one, where CO is formed, it also occurs CO methanation, it was important to verify the influence of all the compounds present in the reactor in the kinetics of the three reactions.

The experimental data obtained for CO_2 methanation was tested in the models found in literature and it showed that none of them was appropriate to describe the kinetic of the reactions in this catalyst. However, a model proposed for water-gas shift by Wheeler *et al* showed to be very accurate with the results obtained. It was also used the same model for CO methanation and reverse water-gas shift. Although it seemed a good model for RWGS, it doesn't describe a redox mechanism as it is suggested in the literature, and as it is possible to observe no influence of hydrogen in the reaction. For that, a redox model was proposed and tested and it showed to be the best one for the purpose.

The three models were also tested in the presence of the products at the inlet, where it was possible to observe that it is more likely to occur dissociative adsorption of water than molecular one. This was the only alteration at the original model of Wheeler *et al*, and it was also suitable for the redox model for RWGS.

Finally, all the models were simulated in an isothermal plug flow reactor and compared with the experimental data. The kinetic parameters calculated previously were adjusted to better describe the results expected.

Through the results obtained it can be concluded the catalyst is more reactive to CO when there is a mixture of CO_2 and CO at the inlet, being necessary less mass of catalyst to reach the thermodynamic equilibrium. This is proven by the case where there is only CO_2 at the inlet, where there is formation of CO at the beginning and then its fast consumption. As the only source of CO in this case is from reverse water-gas shift, the CO_2 forms preferentially CO than CH_4. It is also observed the methane formed has a significant contribution of CO methanation, what implies the assumption made in the beginning of the catalytic test is not valid. This can be a possible explanation for the need of such big adjustment of the kinetic parameters.

In reality, it is difficult to have a totally isothermal reactor, as there is heat transfer through the walls, convection inside and outside of the reactor and a radial and axial diffusion of the heat through the catalytic bed. The first aspect was taken into account in a simulation of a non-isothermal plug flow reactor. All the others were neglected due to difficulty in its calculation. It was observed a strong increase of the temperature in the first layers of the catalytic bed (when the amount of catalyst is significantly high) and a diffusion of the heat performed by the end of the catalytic bed. The difference between the inlet and outlet temperature was observed experimentally.

References

[1] "Topsoe," [Online]. Available: http://www.topsoe.com/sites/default/files/henriksen.pdf. [Accessed June 2016].

[2] "ITM Power," [Online]. Available: http://www.itm-power.com/sectors/power-to-gas-energy-storage. [Accessed June 2016].

[3] "Hydrogenics," [Online]. Available: http://www.hydrogenics.com/hydrogen-products-solutions/energy-storage-fueling-solutions/power-to-gas. [Accessed June 2016].

[4] "CEA," [Online]. Available: http://www.cea.fr/presse/Pages/actualites-communiques/energies/Stockage-electricite-CEA-participe-au-projet-Power-to-Gas-Jupiter-1000-.aspx. [Accessed June 2016].

[5] "E.ON," [Online]. Available: http://www.eon.com/en/media/news/press-releases/2014/9/1/eon-power-to-gas-pilot-unit-falkenhagen.html. [Accessed June 2016].

[6] L. Dietz, "Thesys "First-Principles Assessment of CO2 activation over metal catalysts"," Trieste, Italy, 2012-2013.

[7] S. Rönsch, J. Schneider, S. Matthischke, M. Schlüter, M. Götz, J. Lefebvre, P. Prabhakaran and S. Bajohr, "Review on methanation - From fundamentals to current projects," *Fuel*, vol. 166, pp. 276-296, 2015.

[8] T. Schaaf, J. Grünig, M. R. Schuster, T. Rothenfluh and A. Orth, "Methanation of CO2 - storage of renewable energy in a gas distribution system," *Energy, Sustainability and Society - SpringerOpen Journal*, pp. 1-14, 2014.

[9] "Webbook," [Online]. Available: http://webbook.nist.gov/chemistry/. [Accessed February 2016].

[10] D. J. Darensbourg, C. G. Bauch and C. Ovalles, "Mechanistic Aspects of Catalytic Carbon Dioxide Methanation," *Reviews in Inorganic Chemistry*, vol. 7 No. 4, pp. 315-339, 1985.

[11] S. Medsforth, "Promotion of Catalytic Reactions," *J. Chem. Soc., Trans.*, vol. 123, pp. 1542-1469, 1923.

[12] T. V. Herwijnen, H. V. Doesburg and W. A. Jong, "Kinetics of the Methanation of CO and CO2 on a Nickel Catalyst," *Journal of Catalysis*, vol. 28, pp. 391-402, 1973.

[13] B. R. Franko, G. Gruber, L. Seglin and R. Geosits, "Survey of Methanation Chemistry and Processes," in *Methanation of Synthesis Gas*, Len Seglin, 1975, pp. 1-30.

[14] V. M. Vlasenko and G. E. Uzefovich, *Russ. Chem. Rev.*, vol. 38 , no. 9, p. 728, 1969.

[15] G. G. Binder and R. R. White, *Chem. Eng. Prog.* , vol. 46, no. 11, p. 563, 1950.

[16] J.-A. Dalmon and G. A. Martin, "Intermediates in CO and CO2 hydrogenation over Ni catalysts," *J. Chem. Soc., Faraday Trans. 1,* vol. 75, pp. 1011-1015, 1979.

[17] C. H. Bartholomew and G. D. Weatherbee, "Hydrogenation of CO2 on Group VIII Metals - Kinetics and Mechanism of CO2 Hydrogenation on Nickel," *Journal of Catalysis,* vol. 77, pp. 460-472, 1982.

[18] J. Xu and G. F. Froment, "Methane Steam Reforming, Methanation and Water-Gas Shift: I. Intrinsic Kinetics," *AIChE Journal,* vol. 35, no. 1, pp. 88-96, January 1989.

[19] Z. A. Ibraeva, N. V. Nekrasov, B. S. Gudkov, V. I. Yakerson, Z. T. Beisembaeva, E. Z. Golosman and S. L. Kiperman, "Kinetics of Methanation of Carbon Dioxide on a Nickel Catalyst," *Theoretical and Experimental Chemistry,* vol. 26, no. 5, pp. 584-588, 1991.

[20] J. Gao, Q. Liu, F. Gu, B. Liu, Z. Zhong and F. Su, "Recent advances in methanation catalysts for the production of synthetic natural gas," *RSC Advances,* vol. 5, no. 29, pp. 22759-22776, 2015.

[21] P. A. Aldana, F. Ocampo, K. Kobl, B. Louis, F. Thibault-Starzyk, M. Daturi, P. Bazin, S. Thomas and A. C. Roger, "Catalytic CO2 valorization into CH4 on Ni-based ceria-zirconia. Reaction mechanism by operando IR spectroscopy," *Catalysis Today,* vol. 215, pp. 201-207, 2013.

[22] F. Koschany, D. Schlereth and O. Hinrichsen, "On the kinetics of the methanation of carbon dioxide on coprecipitated NiAl(O)x," *Applied Catalysis B: Environmental,* vol. 181, pp. 504-516, 2016.

[23] J. Kopyscinski, T. J. Schildhauer, F. Vogel, S. Biollaz and A. Wokaun, *J. Catal.* , vol. 271, pp. 262-279, 2010.

[24] W. M. Graven and F. J. Long, "Kinetics and Mechanisms of the Two Opposing Reactions of the Equilibrium CO+ H2O=CO2+H2," *J. Am. Chem. Soc.,* vol. 76, no. 10, pp. 2602-2607, 1954.

[25] D. C. Grenoble and M. M. Estadt, "The Chemistry and Catalysis of the Water Gas Shift Reaction," *Journal of Catalysis,* vol. 67, pp. 90-102, 1981.

[26] C. Wheeler, A. Jhalani, E. J. Klein, S. Tummala and L. D. Schmidt, "The water-gas-shift reaction at short contact times," *Journal of Catalysis,* vol. 223, pp. 191-199, 2004.

[27] C. A. Callaghan, *Kinetics and Catalysis of the Water-Gas-Shift Reaction: A Microkinetic and Graph Theoretic Approach,* Worcester Polytechnic Institute, 2006.

[28] M. I. Temkin, "The kinetic of some industrial heterogeneous catalytic reactions," in *Advances in Catalysis,* New York, Academic Press, 1979, p. 173.

[29] R. J. Byron Smith, L. Muruganandam and S. S. Murthy, “A Review of the Water Gas Shift Reaction Kinetics,” *International Journal of Chemical Reactor Engineering,* vol. 8, pp. 1-32, 2010.

[30] M. L. Ang, U. Oemar, Y. Kathiraser, E. T. Saw, C. K. Lew, Y. Du, A. Borgna and S. Kawi, “High-temperature water-gas shift reaction over Ni/xK/CeO2 catalysts: Suppression of methanation via formation of bridging carbonyls,” *Journal of Catalysis,* vol. 329, pp. 130-143, 2015.

[31] A. Mohsenzadeh, T. Richards and K. Bolton, “DFT study of the water gas shift reaction on Ni(111), Ni(100) and Ni(110) surfaces,” *Surface Science,* vol. 644, pp. 53-63, 2016.

[32] D. Brennan and F. H. Hayes, “HEat of adsorption of hydrogen on evaporated films of tungsten and of nickel,” *Trans. Faraday Soc.,* vol. 60, pp. 589-596, 1964.

[33] C. H. Bartholomew, “Hydrogen Adsorption on Supported Cobalt, Iron, and Nickel,” *Catalysis Letters,* vol. 7, pp. 27-52, 1990.

[34] T. Panczyk, S. Pawel and W. Rudzinski, “Hydrogen Adsorption on Nickel (100) Single-Crystal Face. A Monte Carlo Study of the Equilibrium and Kinetics,” *J. Phys. Chem. B,* vol. 109, pp. 10986-10994, 2005.

[35] J. T. Richardson and T. S. Cale, “Interpretation of Hydrogen Chemisorption on Nickel Catalysts,” *Journal of Catalysis,* vol. 102, no. 2, pp. 419-432, 1986.

[36] S.-G. Wang, D.-B. Cao, Y.-W. Li, J. Wang and H. Jiao, “Chemisorption of CO2 on Nickel Surfaces,” *J. Phys. Chem. B,* vol. 109, pp. 18956-18963, 2005.

[37] M. Rizzi, *Carbon dioxide adsorption and hydrogenation on nickel-based surfaces: a first principles study,* Università degli Studi di Trieste, 2011.

[38] H. Freund and M. W. Roberts, “Surface Chemistry of Carbon Dioxide,” *Surface Science Reports,* vol. 25, pp. 225-273, 1996.

[39] T. Kwan and Y. Fujita, “Adsorption of Carbon Dioxide on Metal Catalysts,” *Chemical Society of Japan,* vol. 24, no. 1, pp. 46-50, 1961.

[40] A. Cabrera, W. Garrido and U. Volkmann, “Studies of carbon monoxide and hydrogen adsorption on nickel and cobalt foils aimed at gaining a better insight into the mechanism of hydrocarbon formation,” *Catalysis Letters,* vol. 25, pp. 115-126, 1994.

[41] M. M. Baker and E. K. Rideal, “The adsorption of carbon monoxide by nickel,” *Trns. Faraday Soc.,* vol. 51, pp. 1597-1601, 1955.

[42] Beeck, “Advances in Catalysis,” *Academic Press N.Y.,* vol. 2, 1950.

G. Ertl, H. Knözinger, F. Schüth and J. Weitkamp, “Characterization of Solid
43] Catalysts,” in *Handbook of Heterogeneous Catalysis Vol 1*, Wiley-VCH, pp. 723-726.

Appendices

A) Patterns obtained by XRD of the samples tested

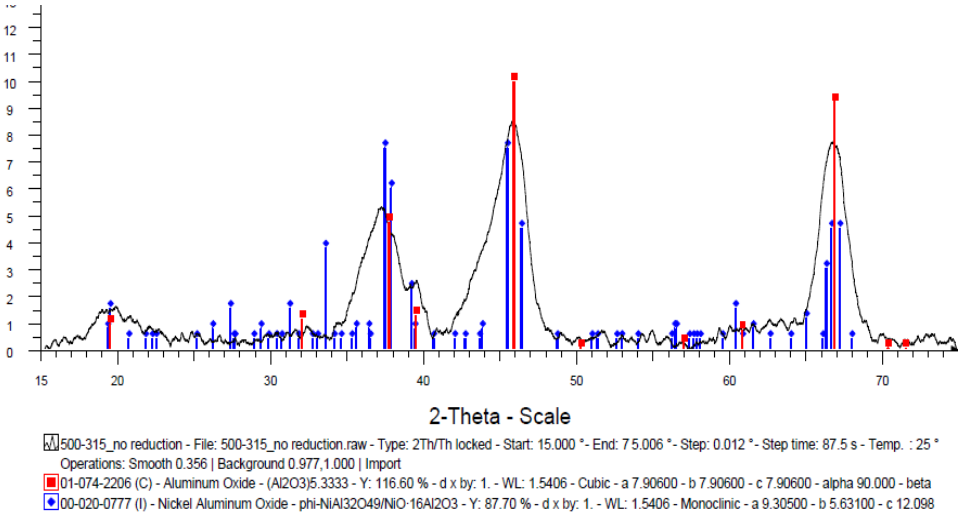

Figure A-1: Pattern of XRD of the sample 500-315 µm without reduction

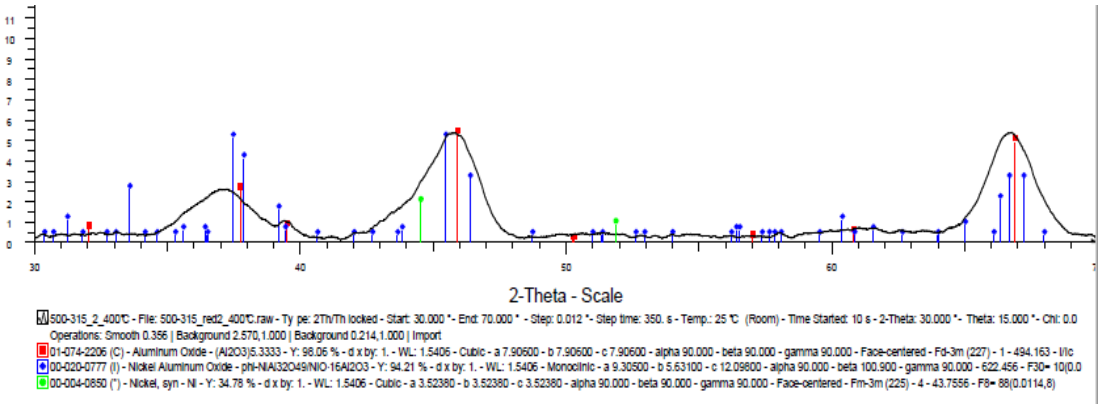

Figure A-2: Pattern of XRD of the sample 500-315 µm after reduction at 400ºC during one hour

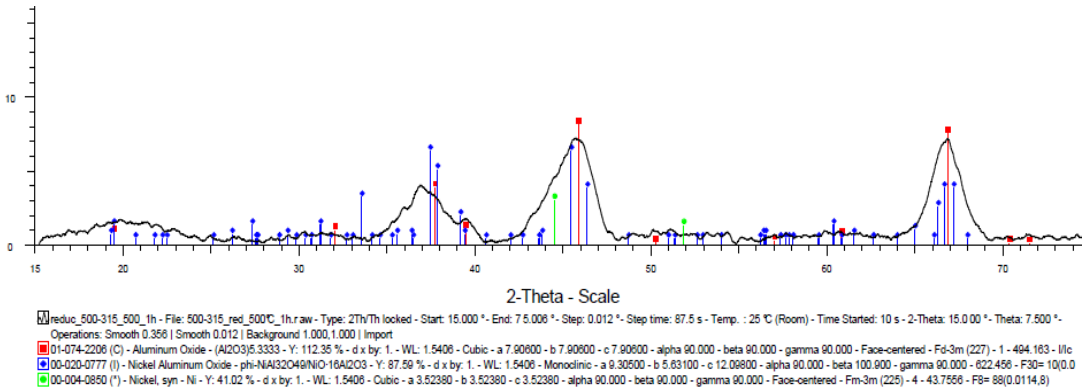

Figure A-3: Pattern of XRD of the sample 500-315 µm after reduction at 500ºC during one hour

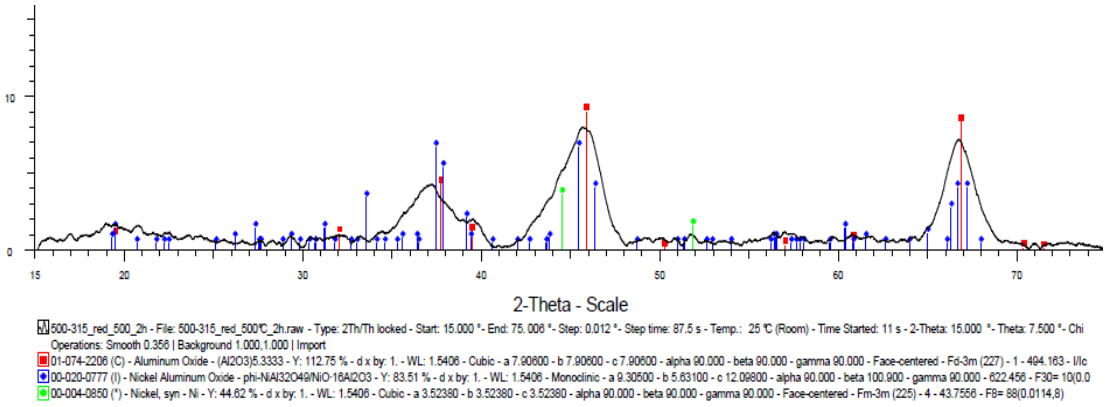

Figure A-4: Pattern of XRD of the sample 500-315 µm after reduction at 500ºC during two hours

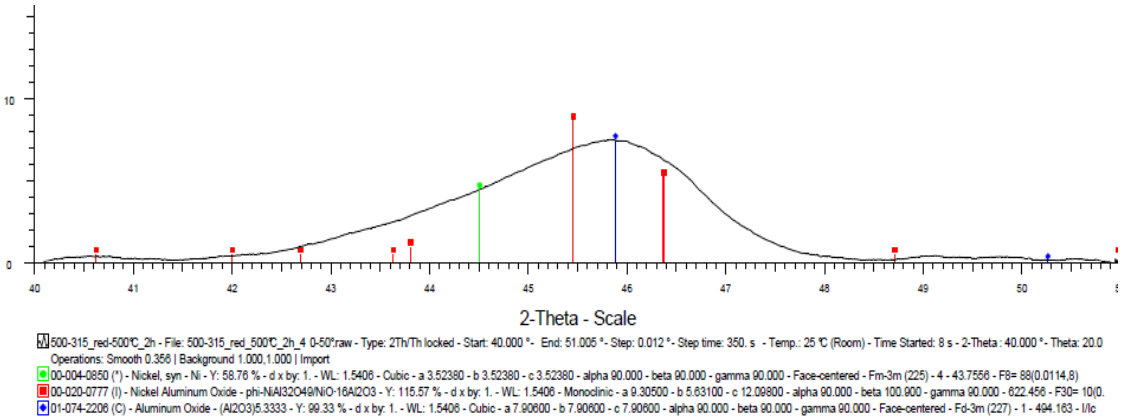

Figure A-5: Pattern of XRD of the sample 500-315 µm after reduction at 500ºC during two hours between 40 and 50º

B) Photos of the reactor

Figure B-1: Mass flow controllers to provide a flow of the components

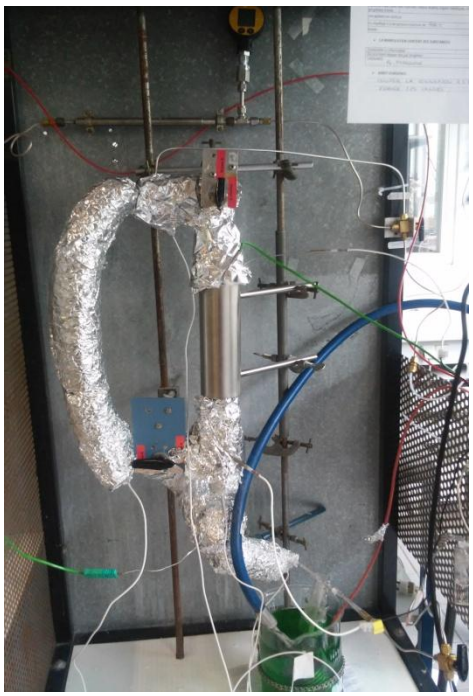

Figure B-2: Reactor involved in the electrical resistance and the cold trap

C) Test of the models presented in literature

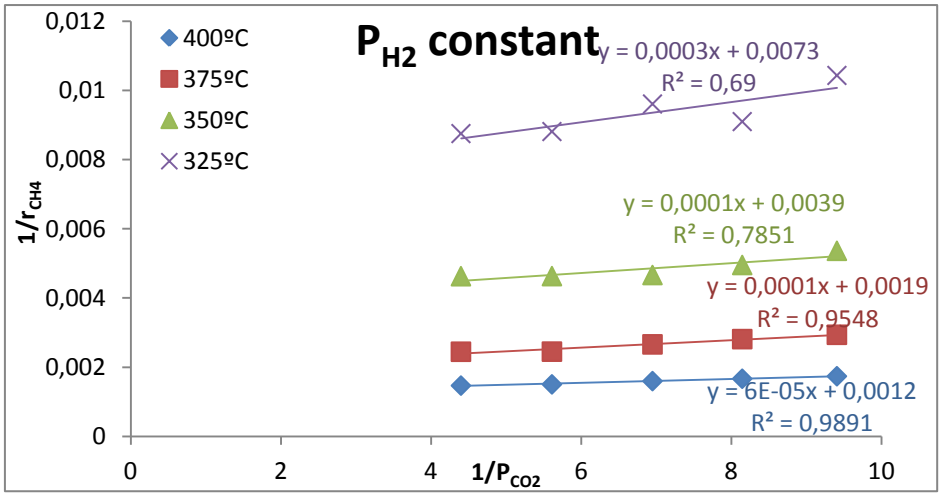

Figure C-1: Test of the model Ibraeva *et al* with constant partial pressure of hydrogen

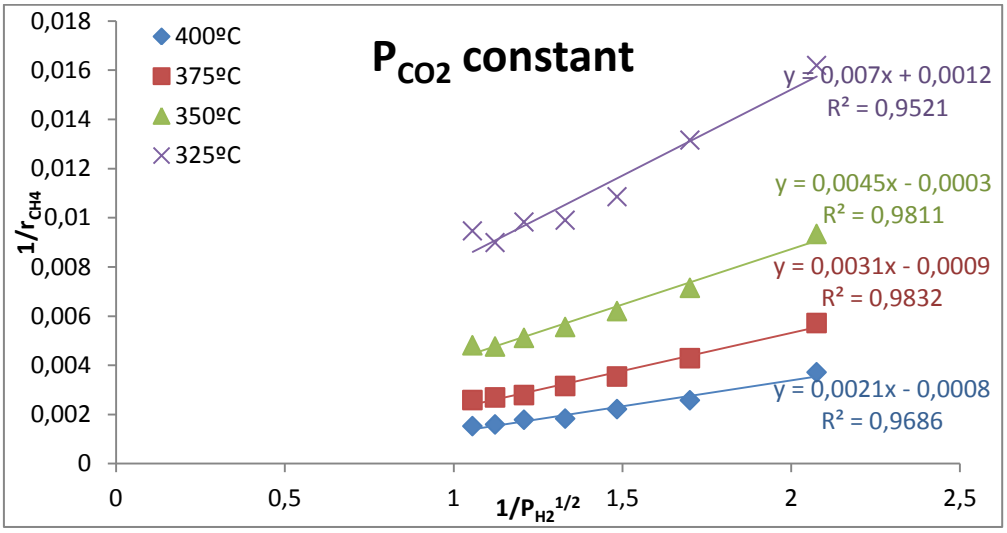

Figure C-2: Test of the model Ibraeva *et al* with constant partial pressure of CO_2

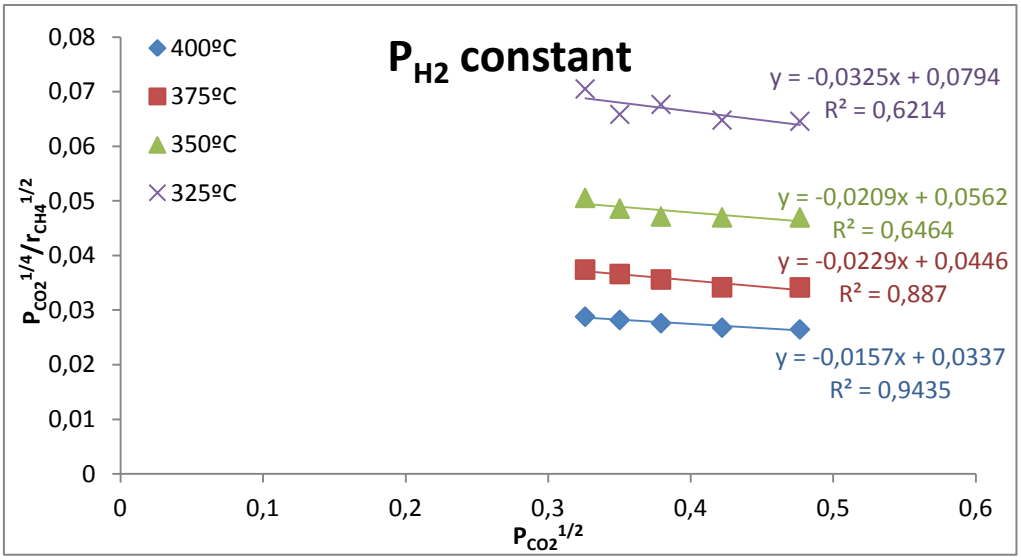

Figure C-3: Test of the model Koschany *et al* with constant partial pressure of hydrogen

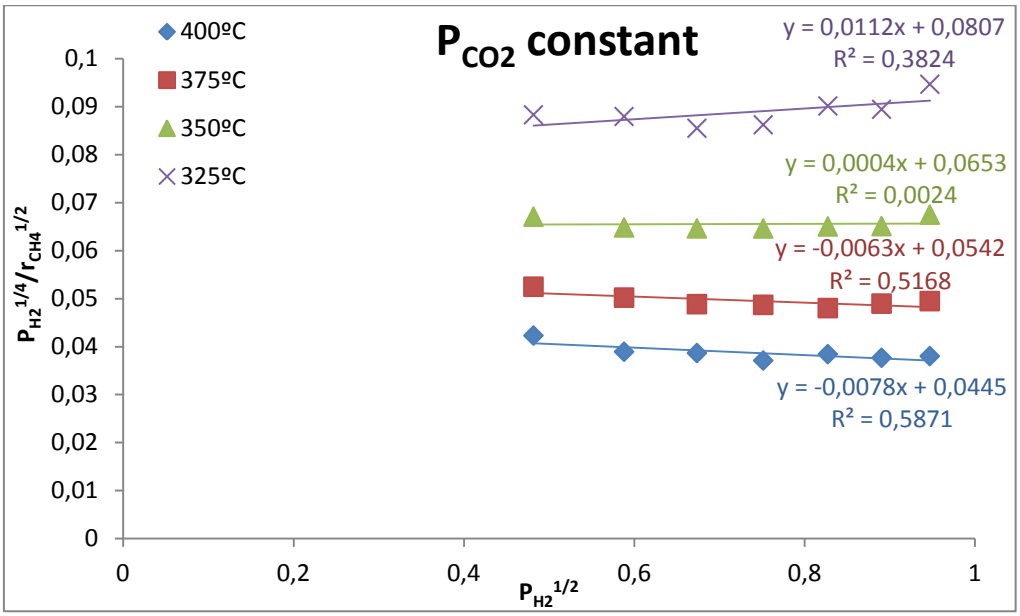

Figure C-4: Test of the model Koschany *et al* with constant partial pressure of CO_2

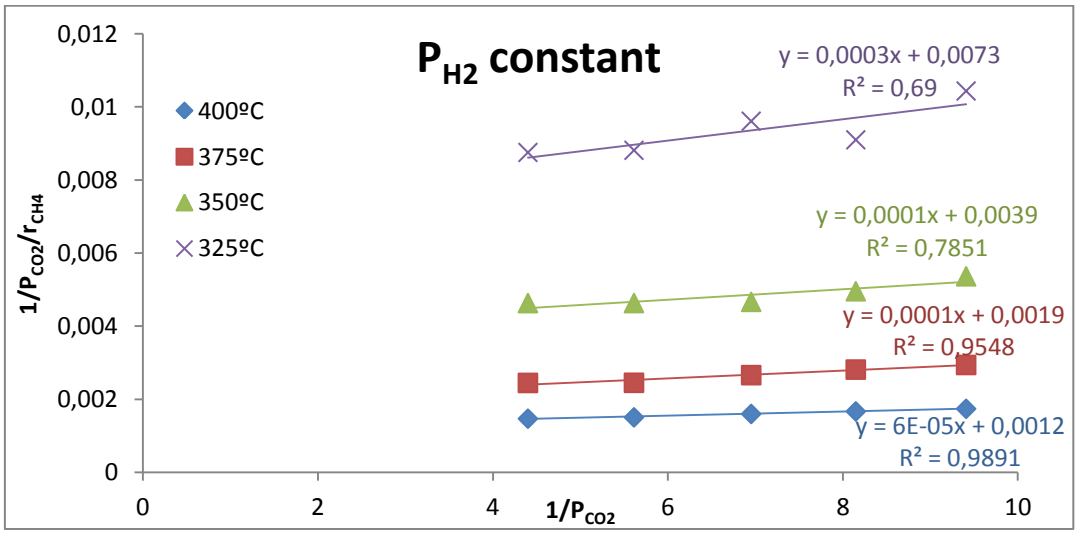

Figure C-5: Test of the model Callaghan with constant partial pressure of hydrogen

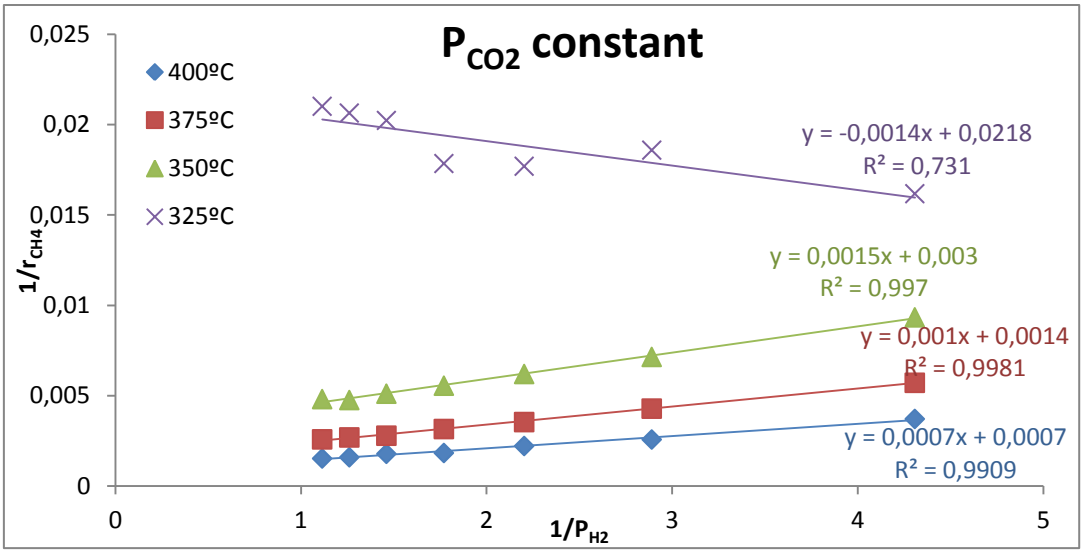

Figure C-6: Test of the model Callaghan with constant partial pressure of CO_2

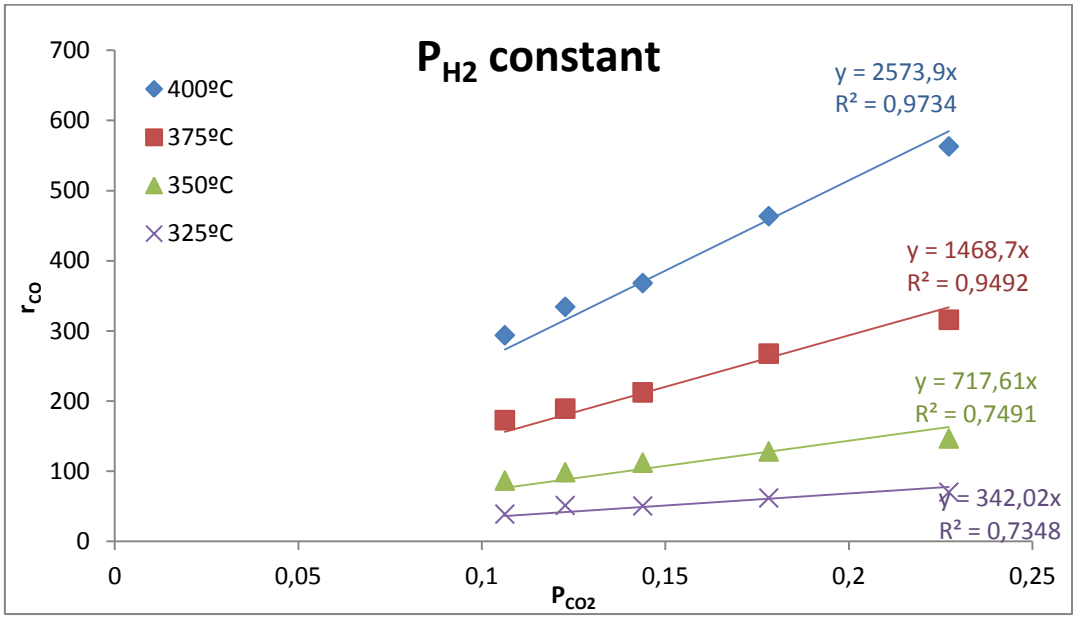

Figure C-7: Test of the model Xu and Froment with constant partial pressure of hydrogen

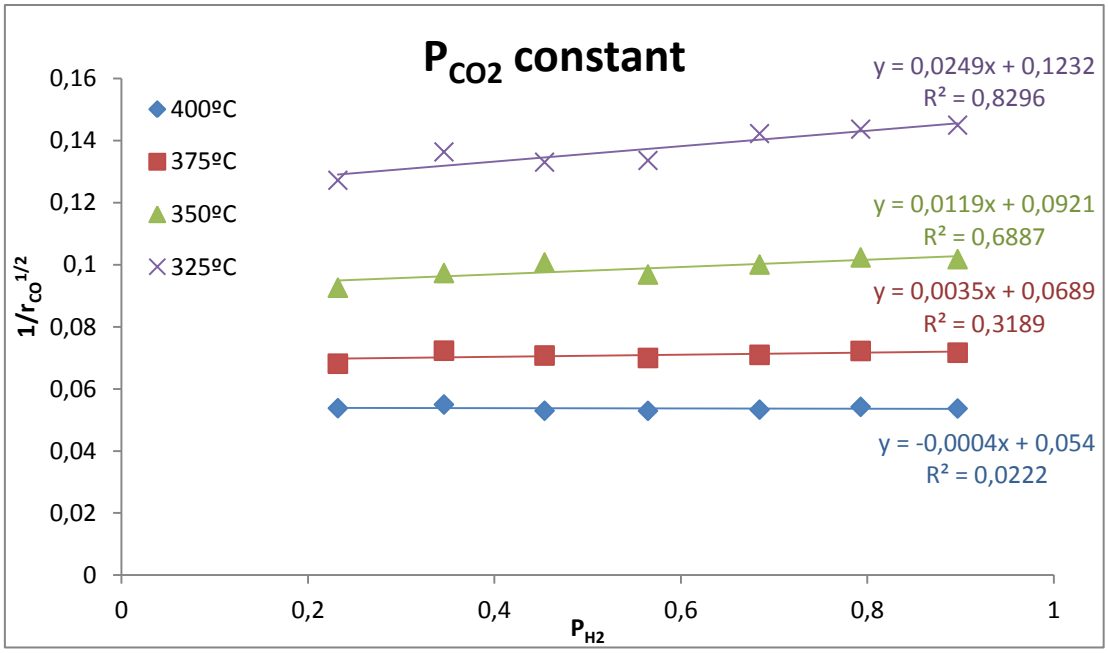

Figure C-8: Test of the model Xu and Froment with constant partial pressure of CO_2

D) Comparison between the model and the experimental results

Next is presented the comparison of the conversions of the reactants given by the experimental test and the models proposed, with different conditions at the inlet.

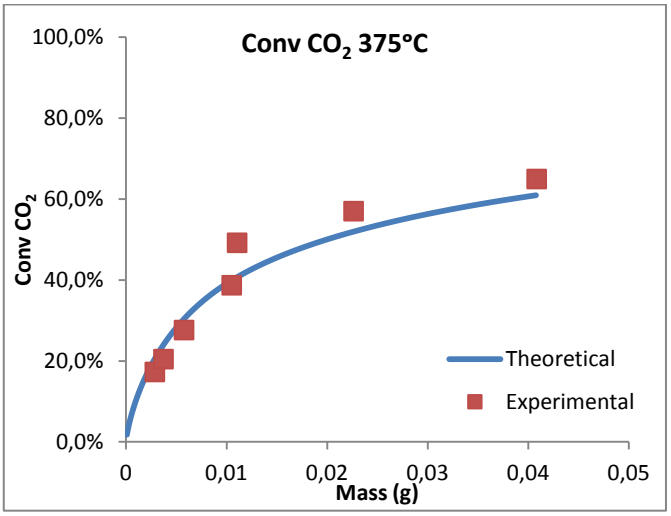

Figure D-1: Behaviour of the experimental and theoretical conversion with only CO_2 at the inlet

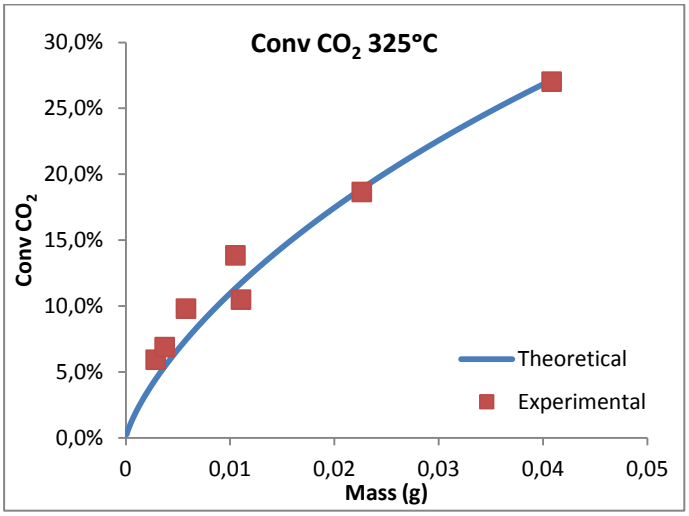

Figure D-2: Behaviour of the experimental and theoretical conversion with only CO_2 at the inlet

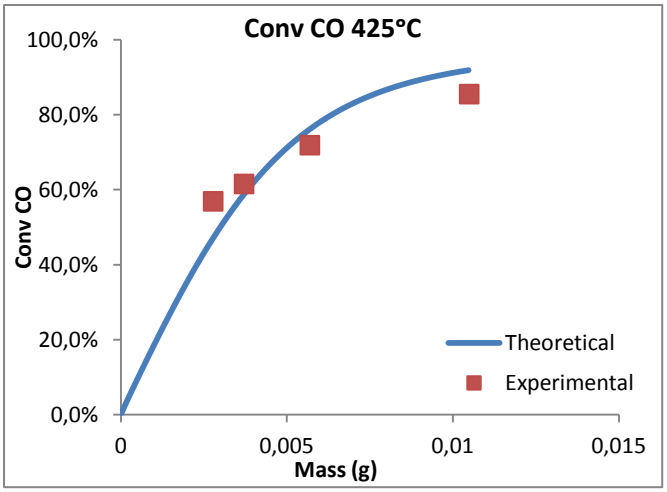

Figure D-3: Behaviour of the experimental and theoretical conversion with only CO at the inlet

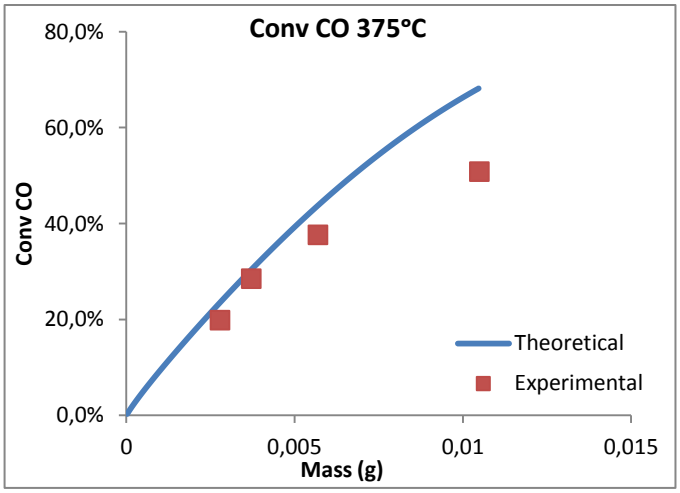

Figure D-4: Behaviour of the experimental and theoretical conversion with only CO at the inlet

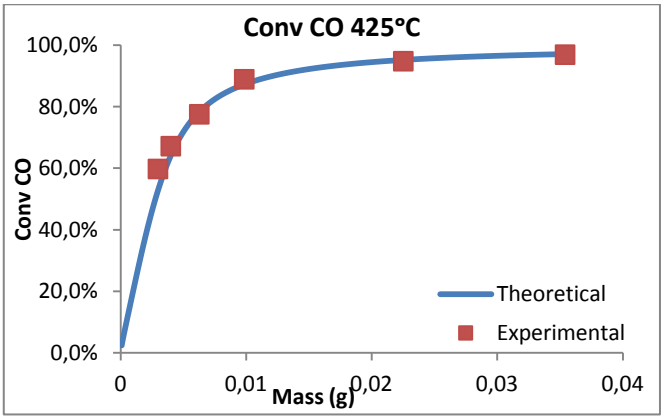

Figure D-5: Behaviour of the experimental and theoretical conversion with CO and CO_2 at the inlet

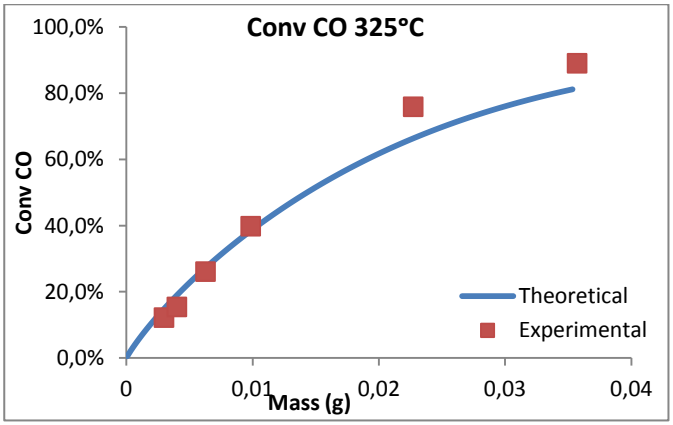

Figure D-6: Behaviour of the experimental and theoretical conversion with CO and CO_2 at the inlet

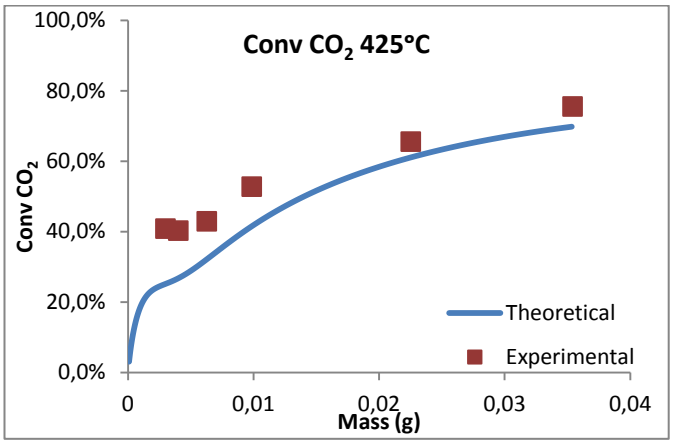

Figure D-7: Behaviour of the experimental and theoretical conversion with CO and CO_2 at the inlet

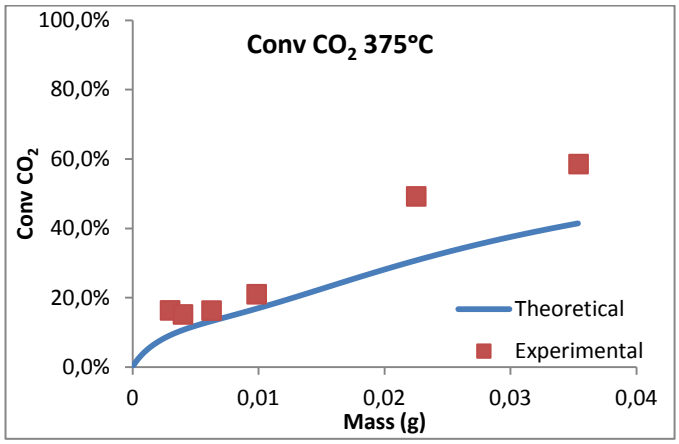

Figure D-8: Behaviour of the experimental and theoretical conversion with CO and CO_2 at the inlet

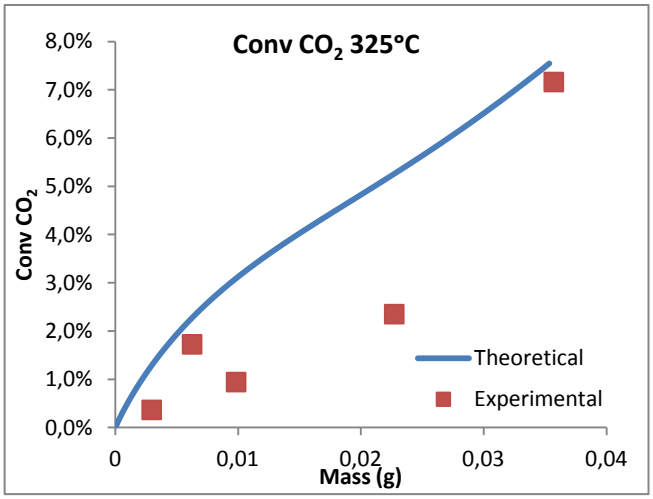

Figure D-9: Behaviour of the experimental and theoretical conversion with CO and CO_2 at the inlet

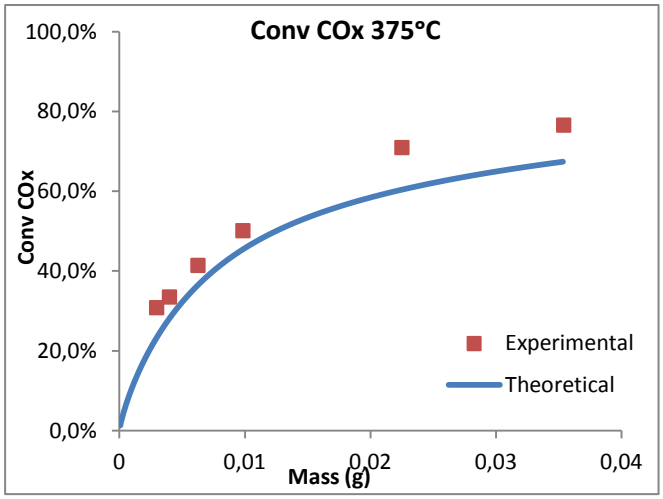

Figure D-10: Behaviour of the experimental and theoretical conversion with CO and CO_2 at the inlet

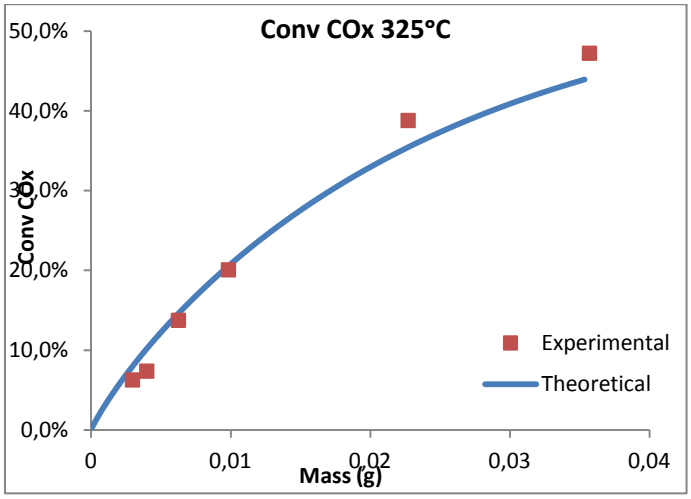

Figure D-11: Behaviour of the experimental and theoretical conversion with CO and CO_2 at the inlet

E) Comparison between the isothermal and non-isothermal models and the experimental results

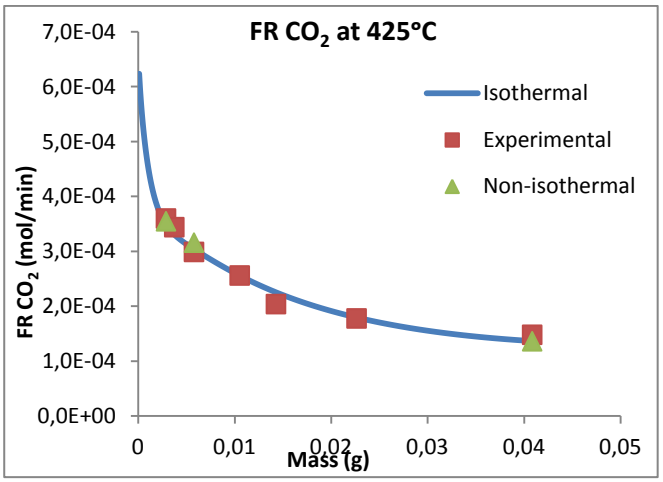

Figure E-1: Behaviour of the experimental and theoretical flow rates with only CO_2 at the inlet

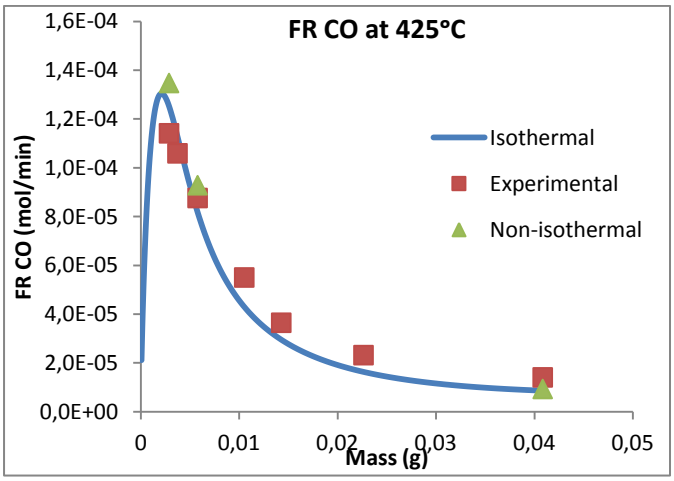

Figure E-2: Behaviour of the experimental and theoretical flow rates with only CO_2 at the inlet

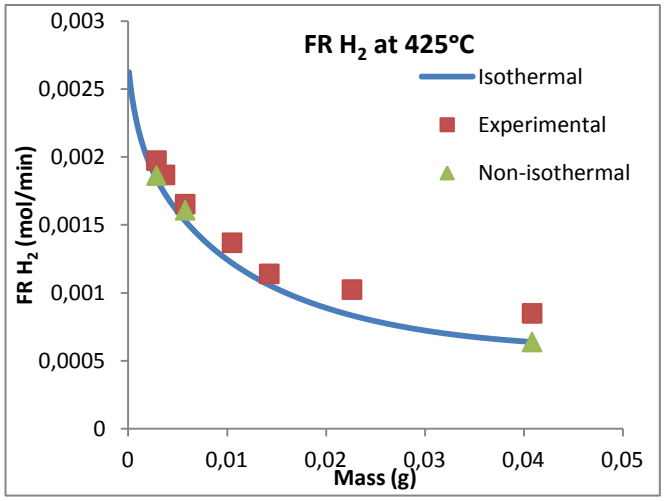

Figure E-3: Behaviour of the experimental and theoretical flow rates with only CO_2 at the inlet

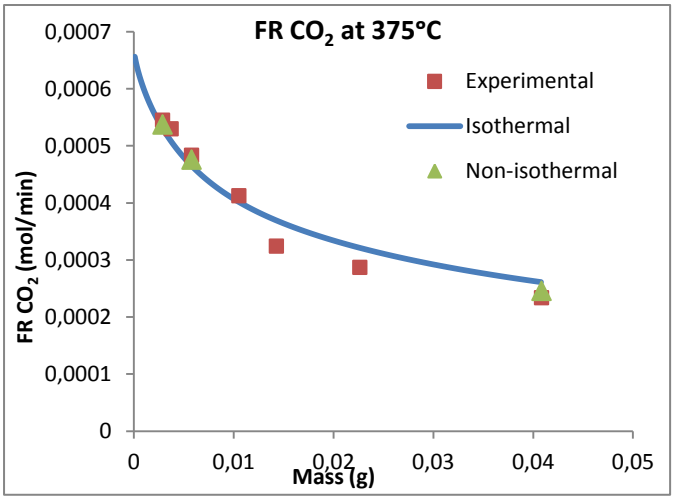

Figure E-4: Behaviour of the experimental and theoretical flow rates with only CO_2 at the inlet

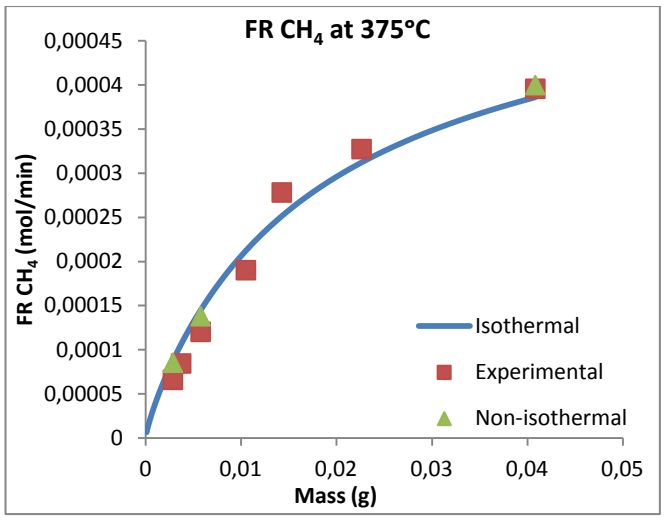

Figure E-5: Behaviour of the experimental and theoretical flow rates with only CO_2 at the inlet

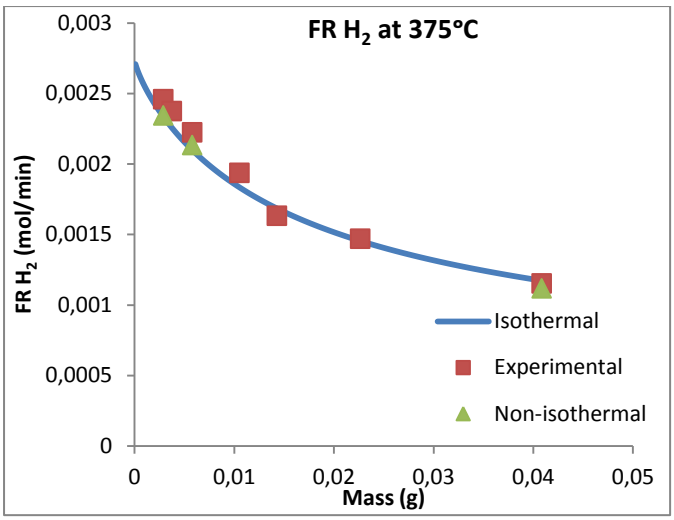

Figure E-6: Behaviour of the experimental and theoretical flow rates with only CO_2 at the inlet

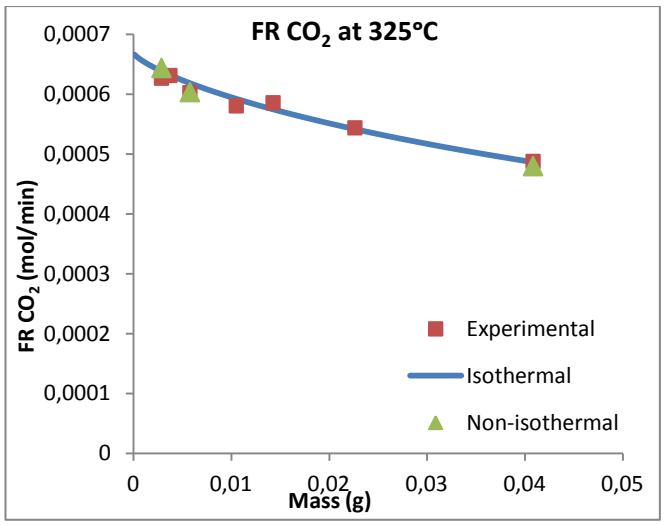

Figure E-7: Behaviour of the experimental and theoretical flow rates with only CO_2 at the inlet

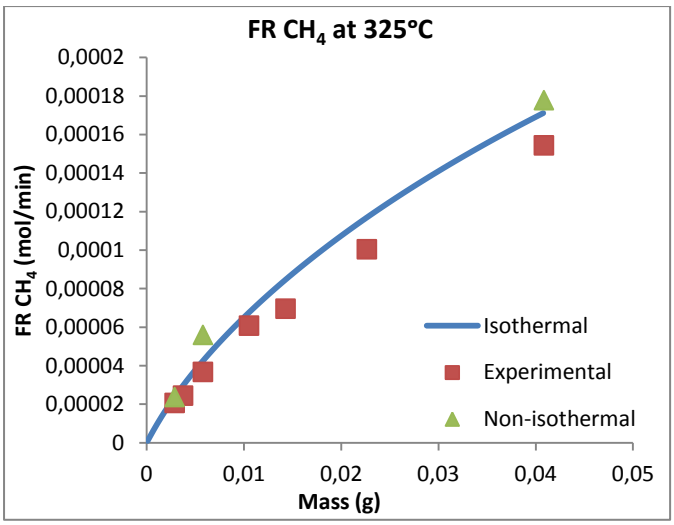

Figure E-8: Behaviour of the experimental and theoretical flow rates with only CO_2 at the inlet

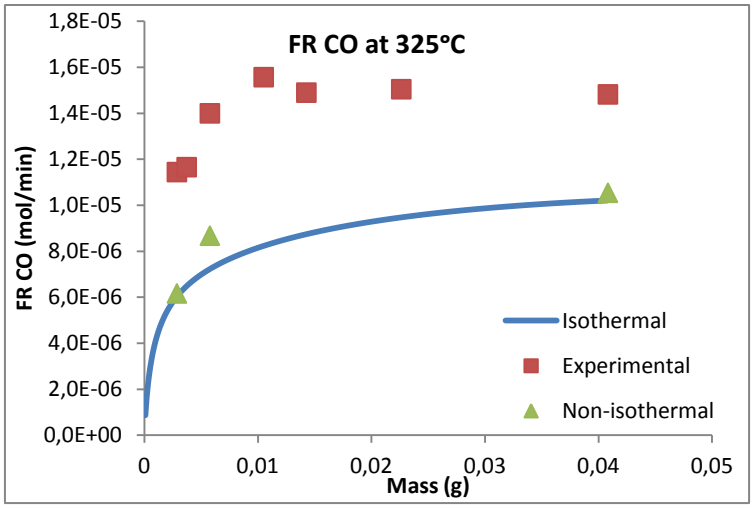

Figure E-9: Behaviour of the experimental and theoretical flow rates with only CO_2 at the inlet

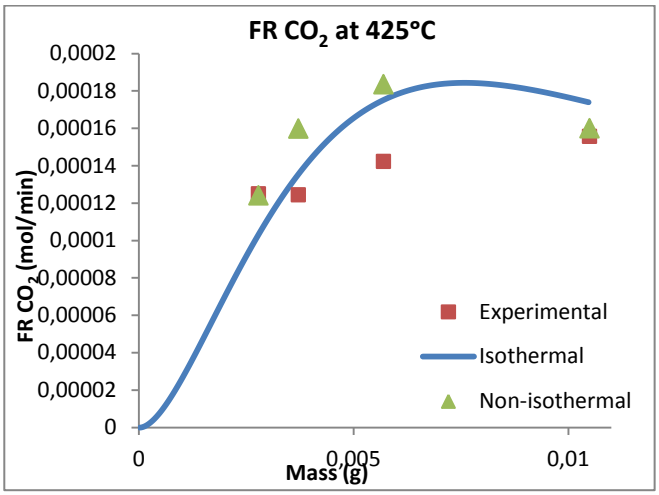

Figure E-10: Behaviour of the experimental and theoretical flow rates with only CO at the inlet

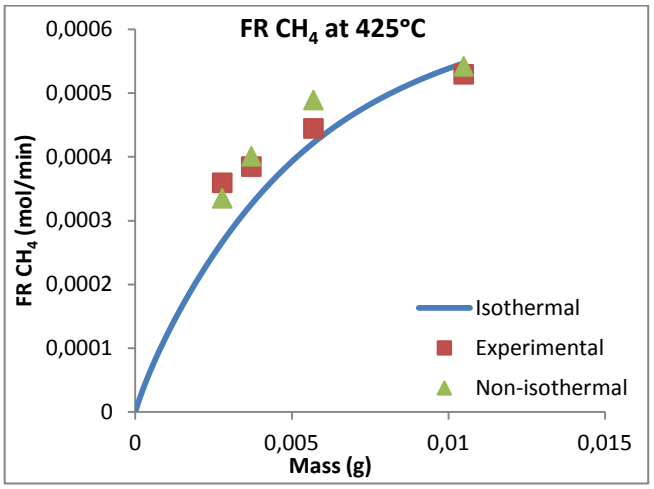

Figure E-11: Behaviour of the experimental and theoretical flow rates with only CO at the inlet

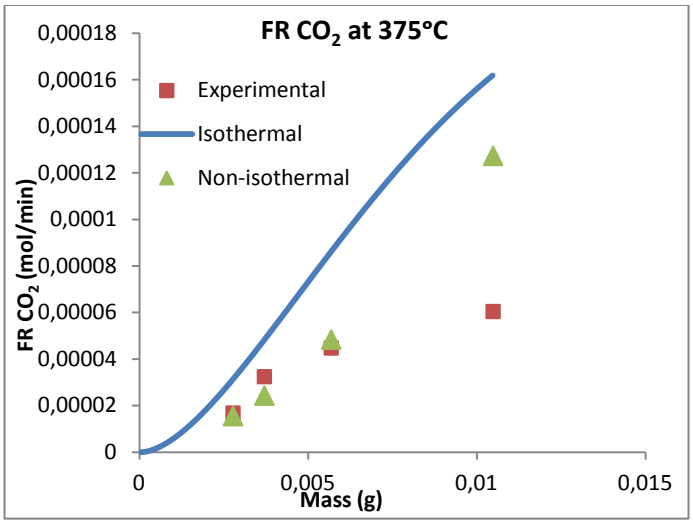

Figure E-12: Behaviour of the experimental and theoretical flow rates with only CO at the inlet

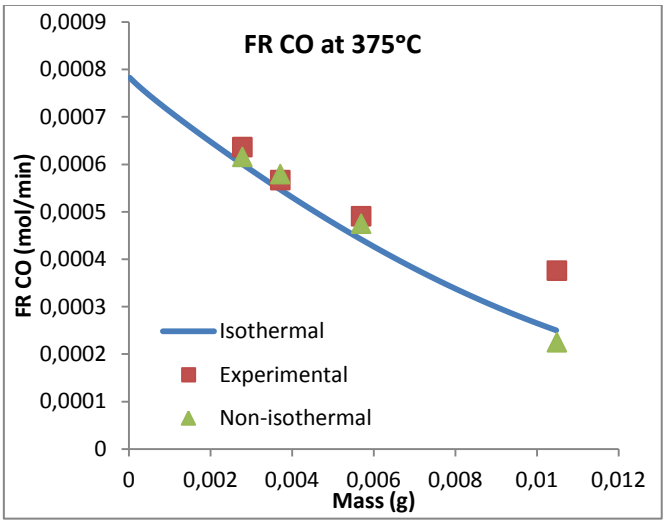

Figure E-13: Behaviour of the experimental and theoretical flow rates with only CO at the inlet

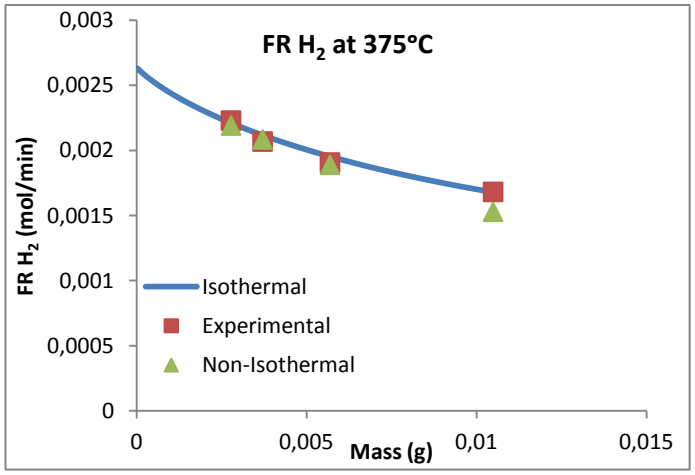

Figure E-14: Behaviour of the experimental and theoretical flow rates with only at the inlet

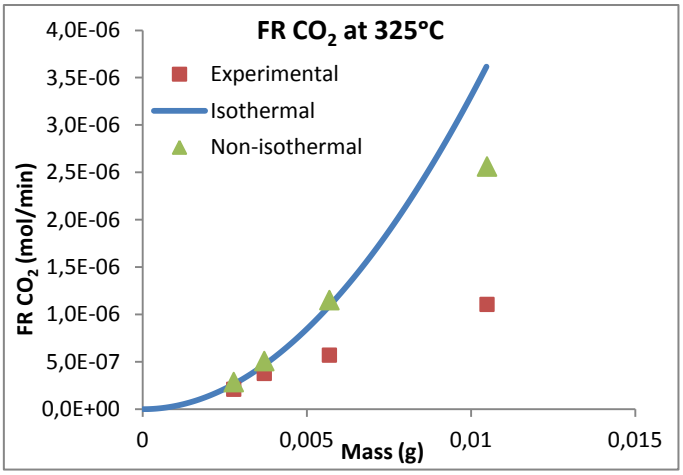

Figure E-15: Behaviour of the experimental and theoretical flow rates with only CO at the inlet

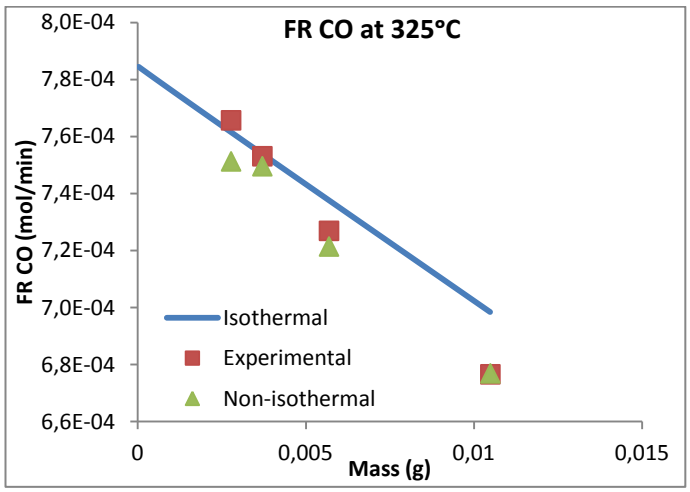

Figure E-16: Behaviour of the experimental and theoretical flow rates with only CO at the inlet

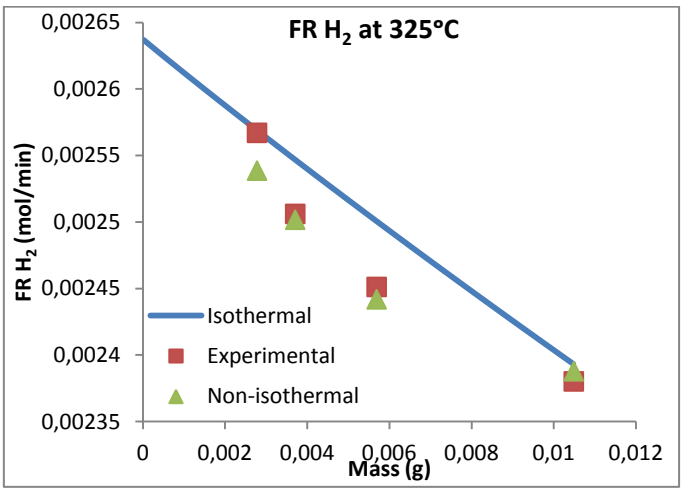

Figure E-17: Behaviour of the experimental and theoretical flow rates with only CO at the inlet

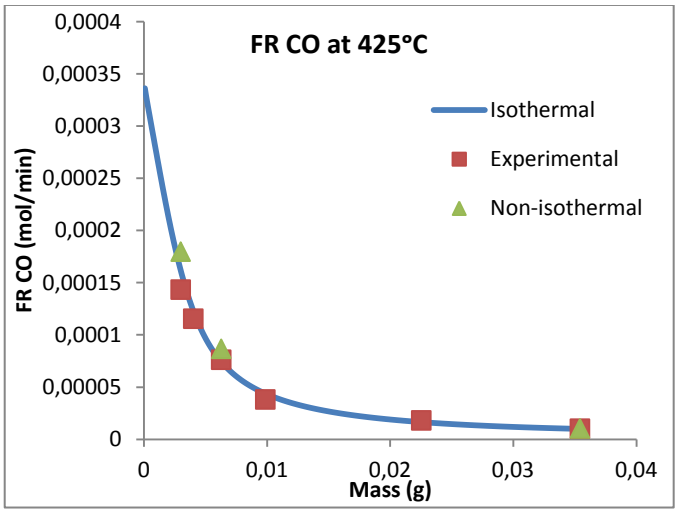

Figure E-18: Behaviour of the experimental and theoretical flow rates with CO and CO_2 at the inlet

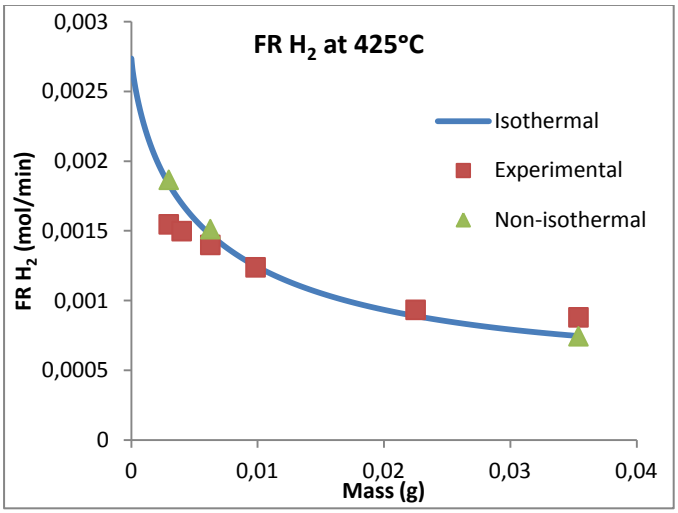

Figure E-19: Behaviour of the experimental and theoretical flow rates with CO and CO_2 at the inlet

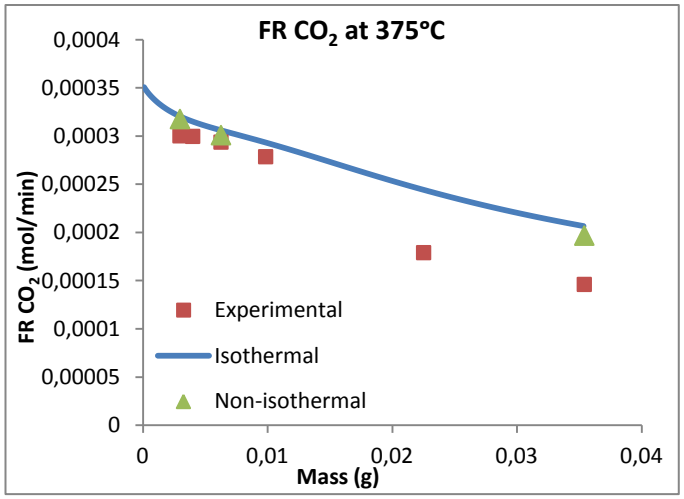

Figure E-20: Behaviour of the experimental and theoretical flow rates with CO and CO_2 at the inlet

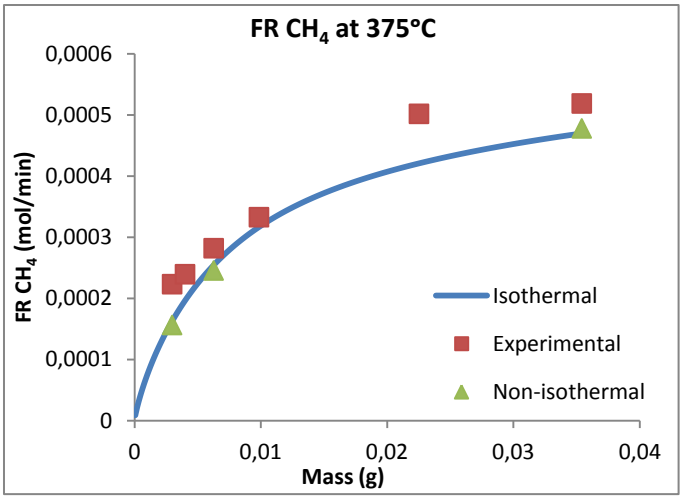

Figure E-21: Behaviour of the experimental and theoretical flow rates with CO and CO_2 at the inlet

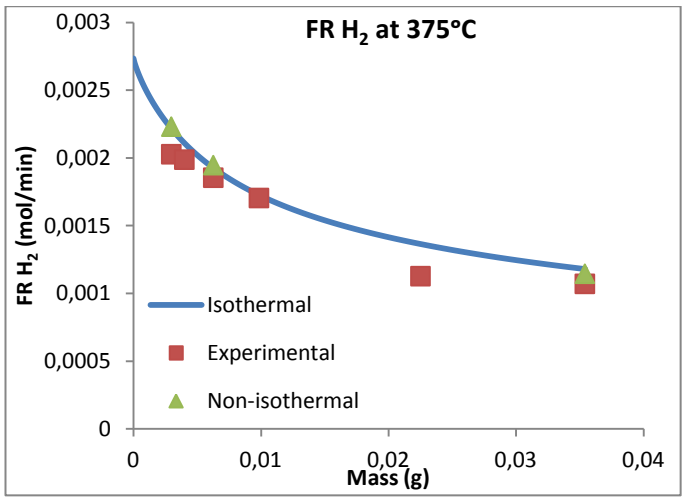

Figure E-22: Behaviour of the experimental and theoretical flow rates with CO and CO_2 at the inlet

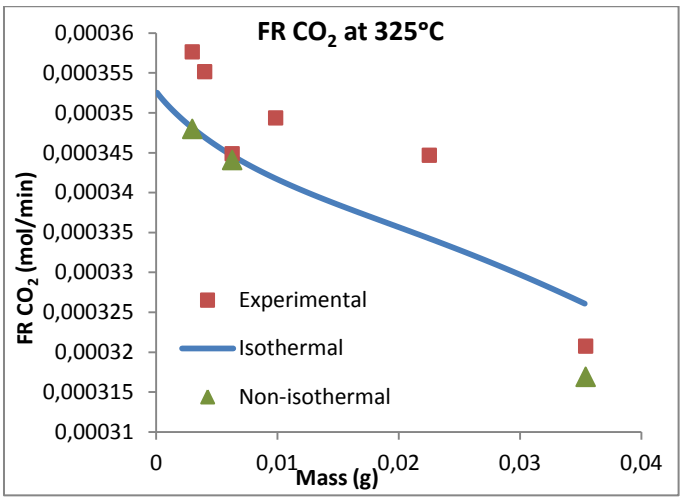

Figure E-23: Behaviour of the experimental and theoretical flow rates with CO and CO_2 at the inlet

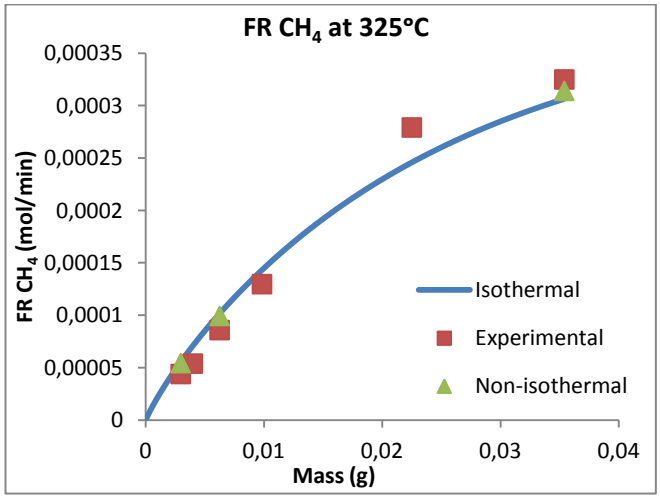

Figure E-24: Behaviour of the experimental and theoretical flow rates with CO and CO_2 at the inlet

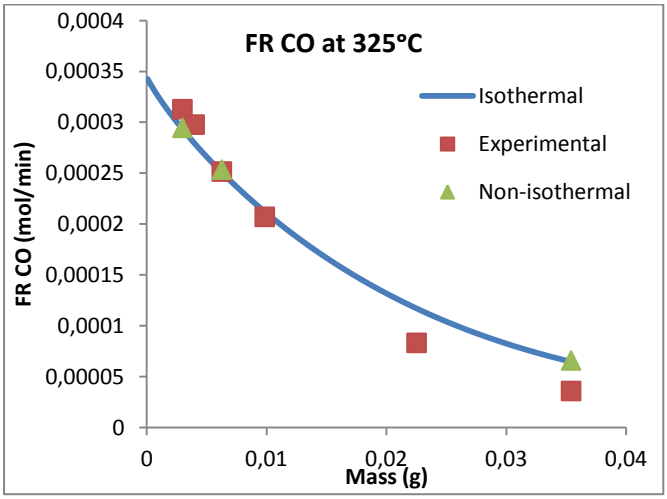

Figure E-25: Behaviour of the experimental and theoretical flow rates with CO and CO_2 at the inlet